

To be published in

A. Narlikar (Ed.)

**“Frontiers in Superconducting Materials”
Springer Verlag, Berlin, 2004**

SUPERCONDUCTIVITY IN HEAVY FERMION COMPOUNDS

P. Thalmeier¹, G. Zwicknagel², O. Stockert¹, G. Sparn¹ and F. Steglich¹

¹Max-Planck-Institut für Chemische Physik fester Stoffe,
01187 Dresden, GERMANY

²Institut für Mathematische Physik,
Technische Universität Braunschweig,
38106 Braunschweig, GERMANY

1 INTRODUCTION

The heavy electron state in intermetallic lanthanide and actinide compounds has its origin in the interplay of strong Coulomb repulsion in the 4f- and 5f- shells and their hybridisation with conduction band states. Heavy quasiparticles have mostly been observed in Ce- and U-based intermetallics which are therefore at the focus of this review. Ideally the ground state in these strongly correlated electron compounds may be described as a Landau Fermi liquid (LFL) state with large enhancement of the effective mass and associated large values of the linear specific heat coefficient γ , Pauli susceptibility χ_0 and A-coefficient of the resistivity. It has recently become clear that the microscopic origin of mass enhancement is quite different in Ce- and U-compounds, as described by the Kondo lattice model and dual model respectively.

The renormalised LFL state is however prone to instabilities at low temperatures due to residual heavy quasiparticle interactions and the sharpness of the Fermi distribution. The most common instabilities are the spontaneous appearance of (spin-)density wave (SDW) and superconducting (SC) order parameters which break at least some of the underlying spatial or internal symmetries like time reversal or gauge symmetry. Via their associated gap functions both type of order parameters are reflected in the modified energies and densities of low lying excitations.

This also changes low temperature properties in the ordered state and may in turn be used as a means to obtain information on the symmetry class of the order parameter. Both SC and SDW gap functions $\Delta(\mathbf{k})$ may be conventional or unconventional depending on whether their \mathbf{k} -dependence has the same or a lower spatial symmetry as the Fermi surface. In the latter case particles (SC) or particles and holes (SDW) pair preferentially at neighboring sites and avoid the strong on-site repulsion of quasiparticles. For this reason the SC states in Ce- and U-based HF compounds are usually of the unconventional type. Their intriguing properties have led to a rich and flourishing field of research, not only in the genuine HF compounds but also in oxides, ruthenates and organic solids.

The stability of the ordered phase may be influenced by changing microscopic control parameters via application of pressure or by chemical substitution. In this way the SDW state may be tuned to a magnetic quantum critical point (QCP) where the staggered moment vanishes. On theoretical grounds it has long been suspected that unconventional SC pairing is favored by magnetic instabilities, triplet pairing in the ferromagnetic and singlet pairing in the antiferromagnetic case. This correlation, however, cannot always be upheld for real HF materials.

The accumulated evidence in the Ce122 (e.g. CeCu_2Si_2), Ce115 (e.g. CeCoIn_5) and Ce218 (e.g. Ce_2CoIn_8) classes of superconductors seems to vindicate this picture, since the SC appears mostly in small 'domes' around the QCP. The connection between critical spin fluctuation properties and the stability of SC pair states has been analysed within strong coupling Eliashberg type theories. The QCP has additional implications beyond SC. In the normal state above the SC dome thermodynamic and transport behaviour show distinctly anomalous non-Fermi liquid (NFL) behaviour as function of temperature and field. This is thought to be the result of a dressing of quasiparticles with soft spin fluctuations leading to entirely different scaling exponents for specific heat, resistivity etc. as compared to the LFL state. This scenario is accepted for most NFL anomalies in Ce-HF compounds. Alternatively they may be caused by the existence of a 'pseudo-gap' associated with a 'hidden order' parameter, e.g. an unconventional SDW. This may indeed play a role in CeCoIn_5 and CeIrIn_5 in a similar way as invoked for the pseudo-gap phase of underdoped cuprates.

In U-based HF superconductors quantum critical behaviour does not play an important role with the possible exception of UBe_{13} . Instead of appearing close to the destruction of SDW order, SC in U-HF compounds is mostly embedded within a stable AF phase of reduced (sometimes very small) ordered moments. Like the different origin of mass enhancement this may be connected with the multi-orbital structure and multiple occupation of 5f shells. Instead of the Kondo lattice picture, a dual model with partly localised and partly itinerant electrons caused by a strongly orbital dependent effective hybridisation is more appropriate for U-HF compounds. In turn this suggests a new SC mechanism: Pair formation is caused by the exchange of magnetic excitons which are CEF excitations of the localised 5f-electrons that have acquired dispersion due to intersite-exchange. Contrary to the critical spin fluctuations in Ce-compounds these propagating bosonic modes are not overdamped. This mechanism has been vindicated in UPd_2Al_3 by the complementary results of quasiparticle tunneling and inelastic neutron scattering (INS) experiments. An equivalent experimental support for the spin fluctuation mechanism is still lacking.

This article reviews the present understanding of Ce-based and some of the U-based HF superconductors, with emphasis on the former. We will not discuss the physics of HF su-

perconductors containing other 4f or 5f elements like Pr skutterudites or trans-uranium based superconductors. For Ce-compounds we focus on the connection to magnetic quantum critical behaviour and the implications of the dual 5f-electron nature are discussed extensively for U-compounds. In sect. 2 we give the theoretical foundation of the different heavy quasiparticle origin in Ce- and U- compounds and present a brief summary of NFL properties in the normal state close to a QCP. In sect. 3 we discuss the known classes of Ce-HF superconductors with emphasis on the Ce122 compounds. We also discuss the new non-centrosymmetric SC CePt₃Si. In sect. 4 we give a description of the different microscopic pairing mechanisms present in the Ce- and U- intermetallics. In sect. 5 we discuss only those two U-based HF superconductors where new results have been obtained recently, namely UBe₁₃ and UPd₂Al₃. Finally sect. 6 gives the summary.

Of the many already existing review articles and monographies on HF systems and their superconducting state we mention here a small selection: The normal state properties of HF metals are at the focus in [1–4]. General reviews on HF superconductors are given in [5, 6] and the monography [7]. The exceptional case of the multicomponent SC UPt₃ is discussed in detail in [8, 9].

2 THEORIES FOR THE NORMAL HF STATE

The theoretical understanding of superconductivity and magnetism in the heavy fermion systems is still in the state of rather schematic or illustrative models. A major difficulty is that the normal state quasiparticles can so far be described only within effective single-particle renormalised band pictures with empirical input parameters. For some compounds like UBe₁₃ and Ce- compounds close to the quantum critical point the SC transition may even take place in a state where the low energy excitations are not simple LFL quasiparticles but are dressed by soft spin fluctuations. This is witnessed by the observation of non-Fermi liquid (NFL) behaviour in thermodynamic and transport quantities. A fully microscopic description in the case where inter-site effects become important is not available. Typical lattice effects are the formation of coherent heavy quasiparticle bands whose Fermi surfaces were observed experimentally. We first discuss the renormalised band theory which provides a way to describe the coherent heavy quasiparticle bands within a Fermi liquid approach. The latter can be calculated from single-particle Hamiltonians where the effective potential is constructed to account for many-body effects. The residual interaction among the quasiparticles eventually leads to the instability of the normal Fermi liquid phase.

2.1 RENORMALISED BAND THEORY FOR HF Ce-COMPOUNDS

The Landau theory assumes that there exists a one-to-one correspondence between the states of the complex interacting system and those of a gas of independent fermions, which may move in an external potential [10–12], [13]. The single-particle orbitals and energies are determined from an effective Hamiltonian. The characteristic properties of a system are reflected in an effective and not necessarily local potential which describes the field of the nuclei and the modifications arising from the presence of the other electrons. The essential many-body aspects

of the problem are then contained in the prescription for constructing the effective potentials which have to be determined for specific problems.

The Landau theory of Fermi liquids is a phenomenological theory. The characteristic properties of the quasiparticles which can hardly be calculated from microscopic theories are expressed in terms of parameters which are determined from experiment. The quasiparticle energies in a crystal

$$\varepsilon(\mathbf{k}) = \mathbf{v}_F(\hat{\mathbf{k}}) \cdot (\mathbf{k} - \mathbf{k}_F(\hat{\mathbf{k}})) \quad (1)$$

are given in terms of the (anisotropic) Fermi wave vector \mathbf{k}_F and the Fermi velocity \mathbf{v}_F which depend upon the direction $\hat{\mathbf{k}}$. The key idea of the renormalized band method is to determine these quantities by computing the band structure for a given effective potential which accounts for the many-body effects. The periodic potential leads to multiple-scattering processes involving scattering off the individual centers as well as the propagation between the centers. The characteristic properties of a given material enter through the information about single center scattering. They can be expressed in terms of properly chosen set of phase shifts $\{\eta_v^i(\varepsilon)\}$ specifying the change in phase of a wave incident on site i with energy E and symmetry v with respect to the scattering center. Within the scattering formulation of the band structure problem the values of the phase shifts at the Fermi energy $\{\eta_v^i(\varepsilon_F)\}$ together with their derivatives $\left\{ (d\eta_v^i/d\varepsilon)_{\varepsilon_F} \right\}$ determine the Fermi wave vectors \mathbf{k}_F and the Fermi velocity \mathbf{v}_F . The scattering formulation of the effective band structure problem provides a highly efficient parametrisation scheme for the quasiparticles. To further reduce the number of phenomenological parameters we refer to the microscopic model for Ce-based HF compounds.

The similarities in the behavior of Ce-based heavy-fermion systems to that of dilute magnetic alloys have led to the assumption that these systems are "Kondo lattices" where the observed anomalous behavior can be explained in terms of periodically repeated resonant Kondo scattering. This ansatz provides a microscopic model for the formation of a singlet ground-state and the existence of heavy quasiparticles. An extensive discussion is given in [4]. Direct evidence for the Kondo scenario comes from photoelectron spectroscopy. The characteristic features of a Kondo system can be summarized as follows [14, 15]: At high temperatures, the combined PES/BIS spectra from photoemission and inverse photoemission exhibit two distinct peaks below and above the Fermi energy. These two features correspond to the valence transitions $f^n \rightarrow f^{n\mp 1}$, respectively. The changes in the occupation of the Ce 4f- shells are associated with energies of order eV. The high-temperature state can be modelled by weakly correlated conduction electrons which are weakly coupled to local f-moments. The f-derived low-energy excitations are those of a system of local moments. The direct manifestation of the low-energy scale is the appearance of a sharp peak near the Fermi energy at low temperatures. In Ce systems, this many-body feature known as "Abrikosov-Suhl" or "Kondo" resonance, is centered at $\varepsilon_F + kT^*$ slightly above the Fermi edge ε_F . The "Kondo temperature" T^* determines the energy scale of the dynamical screening of the impurity spin by conduction electrons [4]. The evolution of the Kondo resonance with temperature was recently observed by high-resolution photoemission experiments [16].

The resonance is a genuine many-body feature reflecting the small admixture of f^0 configurations to the ground state and the low-lying excitations which are mainly built from f^1 -configurations. At sufficiently low temperatures $T \ll T^*$, the contribution of the narrow reso-

nance peak to the thermodynamic and transport properties can be described in terms of a Landau theory with heavy fermionic quasiparticles [17]. Based on the corresponding effective Hamiltonian Nozières [18] introduced a resonant phase shift to account for the impurity contribution to the low-energy properties.

The novel feature observed in stoichiometric Ce-compounds is the formation of narrow coherent bands of low-energy excitations. The heavy fermions arise from a decoherence-coherence crossover occurring at low temperatures.

The calculation of realistic quasiparticle bands in Ce-based Heavy Fermion compounds proceeds in several steps. For a detailed description see [19]. The first step is a standard LDA band structure calculation by means of which the effective single-particle potentials are self-consistently generated. The calculation starts, like any other ab-initio calculation, from atomic potentials and structure information. In this step, no adjustable parameters are introduced. The effective potentials and hence the phase shifts of the conduction states are determined from first principles to the same level as in the case of “ordinary” metals. The f-phase shifts at the lanthanide and actinide sites, on the other hand, are described by an empirical resonance type expression

$$\eta_{\hat{f}} \simeq \tan^{-1} \frac{\Gamma_{\hat{f}}}{\varepsilon - \varepsilon_{\hat{f}}} \quad (2)$$

characterized by the position $\varepsilon_{\hat{f}}$ and the width $\Gamma_{\hat{f}}$ of the many-body resonance. One of these free parameters is eliminated by imposing the condition that the charge distribution is not significantly altered as compared to the LDA calculation by introducing the renormalation. The renormalised band method devised to calculate the quasiparticles in heavy-fermion compounds thus is essentially a one-parameter theory. We mention that spin-orbit and CEF splittings can be accounted for in a straight-forward manner [20].

The strong local correlations in Kondo lattices lead to an observable many-body effect, i. e., the change with temperature of the volume of the Fermi surface. At high temperatures, the f -degrees of freedom appear as localised magnetic moments, and the Fermi surface contains only the itinerant conduction electrons. At low temperatures, however, the f degrees of freedom are now tied into itinerant fermionic quasiparticle excitations and accordingly, have to be included in the Fermi volume following Luttinger’s theorem. Consequently the Fermi surface is strongly modified. This scenario [21] was confirmed experimentally by measurements of the de Haas-van Alphen (dHvA) effect [22–24].

2.2 DUAL MODEL FOR U-BASED SYSTEMS

The Kondo picture, however, does not apply in the case of the actinide compounds. The difficulties with this model have been discussed in [25]. The difference between the Ce-based heavy-fermion compounds and their U-counterparts can be seen directly from the photoemission spectra [14]. In U-based heavy-fermion compounds, the fingerprint character of the transitions $f^n \rightarrow f^{n\pm 1}$ is lost. Instead of the well defined f-derived peaks familiar from the Ce systems we encounter a rather broad f-derived feature. This fact shows that the f-valence in the actinide heavy-fermion systems is not close to integer value as it is the case in Ce-based HF compounds. In fact, the f-valence of the U ions has been discussed rather controversially.

Increasing experimental and theoretical evidence points towards a dual nature of the $5f$ -electrons in actinide-based intermetallic compounds, with some of the $5f$ electrons being localised and others delocalised. The dual model which assumes the coexistence of both delocalised and localised $5f$ -electrons provides a scheme for microscopic calculations of the heavy quasiparticle bands in actinide compounds. The concept is summarised as follows: The “delocalised” $5f$ -states hybridise with the conduction states and form energy bands while their “localised” atomic-like counterparts form multiplets to reduce the local Coulomb repulsion. The two subsystems interact which leads to the mass enhancement of the delocalised quasiparticles. The situation resembles that in Pr metal where a mass enhancement of the conduction electrons by a factor of 5 results from virtual crystal field (CEF) excitations of localised $4f^2$ electrons [26]. The underlying hypothesis is supported by a number of experiments. For an extensive discussion we refer to [27]. Calculations based on the dual model as described above reproduce the dHvA data in UPt_3 [28] and UPd_2Al_3 [29]. The results of the latter calculation will be discussed in sect. 5.2.

The dual nature of the $5f$ states which is found in many actinide intermetallic compounds is a consequence of the interplay between local Coulomb correlations and hybridisation with the conduction electrons. The underlying microscopic mechanism is an area of active current research (see [30] and references therein). LDA calculations show that the effective hopping matrix elements for different $5f$ orbitals are unequal. But it is of interest to understand why only the largest among them is important and why the others are suppressed.

The reason lies in the competition between anisotropic hybridisation and angular correlations in the $5f$ shell which can be seen by exact diagonalisation of small clusters modelling the U sites in heavy fermion compounds [30]. Keeping only the degrees of freedom of the $5f$ shells while accounting for the conduction states by (effective) anisotropic $5f$ -intersite hopping leads to the model Hamiltonian

$$H = - \sum_{\langle nm \rangle, j_z} t_{j_z} \left(c_{j_z}^\dagger(n) c_{j_z}(m) + h.c. \right) + H_C \quad (3)$$

The first sum is over neighboring sites $\langle nm \rangle$. Furthermore $c_{j_z}^\dagger(n)$ ($c_{j_z}(n)$), creates (annihilates) an electron at site n in the $5f$ $j = 5/2$ state with $j_z = -5/2, \dots, 5/2$. The effective hopping between sites results from the hybridisation of the $5f$ states with the orbitals of the ligands and depends generally on the crystal structure. Rather than trying to exhaust all possible different lattice symmetries, we shall concentrate here on the special case that hopping conserves j_z . While this is certainly an idealisation, it allows us to concentrate on our main topic, i. e., a study of the influence of atomic correlations on the renormalisation of hybridisation matrix elements. The parameters t_{j_z} ($= t_{-j_z}$) are chosen in accordance with density-functional calculations for bulk material which use $j j_z$ basis states. The local Coulomb interactions can be written in the form

$$H_C = \frac{1}{2} \sum_n \sum_{j_{z1}, \dots, j_{z4}} U_{j_{z1} j_{z2} j_{z3} j_{z4}} c_{j_{z1}}^\dagger(n) c_{j_{z2}}^\dagger(n) c_{j_{z3}}(n) c_{j_{z4}}(n) \quad (4)$$

where the Coulomb matrix elements $U_{j_{z1} j_{z2} j_{z3} j_{z4}}$ are expressed in terms of the expectation values U_J of the repulsion between electron pairs in states with total angular momentum J . The

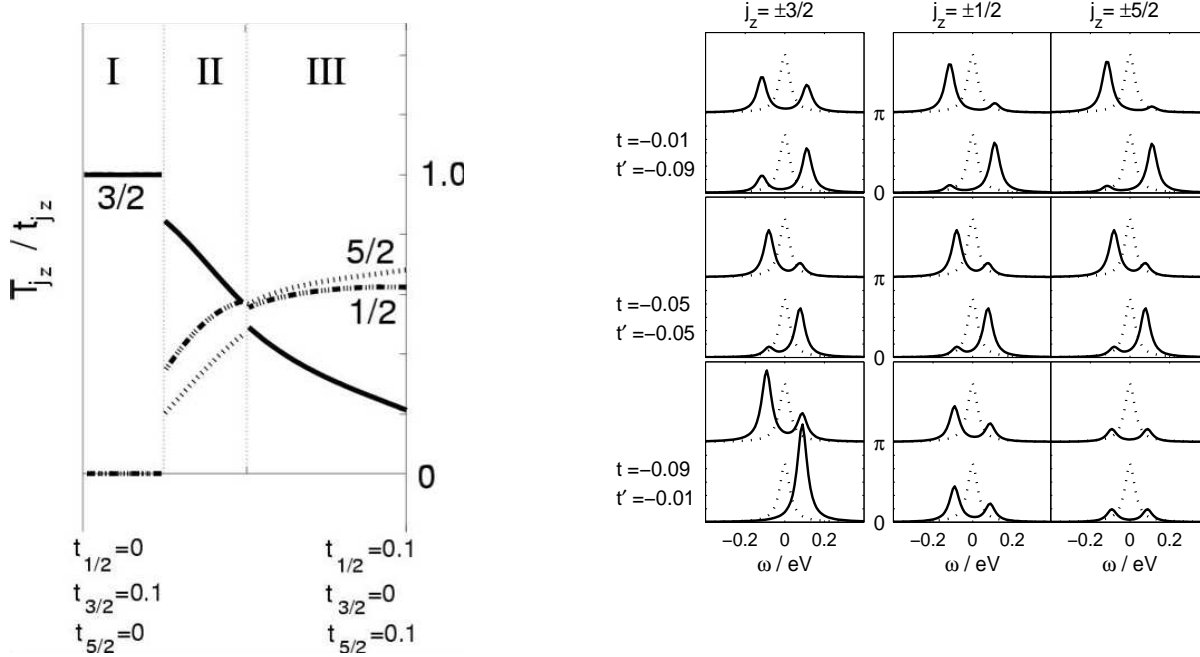


Figure 1: Left panel: Enhancement of hopping anisotropies due to intra-atomic correlations in a two-site cluster. The orbital-projected expectation value of the kinetic energy T_{j_z}/t_{j_z} along the lines connecting linearly the points is written below the figure. Regions with $\mathcal{J}_z = 15/2, 5/2$ and $3/2$, are labeled I, II and III respectively. Right panel: Dispersion of the low-energy peak in the spectral functions ($A_{j_z}(\mathbf{k}, \omega) + A_{-j_z}(\mathbf{k}, \omega)$) for strongly anisotropic systems ($|t_{3/2}| = |t| \ll |t'| = |t_{1/2}| = |t_{5/2}|$) as well as in the isotropic limit ($|t_{3/2}| = |t| = |t'| = |t_{1/2}| = |t_{5/2}|$). For each parameter set of hopping parameters, the spectral functions for $k=0$ and $k=\pi$ are compared. The dotted curve denotes the isotropic peak in the atomic limit.

actual calculations U_J values used in the calculation were determined from LDA wavefunctions for UPt₃ [28], i. e., $U_{J=4} = 17.21$ eV, $U_{J=2} = 18.28$ eV, and $U_{J=0} = 21.00$ eV. We expect $U_{J=4} < U_{J=2} < U_{J=0}$ always to hold for Coulomb interactions, independently of the chemical environment. In contrast, the relative order of the hopping matrix elements will vary strongly from one compound to the next. The average Coulomb repulsion is irrelevant for the low-energy physics of the model. It simply restricts the relevant configurations to states such that each site is occupied either by 2 or 3 f electrons. The low-energy sector is exclusively determined by the differences of the U_J values, which are of the order of 1 eV and thus slightly larger than typical bare f -band widths. The latter are obtained, e.g., from LDA calculations for metallic uranium compounds like UPt₃. To mimic the situation in the U-based heavy-fermion compounds we consider the intermediate valence regime. The Hamiltonian eq. (3) conserves $\mathcal{J}_z = \sum_n J_z(n)$ where \mathcal{J}_z is the z -component of the total angular momentum of the system and the $J_z(n)$ refer to angular momentum projections on individual sites. We shall therefore characterise the eigenstates by their \mathcal{J}_z value. Strong on-site correlations result in a considerable enhancement of anisotropies in the bare hopping matrix elements. This can lead to a localisation of electrons in orbitals with relatively weak hybridisation. The latter is effectively reduced to zero in those

cases.

The degree of localisation or, alternatively, of the reduction of hopping of a given j_z orbital by local correlations, is quantified by the ratio of the j_z - projected kinetic energy T_{j_z} and the bare matrix element t_{j_z}

$$\frac{T_{j_z}}{t_{j_z}} = \sum_{\langle nm \rangle, \pm} \langle \Psi_{gs} | (c_{\pm j_z}^\dagger(n) c_{\pm j_z}(m) + h.c.) | \Psi_{gs} \rangle. \quad (5)$$

The ground-state wavefunction $|\Psi_{gs}\rangle$ contains the strong on-site correlations. A small ratio of T_{j_z}/t_{j_z} indicates partial suppression of hopping for electrons in the $\pm j_z$ orbitals. Two kinds of correlations may contribute to that process. The first one is based on the reduction of charge fluctuations to atomic f^2 and f^3 configurations. This is a result for large values of U_J and can be studied by setting all U_J equal to a value much larger than the different t_{j_z} . The second one is due to differences in the U_J values, i. e. , $U_{J=4} < U_{J=2} < U_{J=0}$. The differences in the U_J values are the basis of Hund's rules. Hopping counteracts Hund's rule correlations and vice versa. What we want to stress is the fact that those correlations can lead to a complete suppression of hopping channels except for the dominant one which shows only little influence.

Results for the ratios T_{j_z}/t_{j_z} are shown in fig. 1 for a two-site model [30]. As the relevant correlations are local the general results qualitatively agree with those found for a three-site cluster and four-site clusters [31]. We can distinguish three different regimes with $\mathcal{J}_z = 15/2$, $5/2$ and $3/2$, labeled I, II and III respectively. One observes that in region I only the dominant hybridisation of the $j_z = 3/2$ orbital survives while that of the $j_z = 1/2$ and $j_z = 5/2$ orbitals is completely suppressed. On the other hand in regions II and III the correlation effects on different orbitals are not very different. These findings demonstrate that in particular Hund's rule correlations strongly enhance anisotropies in the hopping. For a certain range of parameters this may result in a complete suppression of the effective hopping except for the largest one, which remains almost unaffected. This provides a microscopic justification of partial localisation of $5f$ electrons which is observed in a number of experiments on U compounds and which is the basis for further model calculations described later on.

Many aspects of partial localisation in the ground state are described appropriately by both a Gutzwiller type variational wave function and by a treatment which keeps only those interactions which are present in LDA+U calculations [32]. This finding should encourage further applications of LDA+U and related approaches as SIC-LDA for ground-state properties of actinide heavy-fermion materials. The subtle angular correlations which determine the magnetic character are accounted for only in limiting cases. In addition, we cannot expect these schemes to reproduce the small energy scales responsible for the heavy fermion character of the low-energy excitations. The dual nature of the $5f$ states is manifest in the spectral functions $A_{j_z}(\mathbf{k}, \omega)$ and the density of states (DOS) $N(\omega)$ given by

$$N(\omega) = \sum_{\mathbf{k}} \sum_{j_z} A_{j_z}(\mathbf{k}, \omega) \quad . \quad (6)$$

The spectral functions which are defined by

$$\begin{aligned} A_{j_z}(\mathbf{k}, \omega) = & \sum_n \left| \langle \psi_n^{N+1} | c_{j_z}^\dagger(\mathbf{k}) | \psi_0^N \rangle \right|^2 \delta(\omega - (E_n^{N+1} - E_0^N)) + \\ & + \sum_n \left| \langle \psi_n^{N-1} | c_{j_z}(\mathbf{k}) | \psi_0^N \rangle \right|^2 \delta(\omega + (E_n^{N-1} - E_0^N)) \end{aligned} \quad (7)$$

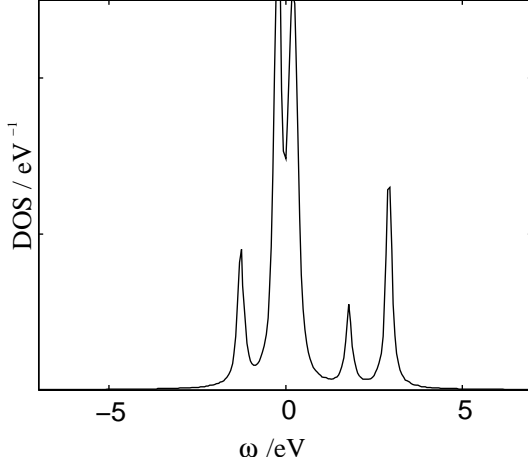


Figure 2: Density of states for a linear chain calculated within CPT. The short-range correlations are treated within a two-site cluster. The hopping parameters are $|t_{3/2}| = 0.2$ eV and $|t_{1/2}| = |t_{5/2}| = 0$. The high-energy side-bands have predominantly $j_z = \pm 5/2$ character.

measure the weights for removing an electrons in state $(\mathbf{k}j_z)$ from the ground state (negative energies) or adding on to it (positive energies). Here $|\psi_0^N\rangle$ denotes the exact ground state of an N -particle system with ground state energy $E_0^{(N)}$ while $|\psi_n^{N+1}\rangle$ and $|\psi_n^{N-1}\rangle$ are complete sets of eigenstates of the $N+1$ - and $N-1$ -particle systems with energies $E_n^{(N+1)}$ and $E_n^{(N-1)}$, respectively. Technically, the spectral functions are obtained from the one-particle Green's functions according to

$$A_{j_z}(\mathbf{k}, \omega) = -\frac{1}{\pi} \text{Im} G_{j_z}(\mathbf{k}, \omega) \quad (8)$$

which are approximately calculated for a cluster following [33]. As a first step towards a microscopic treatment of partial localisation in extended systems the one-particle Green's functions are calculated within cluster perturbation theory. The method combines exact diagonalisation of small clusters with strong-coupling perturbation theory [34]. The many-particle states of the clusters are determined by means of the Jacobi-Davidson method [35]. The formation of the heavy quasiparticles, i. e., the enhancement of the effective mass over the bare band mass is related to the transfer of spectral weight from low energies to high-energy satellites. Different kinds of processes may contribute to this phenomenon. First, there is the suppression of charge fluctuations which effectively restricts the ground state in the mixed-valent regime to f^2 and f^3 configurations. Neglecting angular correlations, the spectral function will have a low-energy peak from the transitions $f^2 \rightarrow f^3$ and $f^3 \rightarrow f^2$ whose weight will be reduced due to the atomic valence transitions $f^2 \rightarrow f^1$ and $f^3 \rightarrow f^4$. These transition appear in the spectrum at energies well separated from the Fermi level. Second, there are the angular correlations as described by Hund's rules. They transfer spectral weight to atomic side bands which appear at energies $\sim 1 - 2$ eV below (or above) the Fermi edge. These structures can be seen from the DOS displayed in fig. 2. Experimentally, the ‘‘Hund's rule structures’’ are observed as ‘‘humped features’’ in photoemission experiments [36]. Due to the atomic transitions the overall width is much larger than the value predicted by standard band structure calculations.

Suppression of charge fluctuations and angular correlations reduce the weight of the low-energy peak to 0.41. This reduction corresponds to an isotropic enhancement of the quasiparticle mass by ~ 2.5 . The quasiparticle weight is further reduced by hopping between the sites. The latter introduces dispersion effects and orbital-dependence as can be seen from fig. 1 (right

panel). The spectral weight of the isotropic “atomic” peak is distributed over a rather broad energy range. The strong local correlations result in a considerable enhancement of anisotropies in the bare hopping matrix elements. The j_z channels with the dominant hopping exhibit well-defined dispersive quasiparticle peaks in the low-energy regime whereas the remaining channels contribute a non-dispersive incoherent background. The results are consistent with previous results the orbital-projected expectation values of the kinetic energy.

2.3 THE NFL STATE AND ITS SCALING LAWS

In the vicinity of a second order phase transition the behavior of various physical properties exhibit singularities which can be characterised by critical exponents [37]. The latter are universal in the sense that they do not depend upon the detailed microscopic nature of the system. They are determined by the dimensionality of the system and the degrees of freedom associated with the long-range correlations in the ordered phase. As a consequence, the critical exponents have been successfully used to classify the critical behavior in classical systems. The universality reflects the fact that the characteristic length and time scales, i.e., the correlation length ξ and the relaxation time τ diverge like

$$\xi \sim |g|^{-\nu} \text{ and } \tau \sim |g|^{-\nu z} \quad (9)$$

for $|g| \rightarrow 0$ (see e. g. [38, 39]) where $g = t, r$ measures the distance to the critical point according to

$$t = \frac{T - T_c}{T_c}, \quad r = \frac{p - p_c}{p_c} \quad \text{or} \quad r = \frac{H - H_c}{H_c} \quad (10)$$

Here T , p and H are temperature, pressure and field while T_c , p_c and H_c are their critical values. It is important to note that the critical exponents are not independent. They are related by scaling relations and, in addition, they are connected with the dimension d of the system by hyperscaling relations. On approaching T_c from above ($t \rightarrow 0^+$) the growing amplitude of thermally excited collective modes drives the system to a new state with spontaneously broken symmetry characterised by an order parameter.

On the other hand quantum phase transitions (QPT) which take place at zero temperature ($T_c=0$) are driven by the contribution of quantum fluctuations to the ground state energy which depends on a control parameter $r \rightarrow 0^+$ associated with pressure or field. In this case the effective dimensionality d_{eff} is given by

$$d_{eff} = d + z \quad (11)$$

where z is the dynamical exponent introduced above. Due to the effective increase in dimensionality the latter may reach the upper critical dimension. As a consequence, the critical exponents associated with the QPT may assume mean-field values [40]. In general, the characterisation of a continuous quantum phase transition is more subtle than that of a classical one.

Besides specific heat, susceptibility and resistivity the Grüneisen ratio Γ has turned out to be a sensitive quantity to characterise the vicinity of the QCP. Zhu et al. [41] have shown that the

Γ ratio defined in terms of the molar specific heat $c_p = \frac{T}{N} (\partial S / \partial T)_p$ and the thermal expansion $\alpha = \frac{1}{V} (\partial V / \partial T)_{p,N} = \frac{1}{V} (\partial S / \partial p)_{T,N}$, namely

$$\Gamma = \frac{\alpha}{c_p} = -\frac{1}{V_m T} \frac{(\partial S / \partial p)_T}{(\partial S / \partial T)_p} \quad (12)$$

diverges at any QCP. Here S is the entropy and $V_m = \frac{V}{N}$ is the molar volume. Away from the QCP when the low-temperature behavior is characterised by a single energy scale E^* the Grüneisen ratio in eq. (12) reduces to

$$\Gamma \simeq \frac{1}{V_m E^*} \frac{\partial E^*}{\partial p} \quad (13)$$

This form was already introduced and discussed in [42–45]. Instead of pressure, an external magnetic field H may be used as control parameter. In this case, the ratio

$$\Gamma_H = -\frac{1}{c_H} \left(\frac{\partial M}{\partial T} \right)_H = -\frac{1}{T} \frac{(\partial S / \partial H)_T}{(\partial S / \partial T)_H} = -\frac{1}{T} \left(\frac{\partial T}{\partial H} \right)_S \quad (14)$$

can be determined directly from the magneto-caloric effect. The Grüneisen ratio Γ and its magnetic counterpart Γ_H owe their importance to the fact that at the critical value $r = 0$ the temperature dependence is given by

$$\Gamma(T, r = 0) \sim T^{-\frac{1}{vz}} \quad (15)$$

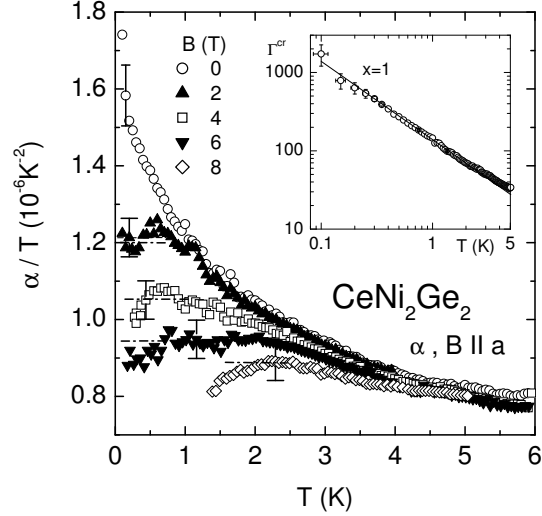
and consequently permits to measure vz . Comparison with experiment usually requires to account for corrections to the simple scaling ansatz from which eq. (15) is derived. The corrections, however, have to be evaluated from a microscopic model. For a discussion of the validity of eq.(15) we refer to [46, 47].

Neutron diffraction results for the A-phase in CeCu_2Si_2 suggest that the magnetic quantum phase transition in stoichiometric heavy fermion compounds arises from the instability of the strongly renormalised Fermi liquid with respect to the formation of a SDW. Model studies for the SDW transition therefore deserve special attention. Using the Ginzburg-Landau-Wilson functional for the effective action [40]

$$\begin{aligned} S[\phi] &= \sum_{\mathbf{q}, i\omega_n} \left(r + q^2 + \frac{|\omega_n|}{\Gamma_q} \right) |\Phi_{\mathbf{q}, i\omega_n}|^2 + S^{(4)} \quad \text{with} \quad \Gamma_{\mathbf{q}} = \Gamma_0 q^{z-2} \\ S^{(4)} &= u \int_0^\beta \int d^d \mathbf{r} |\Phi(\mathbf{r}, \tau)|^4 \end{aligned} \quad (16)$$

the thermal expansion and Grüneisen ratio were calculated on the nonmagnetic side of the phase diagram [41]. Here Φ is the order parameter that fluctuates in space and imaginary time, $\beta = 1/kT$ is the inverse temperature and $\omega_n = 2n\pi T$ are bosonic Matsubara frequencies. The parameter r controls the distance from the critical point. The Landau damping which is linear in $|\omega|$ is due to the scattering of quasiparticles by spin fluctuations. It is characterised by the dynamical exponent z . The theory starts on the Fermi liquid side ($r > r_c$) which is characterised by a large Fermi surface including the f-degrees of freedom. The low-energy excitations are

Figure 3: Thermal expansion showing the suppression of NFL behaviour as function of field. The inset shows that for $B = 0$ the critical contribution to the Grüneisen ratio of CeNi_2Ge_2 (sect. 3.2) scales like $\Gamma \sim 1/T^x$ with $x = 1$. After eq.(15) this means (assuming $z = 2$ for AF SDW) a mean field correlation length exponent $\nu = 1/2$ which is in agreement with $d_{\text{eff}} = d+z = 5$ for the effective dimension [48].



fermionic quasiparticles and their collective excitations. Close to the QCP the static susceptibility is assumed to diverge at a specific wave vector \mathbf{Q} which signifies the transition into the SDW state. The quasiparticles are strongly scattered along “hot lines” which are connected by \mathbf{Q} [49]. This strong scattering modifies the low-temperature thermodynamic and transport properties which exhibit anomalous scaling relations close to QCP. They differ from those familiar from Fermi liquids. The scaling relations are derived adopting the renormalisation scheme of Millis [50, 51] which proceeds in close analogy to the spin-fluctuation theory of ferromagnetism [52]. The scaling behavior obtained for various models and many non-Fermi liquid compounds are summarised in [53].

The model calculations in [41] classify transitions according to various types of magnetic order. Two-dimensional ($d=2$) as well as three-dimensional ($d=3$) systems are considered assuming the values $z = 2, 3$ for the dynamical exponents. Comparison of calculated Grüneisen ratios with experiments in CeNi_2Ge_2 [48] shows that the QCP in this stoichiometric HF compound are consistent with the SDW scenario for three-dimensional critical AF spin fluctuations (fig. 3).

3 CERIUM-BASED HF SUPERCONDUCTORS

Since the discovery of heavy electrons and their superconducting state [54] in CeCu_2Si_2 the Ce-based tetragonal 112-compounds (space group $I4/mmm$, see fig. 4) have been at the focus of investigation. This class of materials offers a unique stage to watch the interplay of quantum-criticality, heavy Landau Fermi liquid (LFL) and non-Fermi liquid (NFL) behaviour as well as unconventional superconductivity. Although it has a long history, major aspects of the parent compound CeCu_2Si_2 of this class were only understood very recently: Firstly the long mysterious ‘A-phase’ associated with the low pressure quantum critical point, has finally been identified as an incommensurate (IC) SDW phase caused by the nesting of heavy quasiparticle FS sheets [55]. In fact it is now possible to follow the continuous evolution of the SDW wave vector and moment size of magnetic phases in $\text{CeCu}_2(\text{Si}_{1-x}\text{Ge}_x)_2$ from the small moment IC-SDW in CeCu_2Si_2 to the atomic moment commensurate antiferromagnetism in CeCu_2Ge_2 [56].

Secondly the anomalous stability of SC in CeCu_2Si_2 for pressures far above the A-phase QCP [57] which did not exhibit the typical dome-shape around the QCP pressure has now been understood. Likewise CeCu_2Ge_2 does not have a dome-shaped SC $T_c(p)$ curve once AF order is suppressed. Employing a negative pressure shift caused by the larger Ge- radius it looks rather similar to that of CeCu_2Si_2 . Artificial reduction of the SC condensation energy in CeCu_2Si_2 by Ge- alloying and applying positive shifts with hydrostatic pressure leads to a breakup of the SC region into two isolated domes which are associated with the previous A-phase magnetic QCP and a new high pressure valence transition QCP respectively [58]. This also suggests that SC phases and pairing mechanisms in the isolated SC regimes are different. Quantum criticality in the $\text{CeCu}_2(\text{Si}_{1-x}\text{Ge}_x)_2$ system is connected with distinct NFL anomalies that can only partly be explained within the standard nearly AF Fermi liquid picture, notably the discrepancy of the temperature scaling of resistivity and γ - coefficients at higher fields close to the A- phase QCP may require different concepts.

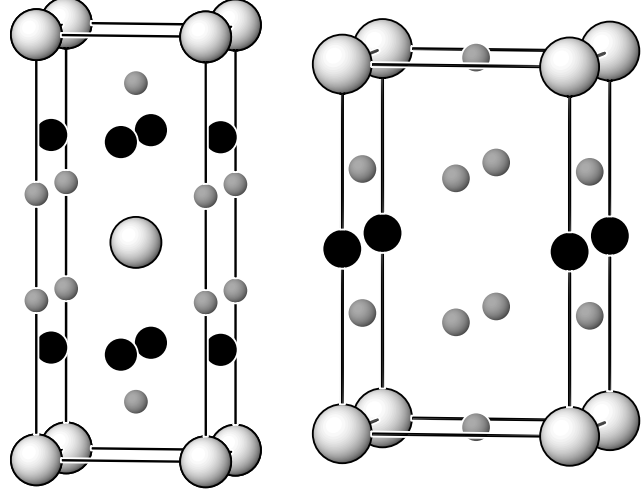
The HF compounds CeRh_2Si_2 and CePd_2Si_2 also become superconducting only under application of pressure like CeCu_2Ge_2 . As in CeCu_2Ge_2 AF order in CeRh_2Si_2 vanishes in a first order phase transition at the critical pressure p_c . SC in the latter appears only in an extremely narrow region around p_c , unlike in the former compound. Due to the first order transition both CeCu_2Ge_2 and CeRh_2Si_2 are in a LFL state close to p_c . For CePd_2Si_2 on the other hand a QCP where AF order vanishes continuously leads to a SC p-T phase diagram which is of the canonical single dome shape centered at p_c where clear cut NFL behaviour in the resistivity is observed. Finally CeNi_2Ge_2 is quite unique because it is not magnetic but rather displays almost ideal NFL behaviour at ambient pressure although incipient superconductivity is found at very low temperatures in highest-purity samples.

A comparison of the various Ce122 compounds leads one to conclude that the existence of an AF QCP with associated NFL behaviour is sufficient to induce superconductivity around p_c . Indeed the AF spin fluctuation theory (sect. 4) predicts a stabilisation of the SC state when the QCP is approached. However, as the examples of CeCu_2Ge_2 and CeRh_2Si_2 show, SC in Ce122 compounds may just as well appear in the normal LFL state.

It took more than 20 years to discover an additional class of Ce-based HF superconductors with the general formula $\text{Ce}_n\text{M}_m\text{In}_{3n+2m}$ ($\text{M} = \text{Co}, \text{Ir}$ and Rh). This belongs to the tetragonal layer type materials derived from the 'infinite layer' parent compound CeIn_3 by stacking n 'CeIn₃' and m 'MIn₂' subunits along the tetragonal axis. While CeCoIn_5 and CeIrIn_5 are single layer ($n=1$) HF compounds which are superconducting at ambient pressure [59], CeRhIn_5 is a local moment AF which becomes SC only under pressure. Likewise in the bilayer ($n=2$) compounds SC appears both at ambient pressure for Ce_2CoIn_8 and Ce_2IrIn_8 and at finite pressure for Ce_2RhIn_8 . Especially CeCoIn_5 has turned out to be of great interest. Its comparatively large T_c has allowed to determine the d-wave symmetry of the SC gap function by field-angle resolved magnetothermal conductivity [60] and specific heat [61] measurements. High-field specific heat [62] and ultrasonic attenuation measurements [63] have indicated that firstly the SC transition evolves to first order at larger fields, and secondly evidence for the long-sought FFLO phase with SC pairing at finite momentum exists. As in the Ce122 class SC appears preferably in the vicinity of magnetic QCPs and the corresponding AF/SC phase diagrams have been determined in pressure experiments. Likewise NFL phenomena above the AF QCP have been observed.

Another exotic HF Ce- superconductor, CePt_3Si has now been discovered which is the first

Figure 4: Left: Tetragonal unit cells of the ThCr_2Si_2 and CeM_2X_2 (Ce122) structure where $\text{M} = \text{Cu, Ni, Ru, Rh, Pd, Au, ...}$ (black circles); $\text{X} = \text{Si, Ge}$ (small grey circles) and Ce (large grey circles). Right: Conventional unit cell of the CeMIn_5 (Ce115) structure with $\text{M} = \text{Co, Ir, Rh}$ (black circles); In (small grey circles) and Ce (large grey circles).



with a non-centrosymmetric structure [64]. Superconductivity in crystals without inversion center was discussed theoretically first in [65]. The lack of inversion symmetry raises fundamental questions of classification of the SC states according to odd and even parity [66]. It remains to be seen whether this compound is the first member of a new class of HF SC.

3.1 QUANTUM CRITICAL BEHAVIOUR AND SUPERCONDUCTIVITY IN CeCu_2Si_2 AND THE ALLOY SERIES $\text{CeCu}_2(\text{Si}_{1-x}\text{Ge}_x)_2$

The first Ce- based HF metal and superconductor [54] has for a considerable time served as a most fruitful model for investigating strongly correlated electron systems. Until rather recently it was also the only HF Ce compound exhibiting superconductivity. Most importantly in CeCu_2Si_2 Si can be continuously substituted by Ge while the compound changes from a HF superconductor to a normal antiferromagnet [56]. The Ge substitution acts like a negative chemical pressure, likewise fully substituted CeCu_2Ge_2 under positive hydrostatic pressure behaves similar as CeCu_2Si_2 under ambient pressure. Ge- substitution and application of hydrostatic pressure therefore allows to vary the coexistence and competition behaviour of superconducting and other order parameters in the alloy series $\text{CeCu}_2(\text{Si}_{1-x}\text{Ge}_x)_2$.

Indeed already stoichiometric CeCu_2Si_2 at ambient pressure shows an additional 'A-phase' which envelops SC in the B-T phase diagram [67] (fig. 5). When T_c and T_A are close they do not coexist and the A-phase is expelled from the SC region of the B-T plane. Ge-substitution or suitable deficit of Cu however stabilises the A-phase ($T_A > T_c$) and coexistence of both phases results. Hydrostatic pressure and Cu excess on the other hand reduces T_A to zero at the quantum critical point (QCP). Even after single crystals became available [68] the nature of the A-phase has remained mysterious. Later, neutron diffraction on weakly Ge- substituted $\text{CeCu}_2(\text{Si}_{1-x}\text{Ge}_x)_2$ samples have shown that the magnetic order observed in the stoichiometric CeCu_2Ge_2 compound is still present, although with continuously decreasing moment [69]. The slightly incommensurate (IC) modulation vector did not change very much as function of x (Ge concentration). Finally IC magnetic order with $\mathbf{Q} = (0.215, 0.215, 0.530)$ (r.l.u) has been found in the stoichiometric compound CeCu_2Si_2 by neutron diffraction [55], which identified the A-phase as a conventional IC-SDW phase with rather low moment $\sim 0.1 \mu_B$ per Ce

| | γ [mJ/molK ²] | T_N [K] | μ [μ_B] | $T_c(p=0)$ [K] | $T_c^m(p_m)$ [K] |
|-----------------------------------|----------------------------------|-----------|-------------------|----------------|------------------|
| CeCu ₂ Si ₂ | 700 | 0.8 | 0.10 | 0.7 | 2.3 (3 GPa) |
| CeCu ₂ Ge ₂ | 1200 ⁽¹⁾ | 4.3 | 1.05 | - | 1.7 (16 GPa) |
| CeNi ₂ Ge ₂ | 350 | - | - | - | 0.4 (2.2 GPa) |

Table 1: Material parameters of Ce- based HF superconductors. ⁽¹⁾ Value extrapolated to $T = 0$ by fitting the $S=1/2$ Bethe ansatz result to data for $T > T_N$ using $T^* = 6K$.

site (fig. 6). The ordering wave vector nicely agrees with the nesting wave vector of heavy FS sheets in CeCu₂Si₂ found by Zwicknagl et al. [20, 55]. It is clear now that the A-phase of CeCu₂Si₂ evolves continuously from the magnetic phase of CeCu₂Ge₂, when x is reduced from $x = 1$ progressively. Taken together the pressure and Ge- substitution dependences at first sight do not support the idea that SC appears around the QCP of the A-phase because the $T_c(x,p)$ curve (full dots in fig. 7) lacks the typical 'dome shape'. Specifically $T_c(p)$ strongly increases for increasing hydrostatic pressure p [57] and reaches its maximum far away from the QCP (fig. 7). This feature is very different from the conventional SC/AF QCP phase diagram which applies for other Ce- based HF superconductors like CePd₂Si₂ and CeRh₂Si₂ (fig. 16). However it is now clear [58] that this anomalous high pressure maximum in T_c is due to the presence of an additional high pressure QCP associated with an only weakly first order valence phase transition of Ce which does not break any symmetry [70]. The charge fluctuations associated with the valence transition have been proposed to mediate the SC pairing around the high pressure maximum [71] which is distinct from both spin fluctuation and magnetic exciton mechanism invoked for other Ce- and U-HF compounds respectively. The appropriate dome shape of two separated QCPs has been revealed by using simultaneous tuning with Ge-substitution and hydrostatic pressure. The latter compensates the effect of the former, but the mean free path is decreased which destabilises the unconventional SC order parameter and reduces its T_c . In this way the large stability region of stoichiometric CeCu₂Si₂ may be broken into the two domes associated with the magnetic and valence transition QCPs (fig.7). It seems now that CeCu₂Si₂ and substitutes also fit into the generic QCP scenario of Ce-HF superconductors albeit with the surprise of an additional qualitatively new QCP.

3.1.1 QUANTUM CRITICAL POINTS AND THE B-T PHASE DIAGRAM

Like the other Ce122 compounds the CeCu₂(Si_{1-x}Ge_x)₂ series crystallises in the tetragonal body centered ThCr₂Si₂ structure (fig. 4). The stability of A and SC phases is extremely sensitive to the stoichiometry of the constituent elements. The homogeneity range of CeCu₂Si₂ in the ternary chemical Ce-Cu-Si phase diagram is quite limited and comprises three regions where either A or SC alone are present or A/SC coexist [72]. This agrees with the observation that in the combined Ge- doping and pressure phase diagram shown in (fig. 5) the crossing of T_c and T_A curves is located around the stoichiometric case at ambient pressure. Around the first low pressure magnetic QCP where $T_A \rightarrow 0$ NFL behaviour with $\Delta\rho(T) \sim T^{3/2}$ and $\gamma(T) = \gamma_0 - \alpha T^{1/2}$ was observed for moderately low temperatures and moderately high fields [75]. This low temperature phase diagram which has been composed of different transport and susceptibility mea-

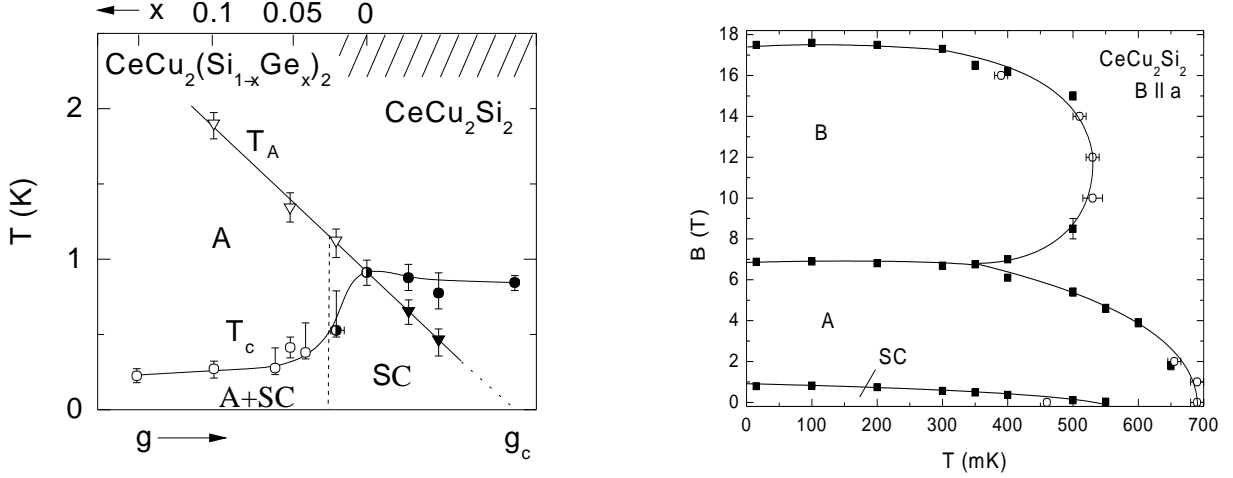
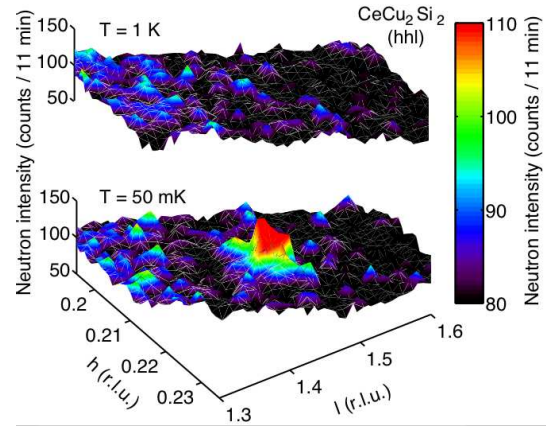


Figure 5: Left panel: Coexistence/competition phase diagram of SC and magnetic A phases close to the magnetic QCP1. Phase boundaries are obtained from susceptibility and resistivity measurements and composed of alloying (negative pressure) and hydrostatic pressure results, separated by a dashed line. Here $g \sim 1-x$ on the left and $g \sim p$ on the right [72] (c.f. theoretical results in fig. 10). Right panel: B-T phase diagram of CeCu_2Si_2 for $B \parallel a$. Original version in [73], completed version from [74]. For this sample the A-phase is expelled from the SC region (no coexistence).

measurements already shows that T_c saturates in a plateau after the T_A -crossing instead of forming the canonical QCP dome shape. Indeed on increasing pressure even further T_c increases steeply reaching a maximum around 3 GPa [76] to 4 GPa [57] (fig. 7). The delicate competition and coexistence behaviour for stoichiometric single crystals of CeCu_2Si_2 has already been obvious from earlier investigations on the B-T phase diagram obtained with ultrasonic methods and dilatometry [73, 74] which is shown in fig. 5 (right panel). For this sample $T_c \leq T_A$ and A/SC phases do not coexist. The expulsion of the A-phase from the SC region in fig. 5 can be clearly seen from sound velocity anomalies across the A and SC phase boundaries. The still poorly understood B phase might be another SDW phase with different propagation vector \mathbf{Q} and/or SDW moment polarisation.

Figure 6: Neutron diffraction intensity in reciprocal (hhl) plane in CeCu_2Si_2 at temperatures above and below the A-phase transition temperature T_A . The magnetic peak appears at $(0.215, 0.215, 1.470)$ corresponding to an incommensurate SDW modulation vector $\mathbf{Q} = (0.215, 0.215, 0.530)$ [55].



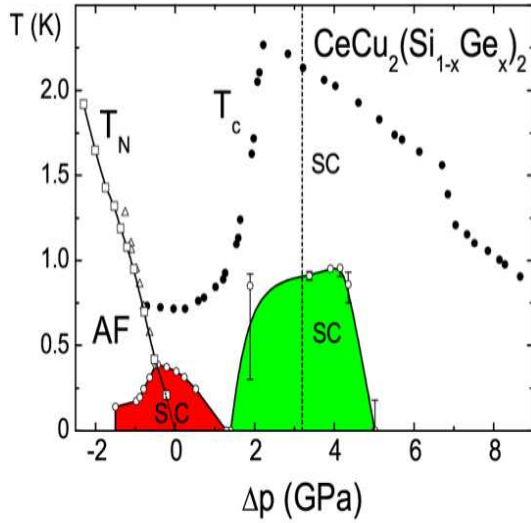


Figure 7: p - T phase diagram of $\text{CeCu}_2(\text{Si}_{1-x}\text{Ge}_x)_2$ composed from pressure (p) dependence and Ge-doping (x) dependence of $\rho(T)$, $C(T)$ and $\chi(T)$. For different substitution level x , the pressure is shifted by the value of its corresponding critical pressure $p_{c1}(x)$ for the magnetic QCP1 ($\Delta p = p - p_{c1}(x)$). Two SC domes are associated with QCP1(p_{c1}) (left dome) of the A- phase and QCP2(p_{c2}) of the integer valence (Kondo) phase (right dome) [58]. The dashed line indicates the valence transition in CeCu_2Ge_2 and T_c (dots [76]) corresponds to stoichiometric CeCu_2Si_2 .

To unravel the puzzling anomalous stability of T_c at high pressure systematic studies with slightly Ge doped single crystal CeCu_2Si_2 were performed [58]. It has been long suspected that the anomalous $T_c(p)$ behaviour is associated with the presence of a second QCP connected with a Ce-valence transition [70]. To support this scenario one has to prove that the region around $T_c \simeq T_A$ and around the maximum T_c correspond to distinct SC phases. This is achieved by the following strategy [58]: i) Due to larger Ge ionic radius slight Ge doping corresponds to application of internal negative pressure which may be compensated again by application of external positive pressure, returning to zero effective pressure. ii) Because the electronic mean free path has decreased due to scattering from Ge impurities, the condensation energy and hence T_c of the anisotropic SC phase will be decreased, destabilising SC. In this way the continuous SC region of stoichiometric CeCu_2Si_2 indeed breaks up into two separate SC domes as shown in fig. 7. The first one centered at $p_{c1}(x)$ is the magnetic QCP associated with the A-phase and its critical line $T_N(\Delta p)$, the second QCP at $p_{c2}(x)$ is supposed to describe the $\text{Ce}^{3+}/\text{Ce}^{4+}$ valence transition where the 4f electron of Ce^{3+} becomes delocalised. This transition does not break any symmetry and therefore its critical line $T_V(\Delta p)$ (not shown in fig. 7) is assumed to end in a critical endpoint. The critical line and its endpoint, however, have so far not been confirmed for these doped $\text{CeCu}_2(\text{Si}_{1-x}\text{Ge}_x)_2$ systems by independent methods. However for pure CeCu_2Ge_2 a weak, symmetry-conserving valence transition was observed via x-ray diffractometry [77] near $p \simeq 15$ GPa, where also $T_c(p)$ assumes its maximum value [57]. Certainly a large volume collapse signifying the 4f delocalisation as in the $\alpha - \gamma$ Ce transition would not be compatible with the presence of the SC phase around $p_{c2}(x)$.

3.1.2 THE A-PHASE AND ELECTRONIC STRUCTURE OF CeCu_2Si_2

The incommensurate magnetic order of the A-phase suggests a SDW origin associated with the itinerant heavy electron FS in CeCu_2Si_2 . To support this conjecture the static magnetic

susceptibility $\chi(\mathbf{q})$ has to be calculated within the context of renormalised band theory [20]. In this approach (sect. 2) resonant phase shifts $\eta_{\hat{f}m}$ for the 4f-states are introduced empirically into the LDA scheme to generate the heavy bands at the Fermi level while charge neutrality and proper f-count are preserved. For the three CEF split Kramers doublets of Ce^{3+} ($J=\frac{5}{2}$) the ansatz for the phase shift is

$$\eta_{\hat{f}m}(\varepsilon) = \tan^{-1} \frac{\Gamma_{\hat{f}}}{\varepsilon - \varepsilon_{\hat{f}m}} \quad \varepsilon_{\hat{f}m} = \varepsilon_{\hat{f}} + \Delta_m \quad (17)$$

Here $\varepsilon_{\hat{f}m}$ defines the centers of heavy bands with $\varepsilon_{\hat{f}}$ denoting the renormalised 4f- level and Δ_m the energies of the three Kramers doublets taken from neutron scattering. The resonance width $\hat{\Gamma}_f$ is an empirical parameter which determines the width kT^* or mass m^* of the heavy electron band. It is adjusted to reproduce the proper experimental value of $\gamma = C/T$. The main heavy electron sheet obtained in [19] is shown in fig. 8. It consists of stacked columns along c . Obviously there are large flat parts on the columns with a nesting vector \mathbf{Q} as indicated. Indeed this leads to a pronounced maximum of $\chi(\mathbf{q})$ at $\mathbf{q} = \mathbf{Q}$ as shown in the contour plot of fig. 8. The experimental IC ordering vector of the A-phase (fig. 6) agrees well with the maximum position of $\chi(\mathbf{q})$ giving credence to the SDW picture for the A phase.

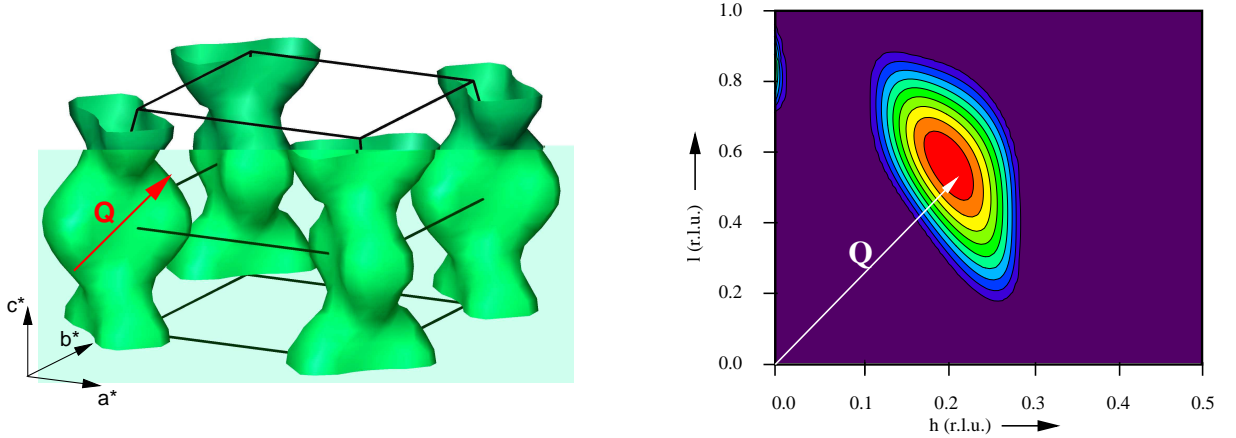


Figure 8: Left panel: Main heavy FS sheet in CeCu_2Si_2 where columnar nesting with wave vector \mathbf{Q} is indicated. Parameters for renormalised band calculations are: $T^* \sim 10$ K and $\Delta_{\text{CEF}} = 330$ K overall CEF splitting. Right panel: Comparison of experimental propagation vector (fig. 6) and contour map of theoretical $\chi(\mathbf{q})$ in (hhl) plane [55].

3.1.3 THE HIGH PRESSURE MIXED VALENT PHASE TRANSITION

The present experimental evidence for the second QCP at high pressure connected with Ce-valence change was described in [70]. A valence transition does not break any spatial symmetry but charge fluctuations and volume strain are strongly coupled which commonly leads to a first order valence transition as in the famed γ - α transition of Ce. No such volume change has been found at p_{c2} of CeCu_2Si_2 making it a rather exceptional case. On the other hand this feature may provide a link to superconductivity as discussed in the next section. The only direct evidence for

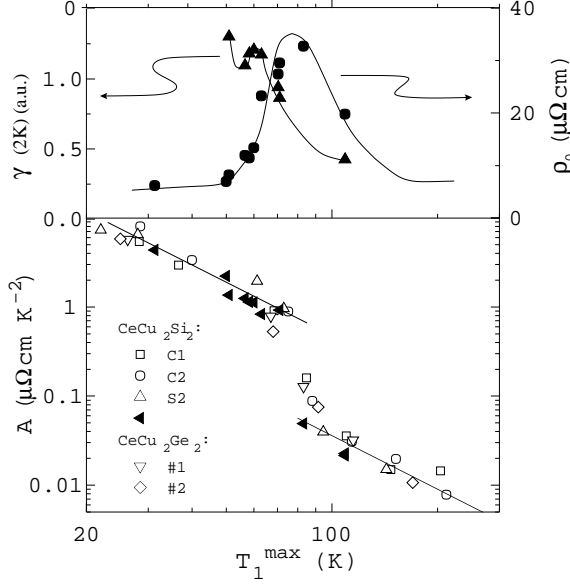


Figure 9: Behaviour of γ -coefficient, residual resistivity ρ_0 and A-coefficient in $\rho(T) = \rho_0 + AT^2$ against $T_1^{\max} \sim T^*$ which scales monotonously with pressure [70].

a small valence change was obtained earlier in L_{III} - x-ray absorption experiments [78]. There is however considerable indirect support for the valence change. The gradual delocalisation of the $4f^1$ - electron under pressure leads to a less strongly correlated electron state, i.e. the effective mass will be reduced according to

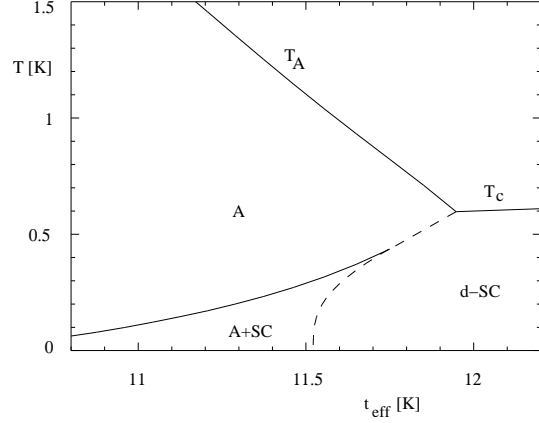
$$\frac{m^*}{m} = \frac{1 - n_f/2}{1 - n_f} \quad (18)$$

when the f-level occupation n_f is reduced significantly below its value in the Kondo limit $n_f \leq 1$. The linear specific heat coefficient $\gamma = C(T)/T$ should reflect this decrease. Likewise the Kadowaki-Woods ratio A/γ^2 should decrease across the valence transition [70]. If it is not of first order, critical valence fluctuations should also lead to a strong increase in the residual resistivity around the transition. These expected fundamental features of a valence transition are indeed present in $CeCu_2Si_2$ as shown in fig. 9. Theoretical models for the present case of a rapid but continuous valence transition under pressure are based on the extended periodic Anderson model (PAM) including a Coulomb repulsion U_{fc} between conduction and f- electrons, in addition to the on-site U_{ff} Coulomb term in the common PAM. Within the more simple impurity model this term has the tendency to decrease the f-occupation and when the energy of the $4f^1$ state, $\epsilon_f + U_{fc}$ approaches ϵ_F , i.e. the energy of the $4f^0$ hole state, n_f is rapidly reduced to values much less than one (fig. 11). External pressure is thought to tune primarily U_{fc} which is an inter-site Coulomb integral and thus cause the valence transitions. For the lattice model the valence change as function of U_{fc} has been calculated within slave boson fluctuation approximation [71].

3.1.4 UNCONVENTIONAL SUPERCONDUCTIVITY AND THE TWO QCP'S

The breakup of the SC region into two independent domes in fig. 7 allows one to speculate that the SC pairing mechanism at each QCP involves exchange of fluctuations of the associated order parameters, magnetic (A-phase transition) or charge fluctuations (valence transition)

Figure 10: Theoretical phase diagram for A and d_{xy} -SC order from a two band model. Full and dashed line correspond to second and first order transitions. A+SC is the coexistence region. The effective tight binding hopping integral t_{eff} scales with p or $1-x$ (c.f. experimental results in fig. 5) [72]



respectively. This may possibly imply a different type of superconducting gap symmetry, although not much is known about the SC state in both regimes, especially for the high pressure SC region. In the magnetic QCP regime Cu NQR experiments under pressure for polycrystalline $\text{CeCu}_2(\text{Si}_{1-x}\text{Ge}_x)_2$ [79] and under ambient pressure for Cu and Ce off-stoichiometric polycrystalline samples [80] show i) $1/T_1 \sim T^3$ behaviour indicating a SC state with gap nodes and ii) the presence of soft magnetic fluctuations close to a pressure or doping regime where the SC is stabilised. This suggests that the magnetic QCP scenario for unconventional HF-SC in CeCu_2Si_2 may be correct. Further knowledge about the nature of the SC gap function can only come from field-angle resolved pure single crystal investigations, e.g. $C(\mathbf{H}, T)$ measurements at very low temperatures.

Model for SC at the magnetic A- phase QCP:

A 2D two-band model for SDW-SC states in $\text{CeCu}_2(\text{Si}_{1-x}\text{Ge}_x)_2$ has been studied in some detail [72]. The microscopic origin of the pair potential is not specified in the BCS type model. A tight binding (TB) band centered at the $\Gamma(0,0)$ point and with $\mathbf{Q} = (\frac{1}{2}, \frac{1}{2})$ nesting feature represents a simplified version of the FS columns in fig. 8 whose nesting properties are known to be responsible for the SDW A-phase. In addition spherical electron pockets which represent the remaining FS sheets of CeCu_2Si_2 are included. The former carries both SDW and SC order parameters, the latter only SC. Therefore a d_{xy} SC state is favored. The A/SC competition-coexistence phase diagram resulting from the coupled gap equations is shown in fig. 10. There t_{eff} is the hopping element of the TB band which is thought to scale linearly with the control parameter g which is $1-x$ ($x = \text{Ge doping}$) or the pressure p . The comparison of the theoretical (fig. 10) and experimental phase diagram (fig. 5) shows a striking resemblance. In this model the tail of the coexistence A+SC regime is stabilised by the SC pairing on the spherical FS sheets. A more elaborate discussion of this issue using the real FS of CeCu_2Si_2 is given in sect. 3.1.6.

Model for SC at the valence transition QCP:

A more microscopic model for the SC mechanism around the high pressure valence transition has been proposed in [71]. The extended PAM mentioned above leads to an electron pairing mainly via the exchange of $c \leftrightarrow f$ charge fluctuations with small wavelength. In weak coupling approximation a d-wave state is found to be stabilised in the regime where appreciable charge

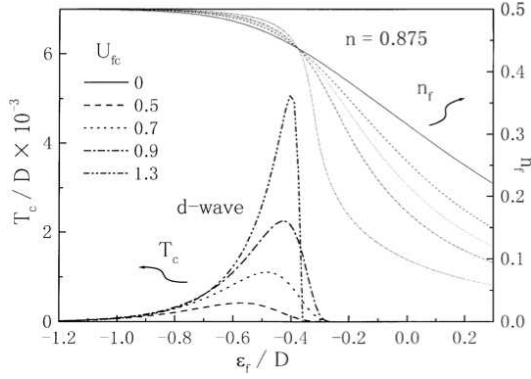


Figure 11: Valence (n_f) transition in the extended (impurity) Anderson model as function of the f-level position ϵ_f (D = conduction band width, $\epsilon_F \equiv 0$). Associated T_c dependence of d-wave SC is also shown. [71]

fluctuations, controlled by the pressure dependent U_{fc} - parameter, set in but the quasiparticle DOS (the mass enhancement) is still sizable. The maximum in T_c scales with the steepness of the continuous valence transition as seen in fig. 11. This does not incorporate realistic FS features but assumes a single spherical conduction band. Also the real change in n_f across the valence transition will certainly be much less than in the theoretical model (fig. 11). Therefore it should be taken as an illustration of the mechanism and not literally as explanation for high pressure SC in $\text{CeCu}_2(\text{Si}_{1-x}\text{Ge}_x)_2$.

3.1.5 NON-FERMI LIQUID STATE AND QUANTUM CRITICAL BEHAVIOUR

Above the SC domes the two QCP's in $\text{CeCu}_2(\text{Si}_{1-x}\text{Ge}_x)_2$ lead to pronounced NFL anomalies in thermodynamic and transport properties. Naturally one would invoke here the quasiparticle scattering from low energy fluctuations of the associated order parameters [49] as one possible mechanism behind NFL behaviour. For the A-phase QCP a detailed comparison of experimentally observed T,B-scaling laws for $\rho(T) = \rho_0 + \Delta\rho(T)$, $\chi(T)$ and $\gamma(T)$ for single crystal CeCu_2Si_2 and polycrystalline samples of various Ge-dopings has been performed [75, 81]. It was found that for samples slightly above $T_A(x) = 0$ the expected NFL scaling laws at a 3D AF QCP

$$\Delta\rho(T) = \beta T^{\frac{3}{2}} \quad \gamma(T) = \gamma_0 - \alpha T^{\frac{1}{2}} \quad (19)$$

are indeed well fulfilled. However there are also distinct deviations, notably the high-field behaviour of $\Delta\rho(T)$ where a crossover of the resistivity exponent from 3/2 to the FL exponent 2 is observed. In contrast $\gamma(T)$ remains qualitatively unchanged [75] at moderately low T and exhibits an upturn at the lowest temperatures which is not yet understood. Such disparities in the scaling of $\Delta\rho(T)$ and $\gamma(T)$ are now also known from other NFL systems and proposals how to account for them have been made [75]. The study of NFL behaviour at the high pressure valence transition QCP on the other hand is still in its beginning. The NFL behaviour in $\Delta\rho(T)$ above the two distinct SC domes of fig. 7 is illustrated in fig. 12.

3.1.6 COEXISTENCE OF SUPERCONDUCTIVITY AND A-PHASE IN CeCu_2Si_2

The central goal in this section is to study the competition-coexistence phase diagram within a more realistic model than above. We start from the real FS sheets of CeCu_2Si_2 as obtained

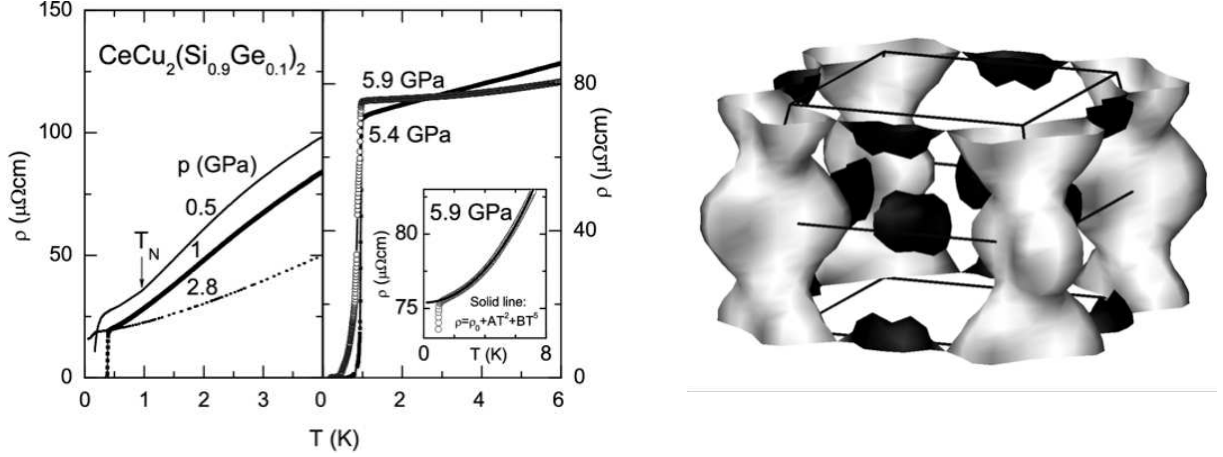


Figure 12: Left panel: NFL behaviour of $\Delta\rho(T)$ in $\text{CeCu}_2(\text{Si}_{1-x}\text{Ge}_x)_2$ close to QCP1 (left) and QCP2 (right) [58]. Right panel: Variation of the SC gap function amplitude $|\Delta(\mathbf{k})|/|\Delta_0(T)| = |\phi_{\Gamma_3}(\mathbf{k})|$ for the (pseudo-) singlet wave function with Γ_3 -symmetry $\phi_{\Gamma_3}(\mathbf{k}) \sim \cos k_x a - \cos k_y a$ on the main sheet of the paramagnetic FS [82, 83]. The amplitude of this SC order parameter is maximal on the kidney-shaped surfaces centered along the Σ -direction which are (almost) unaffected by the formation of the A-phase (dark grey). The dominant contributions to the latter come from the nesting parts on the heavy columns where the superconducting amplitude is small (light gray).

by renormalised band structure calculations. The FS nesting properties determine the observed magnetic structure. Of particular interest are the superconducting states which can either coexist with the A-phase or expel it. The model Hamiltonian is given by

$$H = \sum_{\mathbf{k}s} \epsilon_{\mathbf{k}} c_{\mathbf{k}s}^\dagger c_{\mathbf{k}s} + H_{int} \quad (20)$$

where the first term describes heavy quasiparticles and H_{int} their residual interactions. The creation (annihilation) operators are for quasiparticles with wavevector \mathbf{k} , (pseudo) spins $s = \uparrow, \downarrow$ and energy $\epsilon_{\mathbf{k}}$ are denoted by $c_{\mathbf{k}s}^\dagger (c_{\mathbf{k}s})$. The energies which are measured relative to the Fermi level are calculated within the renormalised band scheme. The residual interactions in the strongly renormalised Fermi liquid is assumed to be repulsive for short separations while being attractive for two quasiparticles of opposite momenta on neighboring sites. The former favors the formation of a SDW while the latter gives rise to the superconducting instability. Within mean-field approximation one has $H_{int} = H_{SDW} + H_{SC}$ where

$$H_{SDW} = - \sum_{\mathbf{k}s} s \frac{1}{2} \sum_{\mathbf{Q}_j} [h(\mathbf{Q}_j) c_{\mathbf{k}s}^\dagger c_{\mathbf{k}+\mathbf{Q}_j s} + h.c.] \quad (21)$$

$$H_{SC} = \frac{1}{2} \sum_{\mathbf{k}ss'} [\Delta_{ss'}(\mathbf{k}) c_{\mathbf{k}s}^\dagger c_{-\mathbf{k}s'}^\dagger + h.c.] \quad (22)$$

The periodically modulated magnetisation $h(\mathbf{Q}_j)$ associated with the eight equivalent SDW propagation vectors \mathbf{Q}_j defined below as well as the superconducting pair potential Δ have to

be determined selfconsistently

$$h(\mathbf{Q}_j) = \frac{U}{L} \sum_{\mathbf{k}_s} \frac{s}{2} \left\langle c_{\mathbf{k}+\mathbf{Q}_j s}^\dagger c_{\mathbf{k}_s} \right\rangle \quad (23)$$

$$\Delta_{ss'}(\mathbf{k}) = \frac{1}{L} \sum g_{ss';s''s'''}(\mathbf{k}, \mathbf{k}') \left\langle c_{-\mathbf{k}' s''} c_{\mathbf{k}' s'''} \right\rangle \quad (24)$$

where the strength U of the local Hubbard-type repulsion is of the order of the quasiparticle band width $k_B T^*$ and $g_{ss';s''s'''}(\mathbf{k}, \mathbf{k}')$ is the effective pair attraction. The \mathbf{k} -summation runs over the entire paramagnetic Brillouin zone and L denotes the number of lattice sites. The expectation values denoted by $\langle \dots \rangle$ have to be evaluated with the eigenstates of the total mean-field Hamiltonian $H_{MF} = H_0 + H_{SDW} + H_{SC}$, and, consequently, depend upon the order parameters. The selfconsistency equations are therefore coupled. The mean-field Hamiltonian implicitly assumes that the amplitudes of both order parameters are small. In particular, we neglect here the pairing amplitudes of the form $\langle c_{-\mathbf{k} s''} c_{\mathbf{k}+\mathbf{Q}_j s'''} \rangle$. The latter are important when the gaps introduced by the antiferromagnetic order into the quasiparticle spectrum are large on the scale set by superconductivity. For a discussion of this point we refer to [84, 85]. The periodically modulated magnetisation associated with the SDW acts on the conduction electrons like a periodic spin-dependent potential which we approximate by

$$h(\mathbf{x}) = \sum_{\mathbf{Q}_j} h(\mathbf{Q}_j) e^{i\mathbf{Q}_j \cdot \mathbf{x}} \quad (25)$$

with identical amplitudes $h(\mathbf{Q}_j) = h_0$ for the eight commensurate wave vectors $\mathbf{Q}_j \in \{(\pm \frac{\pi}{2a}, \pm \frac{\pi}{2a}, \pm \frac{\pi}{c})\}$ which are used for a commensurate approximation to the experimentally found IC SDW. The magnetic superstructure breaks the translational invariance of the underlying lattice but it conserves the point group symmetry. However the mean-field Hamiltonian is invariant under translations with the lattice vectors

$$\mathbf{a}'_1 = (2a, 2a, 0); \quad \mathbf{a}'_2 = (2a, -2a, 0); \quad \mathbf{a}'_3 = (2a, 0, c) \quad (26)$$

The volume of the magnetic supercell is 32 times the volume of the paramagnetic unit cell. As a result, the Brillouin zone is reduced and the quasiparticle states are modified by extra Bragg planes. The opening of new gaps is important at sufficiently low temperatures $T \ll T_A$ where T_A is the SDW transition temperature.

Before proceeding with the SC/SDW coexistence analysis of CeCu_2Si_2 we have to give a brief description of the symmetry classification of unconventional SC gap functions. The fundamental property of $\Delta_{ss'}(\mathbf{k})$ is its behaviour as a two-fermion wave function in many respects. This expresses the fact that an ODLRO order parameter is not the thermal expectation value of a physical observable but rather a complex pseudo-wave function describing quantum phase correlations on the macroscopic scale of the SC coherence length. Its phase is a direct signature of the broken gauge invariance in the SC condensate. The Pauli principle requires $\Delta_{ss'}(\mathbf{k})$ to be antisymmetric under the interchange of particles

$$\Delta_{ss'}(\mathbf{k}) = -\Delta_{s's}(-\mathbf{k}) \quad (27)$$

In addition, it transforms like a two-fermion wave function under rotations in position and spin space and under gauge transformations. The transformation properties yield a general classification scheme for the superconducting order parameter which is represented by a 2×2 -matrix in (pseudo-) spin space. It can be decomposed into an antisymmetric (s) and a symmetric (t) contribution according to $\mathbf{m}\Delta(\mathbf{k}) = \mathbf{m}\Delta_s(\mathbf{k}) + \mathbf{m}\Delta_t(\mathbf{k})$ with

$$\mathbf{m}\Delta_s(\mathbf{k}) = \phi(\mathbf{k})i\mathbf{m}\sigma_2 \quad \mathbf{m}\Delta_t(\mathbf{k}) = \sum_{\mu=1}^3 d_\mu(\mathbf{k})\mathbf{m}\sigma_\mu i\mathbf{m}\sigma_2 \quad (28)$$

where $\mathbf{m}\sigma_\mu$ denote the Pauli matrices. Antisymmetry $\mathbf{m}\Delta(\mathbf{k}) = -\mathbf{m}\Delta^T(-\mathbf{k})$ requires

$$\phi(\mathbf{k}) = \phi(-\mathbf{k}) \quad \text{and} \quad d_\mu(\mathbf{k}) = -d_\mu(-\mathbf{k}) \quad (29)$$

for the complex orbital functions $\phi(\mathbf{k})$ and $d_\mu(\mathbf{k})$ ($\mu = 1-3$). For brevity we will frequently write $\Delta(\mathbf{k})$ for $\phi(\mathbf{k})$ or $|\mathbf{d}(\mathbf{k})|$.

The order parameter can be chosen either as purely antisymmetric ($\mathbf{m}\Delta_s$) or purely symmetric ($\mathbf{m}\Delta_t$) when spin-orbit interaction can be neglected. In the 4f- and 5f- based heavy fermion superconductors spin-orbit interaction is strong. As a consequence classification according to physical pair spins cannot be used. If their high-temperature crystal structures, however, have an inversion center classification according to parity is still possible as is the case in CeCu_2Si_2 .

The general classification scheme for superconducting order parameters proceeds from the behavior under the transformations of the symmetry group \mathcal{G} of the Hamiltonian. It consists of the crystal point group G , the spin rotation group $\text{SU}(2)$, the time-reversal symmetry group \mathcal{K} , and the gauge group $\text{U}(1)$. The appropriate choice of rotations corresponding to weak or strong spin-orbit coupling case is determined by microscopic considerations. Using the above transformation properties the singlet and triplet gap functions $\phi(\mathbf{k})$ and $\mathbf{d}(\mathbf{k})$ respectively may further be decomposed into basis functions $\phi_\Gamma^n(\mathbf{k})$ or $\mathbf{d}_\Gamma^n(\mathbf{k})$ of the irreducible representations Γ (degeneracy index n) of $G \times \text{SU}(2)$ (weak s.o. coupling) or G (strong s.o. coupling). In the latter case the pseudo spin associated with Kramers degeneracy replaces the physical conduction electron spin.

The occurrence of long-range order at a phase transition described by an order parameter is most frequently associated with spontaneous symmetry breaking. The simplest superconductors where only gauge symmetry is broken are called *conventional*. In this case the SC order parameter has the same spatial symmetry as the underlying crystal, i.e. it transforms as a fully symmetric even parity singlet Γ_1 representation of G . It should be noted, however, that conventional is not a synonym for isotropic, for any G one can form Γ_1 representations from angular momentum orbitals of higher order l , for example $l \geq 2$ for tetragonal and hexagonal symmetry and $l \geq 4$ for cubic symmetry. On the other hand, a superconductor with additional broken symmetries besides gauge symmetry is called *unconventional*. It can have either parity. A recent summary is found in the monography [7].

NMR experiments [79, 80] in slightly Ge-doped or Cu-off-stoichiometric samples suggest that the SC gap is unconventional and has line nodes. In our discussion we restrict ourselves to a singlet pair state as revealed by strong Pauli limiting seen in early H_{c2} studies [86]. The singlet state is characterised by a scalar order parameter

$$\Delta(\mathbf{k})_{ss'} = \phi(\mathbf{k})(i\sigma_2)_{ss'} \quad (30)$$

The anisotropic effective pair interaction in the (pseudo-) spin singlet channel can be expanded according to

$$g(\mathbf{k}s, -\mathbf{k}s'; -\mathbf{k}'s'', \mathbf{k}'s''') \rightarrow (i\sigma_2)_{ss'} (i\sigma_2)_{s''s'''} \times \sum_j \frac{1}{2} g(\Gamma^{(j)}) \sum_{\kappa=1}^{d^{(j)}} \phi_{\kappa}^{(j)}(\mathbf{k}) \phi_{\kappa}^{(j)*}(\mathbf{k}') \quad (31)$$

where $\phi_{\kappa}^{(j)}(\mathbf{k})$ is a basis function which belongs to the κ th row, $\kappa = 1, \dots, d^{(j)}$, of the $d^{(j)}$ -dimensional representation $\Gamma^{(j)}$ of the symmetry group. In principle we have to classify the order parameters with respect to the antiferromagnetic lattice. Since the two ordering temperatures are so close we focus on pair states which are compatible with the translational symmetry of the paramagnetic lattice. The corresponding basis functions are listed in [5, 19, 87, 88]. In the explicit calculations, we restrict ourselves to one-dimensional representations for simplicity. The generalisation to multi-dimensional representations is rather straightforward [82].

We further simplify the problem by focussing on the symmetry Γ which yields the strongest quasiparticle attraction g_{Γ} . Assuming that this most stable order parameter is non-degenerate yields the separable interaction kernel

$$g(\mathbf{k}s, -\mathbf{k}s'; -\mathbf{k}'s'', \mathbf{k}'s''') \rightarrow (i\sigma_2)_{ss'} (i\sigma_2)_{s''s'''} \frac{g_{\Gamma}}{2} \phi_{\Gamma}(\mathbf{k}) \phi_{\Gamma}^*(\mathbf{k}') \quad (32)$$

and the selfconsistency condition

$$\Delta(\mathbf{k}) = -g_{\Gamma} \phi_{\Gamma}(\mathbf{k}) \frac{1}{L} \sum_{\mathbf{k}'} \phi_{\Gamma}^*(\mathbf{k}') \langle c_{-\mathbf{k}'\downarrow} c_{\mathbf{k}'\uparrow} \rangle \quad (33)$$

We adopt the Nambu formalism to diagonalise the mean-field Hamiltonian in eq. (22) which allows us to reduce it to single-particle form:

$$H = \sum_{\mathbf{k}}^{AFBZ} \Psi_{\mathbf{k}}^{\dagger} \{ \mathbf{m}\varepsilon(\mathbf{k}) \hat{\tau}_3 + \mathbf{h}\hat{1} + \mathbf{m}\Delta(\mathbf{k}) \hat{\tau}_1 \} \Psi_{\mathbf{k}} \quad (34)$$

where we explicitly exploited the fact that the (pseudo) spin is conserved. The Nambu spinors $\Psi_{\mathbf{k}}$ have 32 components and are defined as

$$\Psi_{\mathbf{k}} = \left(c_{\mathbf{k}\uparrow}, c_{\mathbf{k}+\mathbf{Q}_1\uparrow}, \dots, c_{-\mathbf{k}\downarrow}^{\dagger}, c_{-\mathbf{k}-\mathbf{Q}_1\downarrow}^{\dagger}, \dots \right) \quad (35)$$

They account for the coherent superposition of particles and holes which is the characteristic feature of the superconducting state. Here $\hat{1}$, $\hat{\tau}_1$ and $\hat{\tau}_3$ denote the unit matrix and the Pauli matrices in particle-hole space. The 16 wave vectors $\mathbf{Q}_0 = 0, \mathbf{Q}_1, \dots, \mathbf{Q}_{15}$ are the reciprocal lattice vectors appearing in the antiferromagnetic phase. The set includes the eight propagation vectors of the SDW and their harmonics. The \mathbf{k} -summation is restricted to the reduced Brillouin zone (AFBZ) of the antiferromagnetic state defined by the SDW. The structure of the Hamiltonian matrix in particle-hole space is

$$\hat{H} = \begin{pmatrix} \mathbf{m}\varepsilon(\mathbf{k}) + \mathbf{h} & \mathbf{m}\Delta \\ \mathbf{m}\Delta & -\mathbf{m}\varepsilon(\mathbf{k}) + \mathbf{h} \end{pmatrix} \quad (36)$$

where the 16×16 -diagonal matrix contains the quasiparticle energies of the paramagnetic normal phase

$$\mathbf{m}\varepsilon(\mathbf{k})_{\mathbf{Q}_i\mathbf{Q}_j} = \delta_{\mathbf{Q}_i\mathbf{Q}_j}\varepsilon(\mathbf{k} + \mathbf{Q}_i) \quad (37)$$

The magnetic Umklapp scattering associated with the modulated spin density is accounted for by the matrix

$$\mathbf{h} = -h_0(T)\mathbf{m} \quad (38)$$

whose temperature-dependent amplitude $h_0(T)$ has to be determined selfconsistently while \mathbf{m} is a given matrix. The diagonal matrix

$$\mathbf{m}\Delta(\mathbf{k})_{\mathbf{Q}_i\mathbf{Q}_j} = \Delta_0(T)\mathbf{m}\Phi(\mathbf{k})_{\mathbf{Q}_i\mathbf{Q}_j} = \delta_{\mathbf{Q}_i\mathbf{Q}_j}\Delta_0(T)\phi_\Gamma(\mathbf{k} + \mathbf{Q}_i) \quad (39)$$

contains the superconducting order parameters with the given \mathbf{k} -dependent function $\phi_\Gamma(\mathbf{k})$ and a temperature-dependent amplitude $\Delta_0(T)$. The selfconsistency equations in eq. (24) can be formulated in terms of the off-diagonal elements of the 32×32 -matrix Green's function

$$\hat{G}(i\varepsilon_n, \mathbf{k}) = (i\varepsilon_n \hat{1} - \hat{H}(\mathbf{k}))^{-1} \quad (40)$$

according to

$$\begin{aligned} h_0(T) &= \frac{U}{L} T \sum_{i\varepsilon_n} \sum_{\mathbf{k}}^{\varepsilon_c \text{ AFBZ}} \frac{1}{16} \text{Tr} [\mathbf{m} \hat{1} \mathbf{G}(i\varepsilon_n, \mathbf{k})] \\ \Delta_0(T) &= -\frac{g_\Gamma}{L} T \sum_{i\varepsilon_n} \sum_{\mathbf{k}'}^{\varepsilon_c \text{ AFBZ}} \frac{1}{2} \text{Tr} [\mathbf{m} \Phi(\mathbf{k}') \hat{\tau}_1 \hat{\tau}_3 \mathbf{G}(i\varepsilon_n, \mathbf{k}') \hat{\tau}_3] \end{aligned} \quad (41)$$

Here $i\varepsilon_n = \pi T(2n+1)$ denote the T-dependent Matsubara frequencies and ε_c is the energy cut-off required in weak-coupling theory. The coupling constants U and g_Γ as well as the cut-off ε_c are eliminated in the usual way in favor of the decoupled transition temperatures $T_A^{(0)}$ and $T_c^{(0)}$. The temperature dependence of SDW (A-phase) and SC order parameters is shown in the right panel of fig. 13. On entering the SC regime the A-phase is expelled in a finite temperature interval. This is nicely confirmed by recent neutron diffraction results [89] shown in the left panel of the figure.

3.2 THE (ALMOST) IDEAL NFL COMPOUND CeNi_2Ge_2

This is one of the few Ce-HF compounds which neither order magnetically nor become superconducting, except for incipient SC at very low temperatures in very clean samples. Instead it exhibits clear cut NFL anomalies over more than two temperature decades. Together with the recently discovered YbRh_2Si_2 , CeNi_2Ge_2 is one of the rare cases where one is accidentally very close to a QCP at ambient pressure. This is supported further by the x (Pd-concentration) dependence of the Néel temperature in the alloy series $\text{Ce}(\text{Ni}_{1-x}\text{Pd}_x)_2\text{Ge}_2$ [90]. It is found that $T_N(x)$ extrapolates to zero at a very small positive concentration x_c . Thus CeNi_2Ge_2 is (in contrast to YbRh_2Si_2) slightly on the nonmagnetic side of the QCP. After

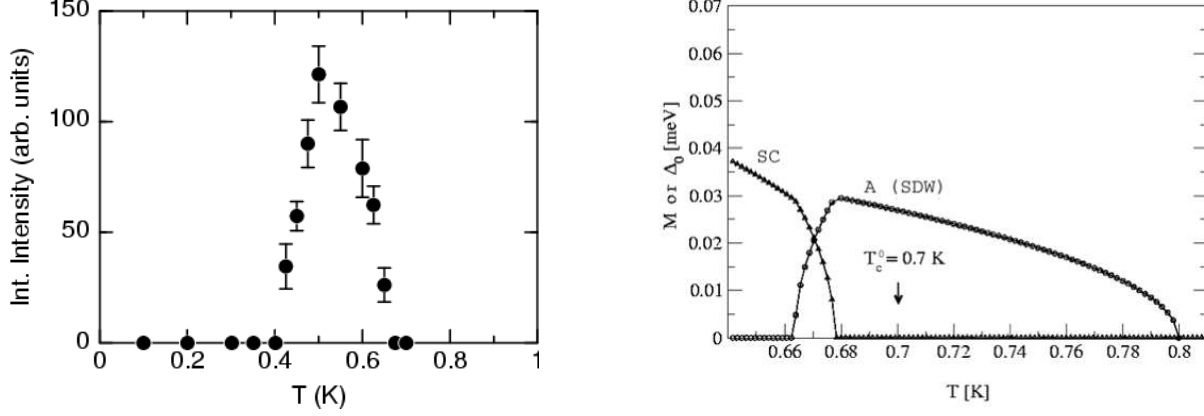


Figure 13: Left panel: Integrated neutron diffraction intensity of the A-phase SDW satellite corresponding to $\mathbf{Q} \simeq (0.215, 0.215, 0.530)$ as a function of temperature. It is proportional to the square of the A-phase order parameter in CeCu_2Si_2 [89]. Right panel: Variation with temperature of the A-phase (SDW) and superconducting order parameters with Γ_3 -symmetry, $\phi_{\Gamma_3}(\mathbf{k}) \sim \cos k_x a - \cos k_y a$ calculated for $T_A^{(0)} = 0.8\text{K} > T_c^{(0)} = 0.7\text{K}$ [82, 83]. For this choice of parameters, the magnetic A-phase initially suppresses the superconducting state which forms at $T_c < T_c^{(0)}$. The two ordering phenomena coexist in a narrow temperature range below T_c . The superconducting correlations, however, suppress the long-range magnetic order which disappears continuously at $T'_A < T_c < T_A^{(0)}$.

some initial doubts [75] it is now accepted [91] that the 3D-SDW QCP scenario analysed in detail in [49] is realised in CeNi_2Ge_2 . This predicts a scaling $\gamma(T) = \gamma_0 - cT^{\frac{1}{2}}$ which is well fulfilled in CeNi_2Ge_2 (fig. 14) down to temperatures around 0.3 K. For even lower temperatures sample dependent upturns in $\gamma(T)$ of unknown origin are present. Likewise the expected NFL resistivity behaviour $\rho(T) = \rho_0 + \beta T^\varepsilon$ with $\varepsilon \geq 1.5$ depending on the sample quality (ρ_0) is found. The very closeness of the AF QCP implies an extreme sensitivity of the scaling to an external field. With increasing field strength one crosses rapidly into a Fermi liquid regime as witnessed by the appearance of a widening plateau in $\gamma(T)$ (fig. 14) and a LFL type resistivity $\rho(T) = \rho_0 + A(B)T^2$. The boundary between the T^ε and T^2 scaling marks the transition from the NFL to the LFL regime (fig. 14). As this boundary is approached from $B > B_c$ the $A(B)$ -coefficient diverges indicating a singular energy dependence of the scattering rate. Thus as the QCP is approached by varying B and T the quasiparticle mass and scattering rates in CeNi_2Ge_2 grow in agreement with the predictions of the 3D SDW scenario for quantum criticality. More recently the NFL behaviour in CeNi_2Ge_2 has also been found in a low temperature divergence of the Grüneisen ratio obtained from thermal expansion as discussed in sect. 2.3.

3.3 SUPERCONDUCTIVITY AND QUANTUM CRITICALITY UNDER PRESSURE IN CePd_2Si_2 AND CeRh_2Si_2

At ambient pressure CeCu_2Si_2 and $\text{CeCu}_2(\text{Si}_{1-x}\text{Ge}_x)_2$ together with CeCoIn_5 and CeIrIn_5 are still the only Ce-based HF superconductors, aside from incipient superconductivity around 100

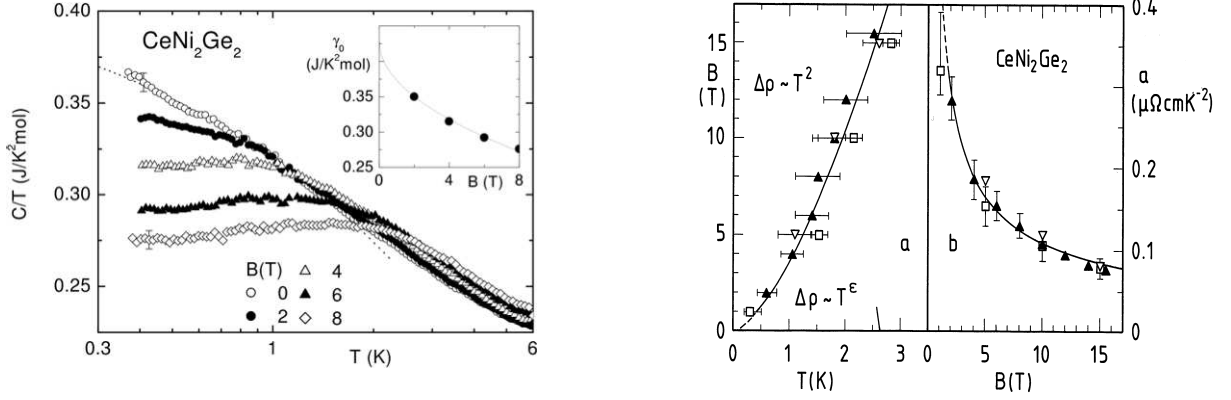


Figure 14: Left panel: Field dependence of $\gamma = C/T$. Dotted line ($B = 0$) indicates $\gamma(T) = \gamma_0 - \beta\sqrt{T}$. Inset shows $\gamma(B)$ in FL (plateau) regime [91]. Right panel: (a) B - T phase boundary separating the FL/NFL regimes; (b) Field dependence of the A -coefficient, solid line indicates $A \sim B^{-0.6}$ [91].

mK in CeNi_2Ge_2 in exceptionally clean samples and the recently discovered non-centrosymmetric SC in CePt_3Si [64]. In the former case this may be due to the accidental closeness of the A-SDW phase QCP at ambient pressure, witnessed by the phase diagram in fig. 5 and the associated NFL anomalies. To find more examples of Ce-based HF superconductors it is therefore an obvious strategy to look for magnetically ordered Ce-HF compounds and drive them to a QCP with applied pressure, hoping that a SC 'dome', however small, might appear. This has been successful for CeCu_2Ge_2 [92] and more recently for CeRh_2Si_2 [93] and also CeIn_3 and CePd_2Si_2 [94]. Note however that strictly speaking CeRh_2Si_2 is not a HF system due to its small mass enhancement visible from the low γ -value at ambient pressure.

The magnetism of these compounds (table 2) and of the Pd-alloy series $\text{Ce}(\text{Rh}_{1-x}\text{Pd}_x)_2\text{Si}_2$ at ambient pressure has been subject to many investigations [94–96]. While there is unanimous agreement on the localised moment nature of CePd_2Si_2 , the interpretation of magnetism in CeRh_2Si_2 is controversial, partly favoring the itinerant picture from resistivity and specific heat measurements [97] and partly a localised picture from dHvA experiments and their interpretation and comparison with band structure calculations for the reference compound LaRh_2Si_2 [98].

The commensurate AF structure of CePd_2Si_2 consists of FM (110) sheets stacked alternately with a wave vector $\mathbf{Q} = (\frac{1}{2}, \frac{1}{2}, 0)$ and moments oriented along [110]. The local moment nature of CePd_2Si_2 can directly be inferred from susceptibility measurements and INS experiments [99]. The former give a tetragonal CEF level scheme of the localised $\text{Ce}^{3+} 4f^1$ electrons as a sequence of three Kramers doublets $\Gamma_7^{(1)}(0)$, $\Gamma_6(19 \text{ meV})$ and $\Gamma_7^{(2)}(24 \text{ meV})$. Well developed AF spin waves with an uniaxial anisotropy gap $\Delta = 0.83 \text{ meV}$ and a dispersion of 2 meV were observed which can be explained within the AF Heisenberg model for local moments. This is further supported by the magnetic phase diagram of the $\text{Ce}(\text{Rh}_{1-x}\text{Pd}_x)_2\text{Si}_2$ alloy series shown in fig. 15 on the Pd-rich side: The monotonous decrease of T_N and simultaneous strong increase of the characteristic HF temperature T^* with Rh-doping ($1-x$) corresponds to the QCP of a Doniach phase diagram for a Kondo-lattice type local moment system. There the destruction of AF

| | $\gamma(p=0)$ [mJ/molK ²] | T_N [K] | μ [μ_B] | $T_c^m(p_m)$ [K] | p_m [GPa] |
|-----------------------------------|---------------------------------------|-----------|-------------------|------------------|-------------|
| CePd ₂ Si ₂ | 250 | 10 | 0.62 | 0.4 | 2.71 |
| CeRh ₂ Si ₂ | 23 | 36 | 1.42 | 0.4 | 1.05 |

Table 2: Material parameters and magnetic properties of the sister compounds CeRh₂Si₂ and CePd₂Si₂.

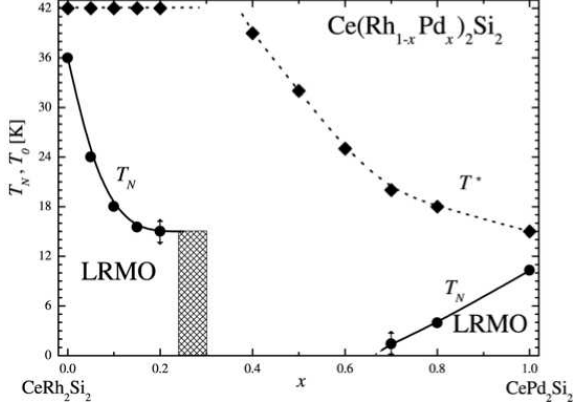


Figure 15: Magnetic x-T phase diagram of Ce(Rh_{1-x}Pd_x)₂Si₂ with Néel temperature $T_N(x)$ (circles) and Kondo temperature $T^*(x)$ (diamonds). Rh-rich side: Itinerant SDW regime. Pd-rich side: Local moment regime with Doniach type phase diagram [97].

order is due to the compensation of magnetic moments in the Fermi sea of conduction electrons.

The magnetism in Ce(Rh_{1-x}Pd_x)₂Si₂ is less well understood. The origin of the exceptionally high $T_{N1} = 36$ K is a longstanding mystery which defies understanding in the local moment system if deGennes scaling of T_{N1} with respect to GdRh₂Si₂ is applied. Like CePd₂Si₂ it orders with $\mathbf{Q} = (\frac{1}{2}, \frac{1}{2}, 0)$, first with a single \mathbf{q} -structure at T_{N1} which changes to a $4\mathbf{q}$ -structure below $T_{N2} = 24$ K (fig. 16). Also the (partly) plateau-like behaviour of $T_N(x)$ and $T^*(x)$ on the Rh-rich side of fig. 15 speaks against the local moment Kondo lattice picture and therefore an itinerant SDW origin of AF in Ce(Rh_{1-x}Pd_x)₂Si₂ has been proposed in [97]. On the other hand the moment size ($1.5\mu_B$, $\mathbf{m} \parallel c$) can be explained within a CEF-split localised $4f^1$ model for Ce which is supported by the entropy gain $\Delta S(T_N) \simeq R \ln 2$ indicating a CEF Kramers doublet. From dHvA experiments [98] it was found that some Fermi surface branches are well explained by LDA results for LaRh₂Si₂ which advocates that $4f$ - electrons in CeRh₂Si₂ do not contribute to the Fermi surface. Alloying leads to an increase of the mean free path and may easily destroy unconventional superconducting states. Therefore, unlike in the CeCu₂(Si_{1-x}Ge_x)₂ system, no superconductivity has been found around the magnetic QCPs of the above T-x magnetic phase diagrams. However the magnetic QCP may also be approached by applying hydrostatic pressure to the pure compounds. Detailed studies of CePd₂Si₂ [95] have revealed the QCP to lie at $p_c = 2.86$ GPa. The almost linear scaling $T_N(p) \sim (p_c - p)$ observed above 1.5 GPa is not in agreement with 3D spin fluctuation theory which predicts a pressure exponent $2/3$. The resistivity at p_c exhibits a NFL-type dependence of $\rho(T) = \rho_0 + BT^\alpha$ with an exponent $\alpha \simeq 1.2$. For samples with sufficiently small ρ_0 an approximately symmetric superconducting dome was indeed identified around p_c as shown in fig. 16. From upper critical field studies the coherence length was estimated as $\xi_0 \simeq 150 \text{ \AA}$.

Likewise hydrostatic pressure application destroys AF in CeRh₂Si₂ [100] at $p_c = 1.05$ GPa. The transition seems to be of first order. Nevertheless in good polycrystalline samples it was

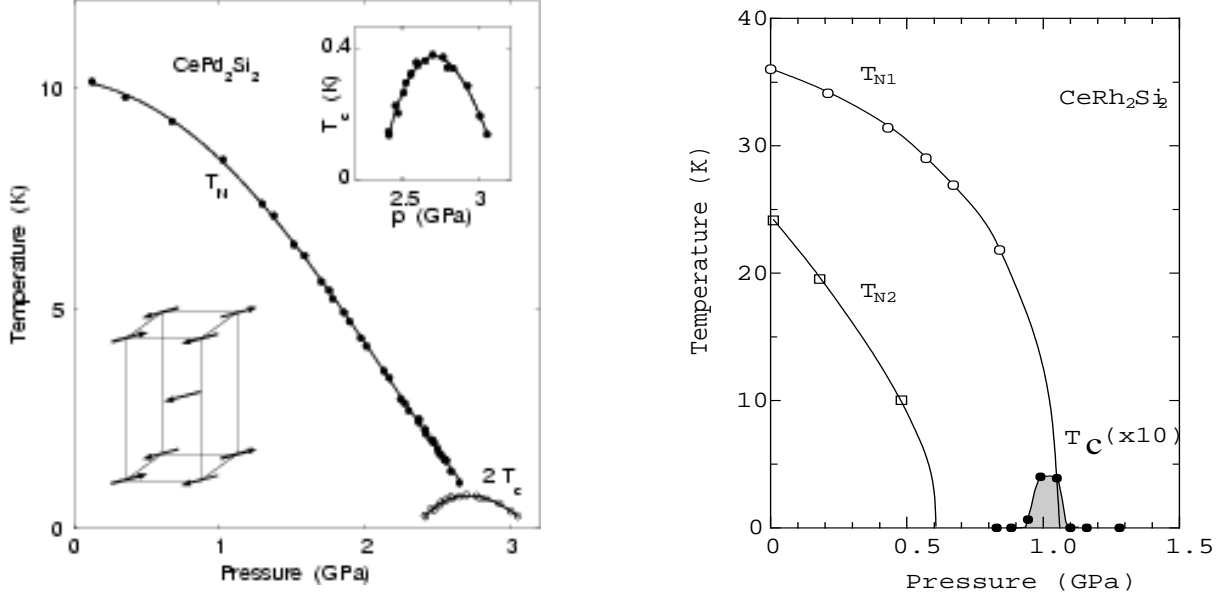


Figure 16: Magnetic and SC phase boundaries under hydrostatic pressure in CePd₂Si₂ (left panel) [95] and CeRh₂Si₂ (right panel) [100]; note the enlarged scales of T_c . In CeRh₂Si₂ the AF structure changes at T_{N2} .

found that SC appears around p_c , albeit in a very small pressure interval from 0.97 to 1.20 GPa, much smaller than previously thought (fig. 16). Again the optimal $T_c \simeq 0.4$ K. From the H_{c2} curves [98] at p_c the coherence lengths $\xi_c \simeq 240\text{\AA}$ and $\xi_a \simeq 310\text{\AA}$ are obtained. The anisotropy of $H_{c2}^{a,c}(0)$ may be caused by the anisotropic paramagnetic limiting effect ($\chi_c/\chi_a = 4$), its observation also suggests a SC singlet pairing state. The dHvA results [100] show a discontinuous change of FS topology at p_c , also the effective masses increase by almost an order of magnitude to $m^*/m \simeq 30$ above p_c . Therefore the transition across the QCP was interpreted as change from the low pressure AF local moment phase with light electrons to the paramagnetic heavy electron state above p_c [100].

Although the superficial appearance of quantum critical phase diagrams in fig. 16 is quite similar for both compounds, there is an important difference: quite opposite to CePd₂Si₂, CeRh₂Si₂ does not show any signature of NFL behaviour around p_c , $\gamma(T)$ has no significant T-dependence below 10 K and its value even increases up to 80 mJ/molK² at p_c due the suppression of AF order [101]. This means there is no direct connection between NFL behaviour in the QCP regime and the appearance of a SC dome. This conclusion can also be drawn from the investigation of Ce155 compounds (sect. 3.4).

Indeed from the theoretical point of view there is no reason to expect such a connection as can be concluded from the discussion in sect. 4. At the QCP the magnetic correlation length ξ_m diverges as described by eq. (9). Accordingly the spectral maximum at an energy $\sim \xi_m^{-2}$ of critical spin fluctuations responsible for NFL behaviour shifts to zero on approaching the QCP (eq.(45)). As explained in sect. 4, this increases the pair breaking effect due to low lying spin excitations and hence should lead even to a suppression of T_c close to the QCP. The soft spin fluctuations responsible for NFL behaviour in the Ce122 compounds close to the QCP are

therefore not essential for the SC pair formation. Therefore compounds like CeCu_2Ge_2 and CeRh_2Si_2 which are in the LFL state around p_c may form the same kind of SC state as NFL compounds like CePd_2Si_2 .

3.4 THE NEW Ce115 AND Ce218 CLASS OF HF SUPERCONDUCTORS

Only recently a new class of promising Ce-based HF superconductors with the general formula $\text{Ce}_n\text{M}_m\text{In}_{3n+2m}$ ($\text{M} = \text{Co}, \text{Ir}, \text{Rh}$) has been discovered. Again the guiding principle of looking for SC close to magnetic QCP's has been succesful, which naturally means that for the members of the family the SC transition takes place out of a pronounced NFL-like normal state. These tetragonal compounds (space group $\text{P4}/\text{mmm}$) are composed of alternating n -fold CeIn_3 layers and m -fold MIn_2 layers derived from the parent compound CeIn_3 ($n=\infty$). The $n=1, m=1$ compounds (fig. 4) CeCoIn_5 and CeIrIn_5 are ambient pressure superconductors and the AF CeRhIn_5 becomes superconducting under pressure similar to the AF $n=2, m=1$ family members Ce_2CoIn_8 and Ce_2RhIn_8 . Although they partly have FS sheets with 2D character like slightly warped cylinders oriented along c , the physical properties, e.g. resistivity and upper critical field are not excessively anisotropic. In fact, an analysis of uniaxial pressure effects of both normal-state and SC properties based on high-resolution thermal expansion measurements reveals that the SC T_c is strongly affected by at least two factors: The lattice anisotropy and the 4f-conduction electron hybridisation which is most sensitive to c -axis lattice distortions [102].

Their electronic structure is well understood and the ambient pressure superconductors CeCoIn_5 and CeIrIn_5 have conduction band states with strong 4f admixture, contrary to the ambient pressure AF compounds which have well localised 4f states witnessed by the similarity of their FS to the La parent compound. Large mass enhancements and specific heat γ coefficients are found but achieving the FL state may require application of a sufficiently large field. Maximum T_c s $\simeq 2.5$ K are achievable under pressure and already realised at ambient pressure for CeCoIn_5 . This is higher than in other families of Ce- or U-HF superconductors, except for CeCu_2Si_2 under pressure, and a factor of ten larger than in the parent compound CeIn_3 . A compilation of physical data is given in table 3, see also [103]. Certainly CeCoIn_5 has turned out to be the most interesting system and is also most thoroughly investigated, partly due to its large ambient pressure T_c and large H_{c2} as well as availability of excellent single crystals. Its unconventional superconducting state with d-wave symmetry is possibly the first which exhibits a change from a second to first order SC transition at $H_{c2}(T)$ below a temperature $T_0 < T_c$. Furthermore specific heat, NMR and ultrasonic attenuation suggest that CeCoIn_5 is the first SC which exhibits the elusive Fulde-Ferrell-Larkin-Ovchinnikov (FFLO) phase at high field and low temperature.

3.4.1 BASICS OF THE ELECTRONIC STRUCTURE

There are extensive LDA calculations and dHvA investigations of the CeMIn_5 and Ce_2MIn_8 electronic structure and FS topology [100, 104–106]. For the reference compound LaRhIn_5 excellent agreement is found and the dHvA frequencies of a few sheets exhibit clear 2D cylindrical structure. The AF compound CeRhIn_5 has localised 4f electrons which are CEF split into three Kramers doublets $\Gamma_7^2(0)$, $\Gamma_7^1(6.9 \text{ meV})$ and $\Gamma_6(23.6 \text{ meV})$ [107]. Therefore CeRhIn_5 should have

| | γ [mJ/molK ²] | T_N [K] | μ [μ_B] | $T_c(p=0)$ [K] | $T_c^m(p_m)$ [K] |
|-----------------------------------|----------------------------------|-----------|-------------------|----------------|------------------|
| CeIn ₃ | 130 | 10.2 | 0.65 | - | 0.25 (2.6 GPa) |
| CeCoIn ₅ | 350 | - | - | 2.3 | 2.5 (1.56 GPa) |
| CeIrIn ₅ | 750 | - | - | 0.4 | - |
| CeRhIn ₅ | 400 | 3.8 | 0.37 | - | 2.2 (2.5 GPa) |
| Ce ₂ CoIn ₈ | 500 | - | - | 0.4 | - |
| Ce ₂ IrIn ₈ | 700 | - | - | - | - |
| Ce ₂ RhIn ₈ | 400 | 2.8 | 0.55 | - | 2.0 (2.3 GPa) |

Table 3: Material parameters of Ce115 and Ce218 HF superconductors.

a similar FS as the La parent. Its AF order introduces many new sheets by folding into the AF BZ but the main FS sheets are indeed in good agreement. On the other hand the almost identical FS of CeCoIn₅ and CeIrIn₅ are well explained by including the 4f states as itinerant electrons in the FS volume which makes them highly different from the above LaRhIn₅ and CeRhIn₅ FS. The selfconsistently calculated f-level occupations for CeCoIn₅ and CeIrIn₅ are indeed close to one [105]. The enhanced γ values are given in table 3 and are generally larger for the itinerant 4f-electron compounds. The different size of mass enhancement for CeCoIn₅ and CeIrIn₅ was attributed to the influence of CEF effects [105]. The mass anisotropies as obtained from upper critical field measurements [104] are considerable, $m_c^*/m_a^* = 4.8$ in CeIrIn₅ and $m_c^*/m_a^* = 5.6$ in CeCoIn₅, reflecting the partly 2D FS topology. As in CeRhIn₅ the AF bilayer compound Ce₂RhIn₈ has largely localised 4f states and therefore again the FS sheets are very similar to the La₂RhIn₈ parent compounds [106], three similar sheets with 2D cylindrical appearance have been found in dHvA experiments and LDA calculations.

3.4.2 AF QUANTUM CRITICAL POINTS AND SUPERCONDUCTIVITY

When magnetic order changes to a different symmetry or vanishes as a function of an external or internal parameter this may be interpreted as a quantum phase transition provided the respective ground state energies are largely determined by the contribution from quantum fluctuations. If the transition is of second order the critical parameter value then defines a proper magnetic quantum critical point (QCP). In its vicinity NFL behaviour and a superconducting phase transition may be induced by spin fluctuations of the type discussed in sect. 4. The Ce115 and Ce218 compounds give considerable support for this scenario.

In the T-p phase diagrams of Ce115 and Ce218 and also Ce122 compounds which are AF at ambient pressure and SC under pressure two typical idealised situations may occur [108]: (1) When $T_N(p=0) \gg T_c(p_c)$ a symmetric SC dome around p_c appears and FL behaviour is observed above T_c and for $p > p_c$, AF order is suppressed inside the SC region. This situation is realised for CeRh₂Si₂ and CePd₂Si₂ as seen in fig. 16. (2) When $T_N(p=0) \geq T_c(p_c)$ the SC region is commonly asymmetric around the QCP and AF order partly coexists with SC. Around p_c and above T_c an extended region of NFL behaviour is observed. This holds for CeCu₂(Si_{1-x}Ge_x)₂, CeRhIn₅ and CeRh_{1-x}Co_xIn₅ (fig.18). This picture is, however, oversimplified as is obvious from the case of CeIn₃ where the conditions (1) are fulfilled but nevertheless

coexistence SC/SDW has been identified in NMR experiments[79]. In fact these results suggest that instead of having a QCP within the SC dome a first order transition with AF/PM phase separation occurs. It remains to be seen whether this also holds true for CePd_2Si_2 . Especially

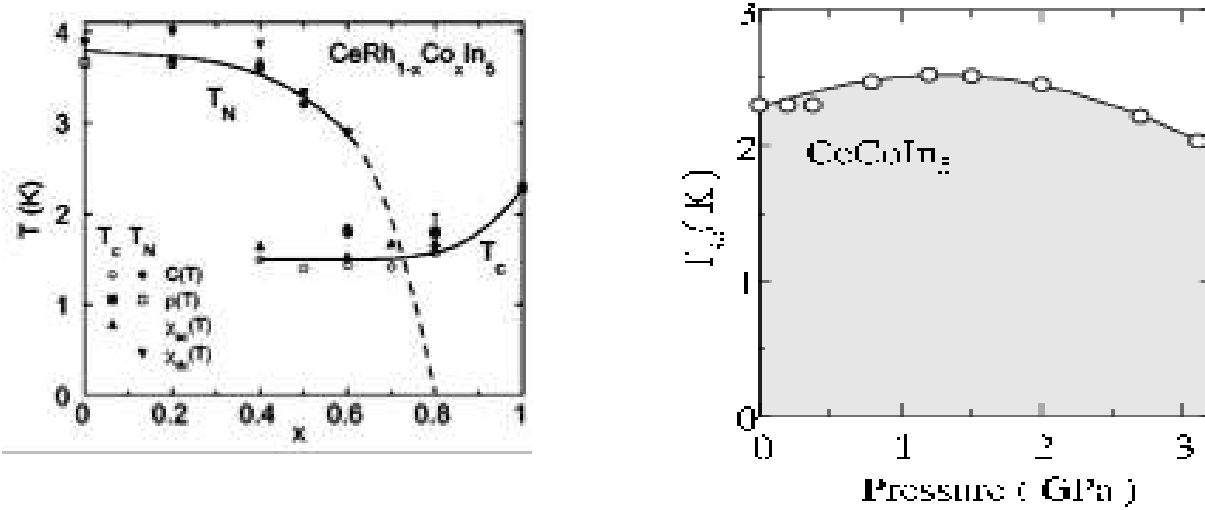


Figure 17: Left panel: Coexistence of AF order and SC in $\text{CeRh}_{1-x}\text{Co}_x\text{In}_5$ ('negative pressure' side) [109]. Right panel: Hydrostatic pressure dependence of T_c in CeCoIn_5 . The critical pressure where $T_c = 0$ is not known [100].

the quantum criticality of CeCoIn_5 and its connection to superconductivity has been clarified by external field and pressure application and by internal pressure through Rh substitution of Co. At ambient pressure CeCoIn_5 is nonmagnetic and the 'large' T_c is almost independent in hydrostatic pressure up to 3 GPa and no magnetic order appears. Apparently doping with Rh, which has a larger ionic radius compared to Co, exerts a 'negative pressure' which for $1-x > 0.2$ Rh doping achieves AF order (fig. 17) while SC persists, albeit with slightly reduced T_c . Thus a considerable regime of AF/SC coexistence appears. Taken together Rh-doping and hydrostatic pressure do not present an ideal dome-shaped SC region, it is rather reminiscent of slightly doped $\text{CeCu}_2(\text{Si}_{1-x}\text{Ge}_x)_2$ under pressure. The combined x, p - T phase diagram of the Rh-doped compound $\text{CeRh}_{1-x}\text{Ir}_x\text{In}_5$ [110] and CeIrIn_5 under hydrostatic pressure [111] is quite similar to fig. 17. $\text{CeRh}_{1-x}\text{Ir}_x\text{In}_5$ also develops AF order that coexists with SC between $0.35 < x < 0.5$ [112]. The $T_c(p)$ curve of CeIrIn_5 starts at $T_c(p=0) = 0.4$ K and reaches $T_c(p_m) = 1.05$ K at $p_m = 2.2$ GPa and finally drops to zero at $p_c = 6$ GPa. This critical pressure for the CeCoIn_5 sister compound is not yet known.

Other family members which are AF at ambient pressure but not SC naturally exhibit better realisations of the canonical AF/SC quantum critical phase diagrams under hydrostatic pressure. This is already true for the AF parent compound CeIn_3 ($T_N = 10$ K) of the Ce115 family [100] with an optimum $T_c = 0.2$ K at 2.5 GPa and especially for the localised 4f compound CeRhIn_5 ($x = 0$ in fig. 17) as is shown in fig. 18. The related AF bilayer compound Ce_2RhIn_8 is another exciting example of AF/SC quantum critical phase diagram (fig. 18). The remarkably high optimum T_c rivals that of ambient pressure CeCoIn_5 and is comparable to its own $T_N(p=0) = 2.8$ K.

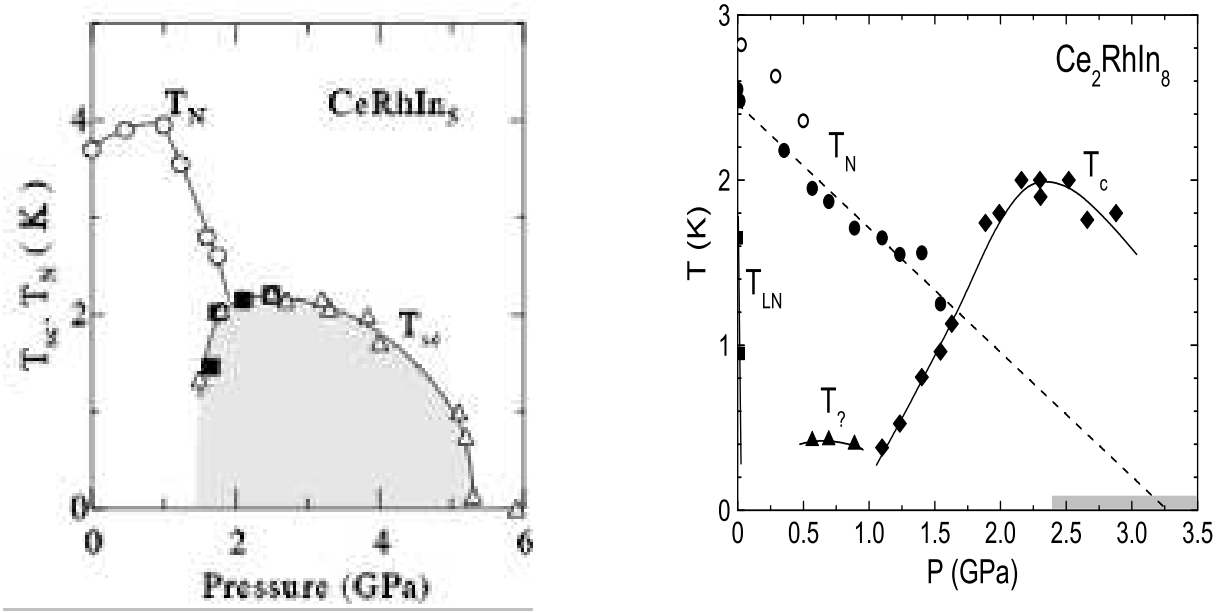


Figure 18: Quantum critical p-T phase diagrams for CeRhIn₅ [100] and Ce₂RhIn₈ [113]. When $T_N \sim T_c^m$ as in Ce₂RhIn₈, AF and SC coexist over considerable pressure range, contrary to the situation in CeRhIn₅ where $T_N \gg T_c^m$.

3.4.3 NFL ANOMALIES IN FIELD AND PRESSURE INDUCED QCP'S

The common signature of a NFL state are anomalous temperature and field scaling exponents for thermodynamic quantities like specific heat, susceptibility, Grüneisen parameters (thermal expansion) and transport quantities like resistivity or Hall coefficient. Their origin and appearance has been briefly discussed in sect. 2.3.

Pronounced NFL anomalies have been identified in the ambient pressure SC CeCoIn₅ and CeIrIn₅, pointing to the closeness of the QCP [114]. This is well illustrated by $\rho(T)$ data for CeCoIn₅ at ambient pressure and zero field. They exhibit linear temperature behaviour above T_c and the logarithmic $\gamma(T)$ variation between 0.4 K and 8 K for fields larger than $H = H_{c2}^{[001]} = 5$ T but smaller than $H = 8$ T (fig. 19) [62]. From systematic $\rho(T, H)$ investigations of CeCoIn₅ a B-T phase diagram may be mapped out showing the development of a field-tuned QCP and associated with it two different NFL regimes. They are characterised by $\rho(T) = \rho_0 + BT^n$ where $n=1$ or $n=\frac{2}{3}$ and a low temperature crossover at T^* to the LFL regime [115] is observed. The $n=1$ regime is similar to the underdoped regime in high T_c superconductors and speculations about the existence of a spin pseudo-gap in CeCoIn₅ and CeRhIn₅ have been made [116]. This is supported by normal state Hall angle and magnetoresistance (MR) measurements [117] which show that in the $n=1$ NFL regime the Hall angle $\Theta_H \sim T^2$ whereas Kohlers rule $\Delta_{xx}(H) \sim H^2$ which holds for LFL systems is strongly violated and a different scaling law is obeyed. The similarities of transport coefficients in CeCoIn₅ to high T_c materials suggests a common origin of NFL behaviour in the critical 2D AF spin fluctuations in both type of compounds. This idea is also supported by an observed giant Nernst effect [118] as in the cuprates. Clear signature of NFL behaviour has also been seen in thermal expansion measurements [119] and the associated

Grüneisen ratio. A compilation of various scaling laws in the NFL regime of the Ce115 and Ce218 compounds may be found in [103, 114]. A kind of inverted behaviour compared to CeCoIn₅ shown in fig. 19 is seen in Ce₂IrIn₈, because in this nonmagnetic HF compound LFL behaviour at zero field changes to NFL behaviour at a field of 13 T, which is interpreted as the appearance of a field induced magnetic QCP [120].

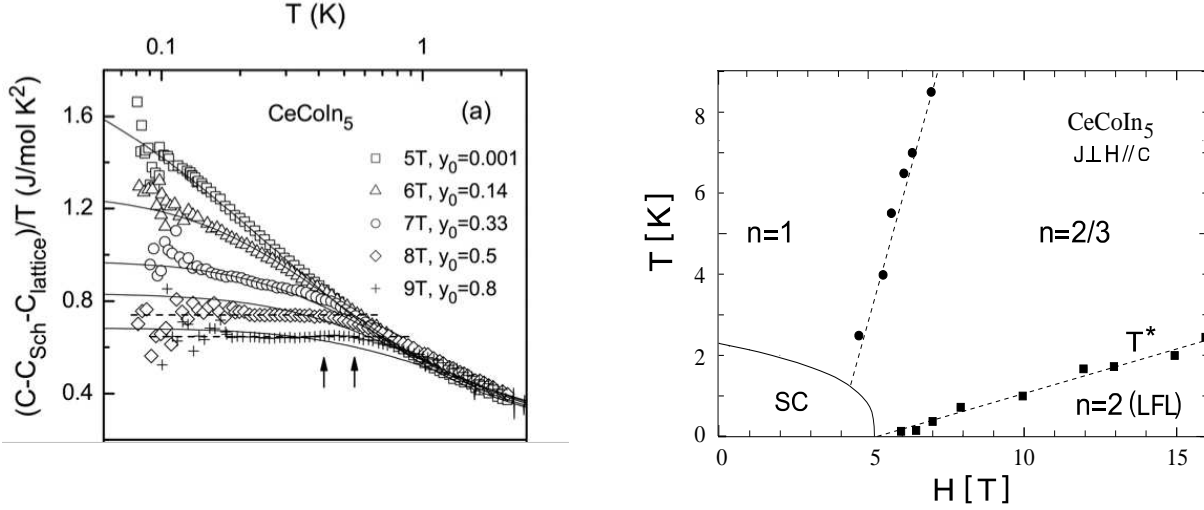
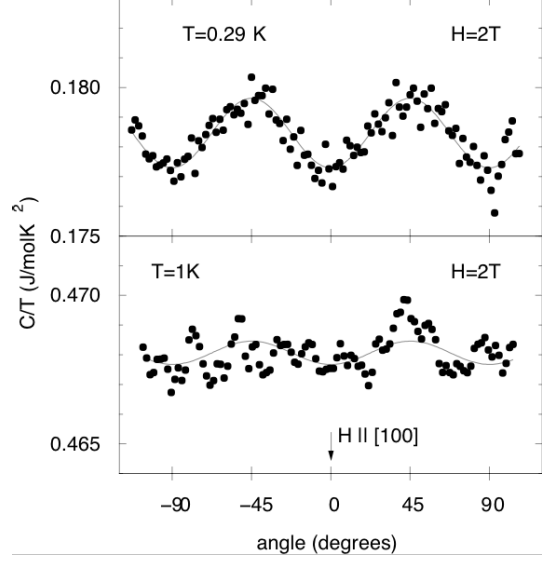


Figure 19: Left panel: Field dependence of $\gamma = C/T$ for $\mathbf{H} \parallel [001]$. Solid lines are fits by Moriya's SCR spin fluctuation theory [62]. Right panel: B-T phase diagram of CeCoIn₅ showing the evolution of two distinct NFL regimes (characterised by different exponents n of $\Delta\rho(T) \sim T^n$) and the high field LFL phase [115].

3.4.4 THE SUPERCONDUCTING GAP FUNCTION IN CeCoIn₅

Heavy Fermion systems are unconventional superconductors regarding their pairing mechanism which is of magnetic origin in most cases and also with respect to non-s-wave symmetry of the order parameter, generally belonging to a non-trivial representation of the total symmetry group. Often, but not necessarily, this is connected with the appearance of nodes or zeroes in the gap function $\Delta(\mathbf{k})$. CeCoIn₅ is the prime and best studied example of unconventional SC in the new family. It is a strong coupling SC with very large BCS ratio $2\Delta/kT_c = 8.86$ at ambient pressure [121] and the gap function is believed to exhibit d-wave symmetry. This has already been suspected from the T^3 -power law behaviour of NMR and NQR relaxation rate $1/T_1$ and the absence of a Hebel-Slichter peak [122]. The same result was found for CeIrIn₅. In addition CeCoIn₅ shows a ¹¹⁵In- Knight shift reduction $K \sim T$ for field along a and c, indicating an isotropic reduction of spin susceptibility in the SC state. The T- dependence of $1/T_1$ and K consistently suggest a singlet pair state with line nodes, e.g. a d-wave state for CeCoIn₅. In subsequent field-angle resolved magnetothermal conductivity [60] and specific heat experiments [61] the position of line nodes, in \mathbf{k} -space have been investigated to identify which irreducible D_{4h} representation among the five d-wave states is realised. In this method a peculiar feature of nodal superconductors in the vortex phase is used as has been first discussed by Volovik [123]. Because of $\Delta(\mathbf{k}) = 0$ along certain directions in \mathbf{k} -space, quasiparticles can

Figure 20: Specific heat γ -coefficient for CeCoIn₅ as function of field angle ϕ with respect to [100] ($\mathbf{H} \perp c$ -axis) in the ab plane. Maxima at [110] correspond to antinodal direction for $\Delta(\mathbf{k})$, suggesting a d_{xy} -gap function. The oscillation amplitude decreases with increasing temperature [61].



tunnel into the inter-vortex region where they acquire a Doppler shift energy $\mathbf{v}_s \cdot \mathbf{k}$ due to the superfluid velocity field $\mathbf{v}_s(\mathbf{r})$. This leads to a finite, field induced residual quasiparticle DOS. For a gap with line nodes one has ($E \ll \Delta$):

$$\frac{N_s(E, \mathbf{H})}{N_n} \simeq \frac{1}{\Delta} \langle \langle |E - \mathbf{v}_s(\mathbf{r}) \cdot \mathbf{k}| \rangle \rangle \quad (42)$$

where a double average over the Fermi surface and the vortex coordinate has to be taken. This contributes to the specific heat and most importantly supports a heat current \perp to the vortices which is not possible in s-wave superconductors for $T \ll T_c$. For $H \ll H_{c2}$ the residual DOS and hence $\gamma(H)$ has a \sqrt{H} dependence characteristic of nodal superconductors [124]. In addition $N_s(E, \mathbf{H})$ depends on the field *direction* with respect to crystal axes and the position of node lines. As a function of polar field angles θ and ϕ the residual DOS and hence the specific heat and thermal conductivity will exhibit angular oscillations whose type and phase allows one to draw direct conclusions on the \mathbf{k} -space positions of nodes in $\Delta(\mathbf{k})$. The Doppler shift phenomenon has now been exploited successfully to clarify the nodal gap structure in many unconventional superconductors [60, 125–128] including CeCoIn₅; see also [129]. There both $\kappa_{xx}(\theta, \phi)$ [60] and $C(\theta, \phi)$ [61] exhibit fourfold oscillations in the azimuthal angle ϕ which means that the gap function $\Delta(\mathbf{k})$ has four line nodes parallel to the c -axis on the main cylindrical FS of CeCoIn₅. The maximum in the oscillation will be achieved when each of them gives a Doppler shift contribution in eq. (42), i.e. when \mathbf{H} points along the anti-nodal direction, the minimum occurs in the nodal direction. Surprisingly the two measurements presently disagree on the position of the line nodes: Thermal conductivity results suggest line nodes along c at [110] and equivalent directions. This means a $d_{x^2-y^2}$ (B_{1g}) symmetry of the SC gap in CeCoIn₅ as for high T_c compounds. On the other hand in the specific heat results of fig. 20 the maxima in the ϕ -oscillations are shifted by 45° , therefore node lines along c should be situated at the tetragonal [100] and equivalent positions meaning a d_{xy} (B_{2g})-type symmetry of the SC gap. This discrepancy is not fully resolved so far.

3.4.5 VORTEX STATE AND FFLO PHASE IN CeCoIn₅

Besides providing important clues on gap function symmetry the vortex state of CeCoIn₅ has proved highly interesting, even unique, in its own right. It was known already for a long time that for low temperatures the SC transition at H_{c2} should change from second to first order. This is due to a competition of orbital- and Pauli-pair breaking effects characterised by the Maki parameter $\alpha = \sqrt{2}H_{c2}/H_P$ where $H_P = \Delta_0/\sqrt{2}\mu_B$ (for $g = 2$) is the Pauli limiting field. Conditions are favorable if the former is weak (large H_{c2} or $\alpha > 1$) compared to the latter and if spin-orbit scattering by impurities is negligible. Neglect of the orbital effect ($\alpha \rightarrow \infty$) leads to $T_0 = 0.55T_c$ for the appearance of the first order transition in an s-wave SC. Apparently these conditions have never been met in superconductors investigated so far. In CeCoIn₅, due to the large effective mass $m^* \simeq 100 m$ and resulting extremely high $H_{c2}^{[110]}(0) = 11.9$ T, and due to excellent sample quality they are much better fulfilled. Indeed in this compound a change from second to first order superconducting transition for field $\mathbf{H} \parallel [001]$ has been found at $T_0 \simeq 0.3T_c$ (corresponding to $\alpha = 3.5$) by specific heat [130, 131] and thermal expansion [102] measurements. The first order transition was also found for $\mathbf{H} \parallel [110]$ from magnetisation [132] and specific heat [62] measurements below $T_0 = 0.5T_c$. (fig 21). The same favorable

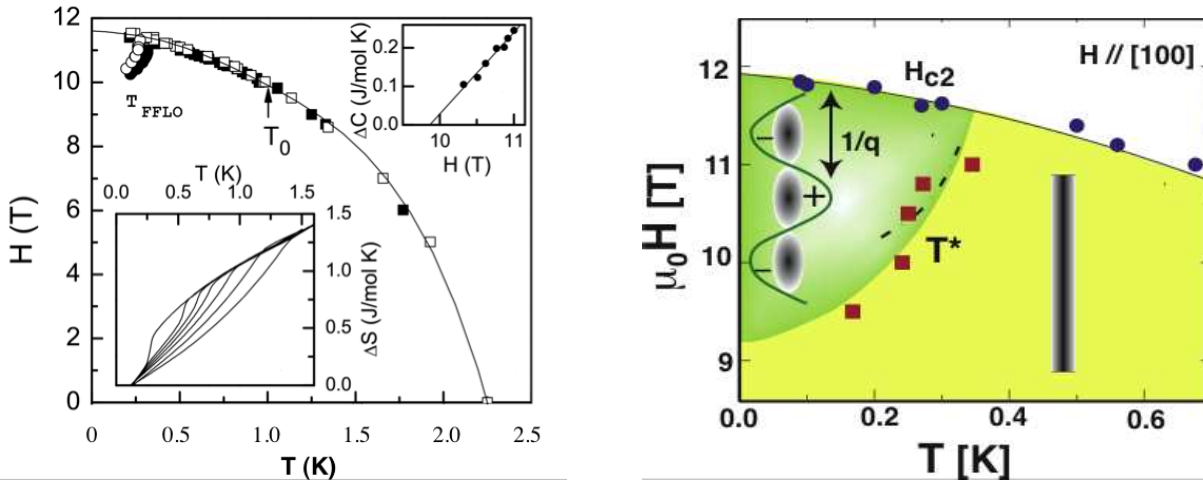


Figure 21: Left panel: H_{c2} curve from specific heat results. At $T_0 \simeq 1.1$ K the SC transition changes from 1st to 2nd order. Lower inset shows entropy gain. Upper inset shows specific heat jump at T_{FFLO} line [62]. Right panel: enlarged FFLO corner determined from sound velocity measurements. Segmentation of vortices in FFLO phase with wave length $1/q$ is indicated [63].

circumstances may explain an even more exotic observation in CeCoIn₅ for $\mathbf{H} \parallel [110]$. At very small temperatures an additional phase appears in the vortex state (fig. 21). It is now considered as the first realisation of the Fulde-Ferrell-Larkin-Ovchinnikov (FFLO) phase where the electrons form Cooper pairs with a finite momentum q . It appears when the Pauli effect largely dominates the orbital effect ($\alpha > 1.8$ [133]) and spin orbit scattering is very small. Apparently CeCoIn₅ is the first SC compound where these conditions are fulfilled leading to the spatially modulated FFLO SC pair state with a wave number $q \simeq 2\mu_B H/\hbar v_F$. In this state the order parameter should have planar nodes perpendicular to the field leading to a segmentation

of vortex lines along the vortex direction. A definite proof for this conjecture by small angle neutron scattering is still lacking, but indirect evidence for the segmentation has been found by sound velocity measurements [63]. The segmentation of vortices on crossing the T_{FFLO} line changes their pinning properties which in turn leads to a Lorentz force anomaly for sound modes with displacement vector $\mathbf{u} \perp \mathbf{H}$. The estimated segmentation length is remarkably close to the calculated modulation length $1/q = 60\text{\AA}$. Also this method allows an independent determination of specific heat results and assures that the new phase is not due to field induced magnetic order since the latter should not have any effect on the vortex pinning. The FFLO corner is clearly visible for \mathbf{H} in the ab - plane but hard to identify for \mathbf{H} along $[001]$ with the smaller H_{c2} in agreement with theoretical predictions. Evidence for the FFLO state for $\mathbf{H} \parallel [110]$ has recently also been found from ^{115}In -NMR measurements [134] which give a $T_{\text{FFLO}}(\mathbf{H})$ -line similar to that from specific heat and sound velocity results and provide direct evidence for the spatial texture of the order parameter in the FFLO phase.

3.5 HF SUPERCONDUCTIVITY WITHOUT INVERSION SYMMETRY IN CePt_3Si

All previously discussed Ce- intermetallic compounds and in fact all HF superconductors known possess centrosymmetric space groups which contain an inversion center. This leads one to a natural classification of SC pairs into even and odd parity or singlet and triplet states. For the singlet channel only time reversal invariance is required in order to assure the necessary degeneracy of paired electron states with opposite momenta and spins. For the formation of triplet pairs however, electron states with opposite momenta but equal spins must also be degenerate which requires inversion symmetry as an additional necessary condition [135]. The lack of an inversion center may also strongly affect the magnetic properties of a superconductor as shown in [65].

The discovery of the first HF superconductor CePt_3Si [64] without inversion symmetry is therefore of considerable fundamental interest. CePt_3Si belongs to the tetragonal space group $P4/\text{mm}$ (fig. 22) where the removal of the inversion center leads to the Ce-point group C_{4v} meaning the loss of the basal plane as mirror plane ($z \rightarrow -z$). The structure can be derived from the hypothetical cubic CePt_3 structure (the same as for CeIn_3) by tetragonal distortion with $c/a=1.336$ and by filling the voids with Si. The $\text{Ce}^{3+}4f$ states of CePt_3Si are well localised as evident from sharp CEF excitations found in INS experiments [137] where the C_{4v} level scheme was determined as $\Gamma_7^{(1)}(0)$, $\Gamma_6(1\text{ meV})$ and $\Gamma_7^{(2)}(24\text{ meV})$. At $T_N = 2.2\text{ K}$ AF magnetic order appears where FM planes are staggered along c with $\mathbf{Q} = (0,0,\frac{1}{2})$. Below $T_c = 0.75\text{ K}$ superconductivity sets in (fig. 23) and coexists microscopically with AF order. Only the second time after A-type CeCu_2Si_2 (fig. 5) this has now been observed for a stoichiometric Ce-compound at ambient pressure. The ordered moments $\mu = 0.16\mu_B$ however are much less than the value of the localised $\Gamma_7^{(1)}$ ground state doublet which suggests a large Kondo screening, and indeed there is an associated mass enhancement of itinerant quasiparticles as is evident from $\gamma_n(\text{CePt}_3\text{Si}) = 390\text{ mJ/mol K}^2$ as compared to $\gamma_n = 9\text{ mJ/mol K}^2$ for LaPt_3Si . A considerable residual $\gamma_s = 180\text{ mJ/mol K}^2$ and a $\Delta C/\gamma_n T_c = 0.25$ much smaller than the BCS value 1.43 has been observed. This raises questions on the quality of the polycrystalline samples although the ξ estimate from H_{c2} indicates that one is not in the dirty limit. Later resistivity measurements on single crystals [138] in a field indeed have identified a coherence length $\xi \simeq 100\text{ \AA} \ll 1$ (mean

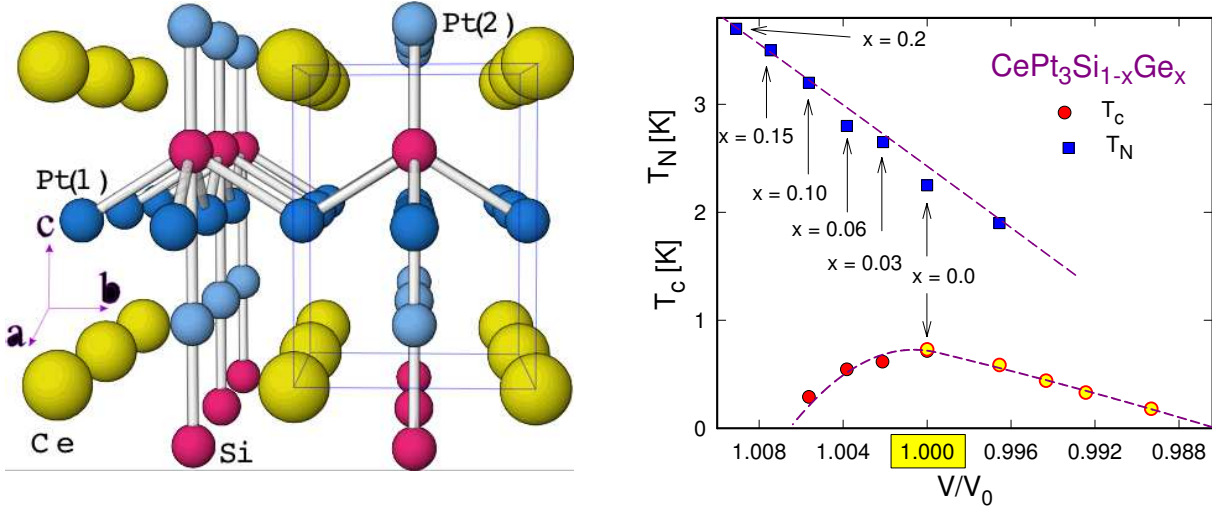


Figure 22: Left panel: Crystal structure of CePt_3Si belongs to the tetragonal space group $P4mm$, the conventional unit cell ($a = 4.072 \text{ \AA}$, $c = 5.442 \text{ \AA}$) is indicated [64]. It lacks the reflection symmetry $z \rightarrow -z$. Right panel: Phase diagram of $\text{CePt}_3\text{Si}_{1-x}\text{Ge}_x$ from ambient pressure (mainly T_N) and hydrostatic pressure results (mainly T_c). Here 1% volume reduction corresponds to 1.5 GPa [136].

free path). There the almost isotropic upper critical fields has been determined as $H_{c2}^a(0) = 3.2 \text{ T}$ and $H_{c2}^c(0) = 2.9 \text{ T}$ (fig. 23) which is considerably larger than the Pauli-Clogston limiting field estimated by $H_P \sim \Delta/\sqrt{2}\mu_B \sim 1.2 \text{ T}$ for $g = 2$. The pressure dependence of T_c which vanishes around $p_c = 1.5 \text{ GPa}$ has still some uncertainty due to the broad appearance of the resistive transition [138]. Nevertheless a combined $p(V)$ - T phase diagram from Ge-doping and hydrostatic pressure results is shown in fig. 22. Whether the AF T_N and the ordered moment vanish continuously and the SC dome extends on both sides of the magnetic phase is presently not known.

The observation of $H_{c2}(0) \gg H_P$ would rather advocate for triplet pairing, this confronts one with two major problems: i) the lack of inversion symmetry should disfavor triplet pairing according to the above arguments. ii) coexistence with fully developed AF order should be destructive for triplet pairs. Proposals to avoid this contradiction have been made in theoretical investigations [66, 139] which include an explicit inversion symmetry breaking but time reversal conserving term in the single particle part of the BCS Hamiltonian. It has the form of a Rashba-type antisymmetric spin-orbit coupling for conduction electrons $c_{\mathbf{k}s}$ which is of the form ($\mathbf{m}\sigma$ = Pauli matrices)

$$H_P = \alpha \sum_{\mathbf{k}, ss'} \mathbf{g}_{\mathbf{k}} \cdot \mathbf{m}\sigma_{ss'} c_{\mathbf{k}s}^\dagger c_{\mathbf{k}s'} \quad (43)$$

where $\mathbf{g}_{\mathbf{k}} = -\mathbf{g}_{-\mathbf{k}}$ is an antisymmetric function which may be obtained from the periodic potential of Bloch states and is conveniently normalised to one on the Fermi surface. For finite α this term lifts the twofold spin degeneracy of conduction bands (but preserves the \mathbf{k} , $s \rightarrow -\mathbf{k}$, $-s$ symmetry). It leads to i) modifications for both singlet and triplet gap equations, ii) a mixing term for singlet and triplet gaps which, however, is of the order $\alpha/\epsilon_F \ll 1$ and therefore can be

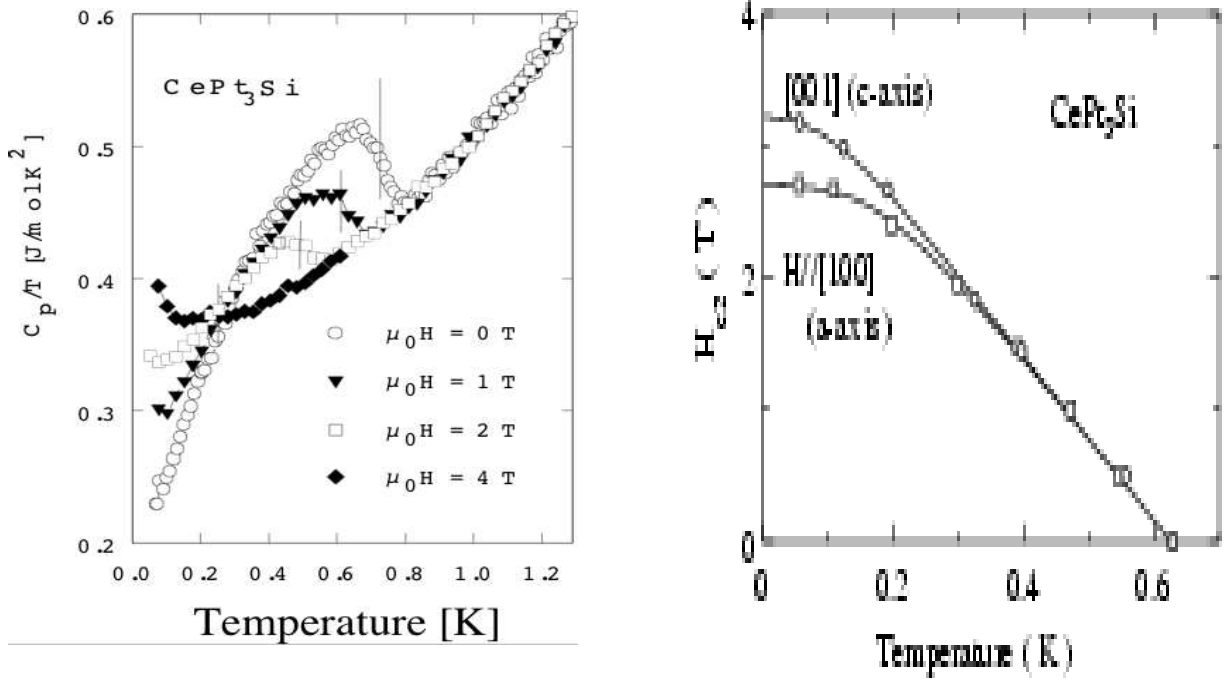


Figure 23: Left panel: Field dependence of C/T in polycrystalline CePt_3Si with SC transition indicated by vertical lines [64]. Right panel: Upper critical field in single crystals from ρ [138].

neglected. Likewise T_c reduction in the singlet case is of order $(\alpha/\varepsilon_F)^2 \ll 1$. The triplet case is more involved and provides important clues on the effect of H_p . For $\alpha = 0$ all triplet states of a given odd l and described by a $\mathbf{d}(\mathbf{k})$ vector gap function have the same T_c . Turning on the I-symmetry breaking ($\alpha > 0$) lifts this degeneracy, the expected T_c -reduction however does not affect all triplet states indiscriminantly, those triplet states with $\mathbf{d}(\mathbf{k}) \parallel \mathbf{g}_\mathbf{k}$ are well protected and have no T_c reduction as in the singlet case. From the C_{4v} point group one may expect $\mathbf{g}_\mathbf{k} \cdot \mathbf{m}\boldsymbol{\sigma} = k_x\sigma_y - k_y\sigma_x$ and then the protected triplet state with unaffected T_c corresponds to the A_{2u} gap function $\mathbf{d}(\mathbf{k}) = \hat{x}k_y - \hat{y}k_x$ which has point nodes. Other triplet states are strongly suppressed for $\alpha \gg T_c$. Thus in principle favorable triplet states are not destroyed by inversion symmetry breaking.

On the other hand the loss of inversion symmetry described by eq. (43) weakens the Pauli-Clogston limiting argument against singlet pairing considerably. It is known that spin-orbit impurity scattering reduces the effect of paramagnetic limiting, the same is true for the anti-symmetric spin-orbit coupling of paired conduction electrons in eq. (43). With increasing α the renormalised H_p increases above its starting value $\Delta/\sqrt{2}\mu_B$ for $\alpha = 0$. For $\alpha/T_c \gg 1$ it becomes arbitrarily large. As a result the observation of a large $H_{c2}(0) \gg \Delta/\sqrt{2}\mu_B$ does not contradict singlet pairing, which in addition would be more compatible with the coexisting AF order.

As a preliminary conclusion one may say that there is no compelling theoretical reason why triplet pairing for SC without inversion symmetry should be prohibited. Likewise the upper critical field observations do not contradict singlet pairing so that the question of gap symmetry in CePt_3Si remains open. Recent NMR relaxation experiments [140] on Pt-sites also did not clarify this question but rather added new puzzles: The low temperature $1/T_1$ behaviour is

neither described by the usual T^3 power law generally observed in HF SC, nor by an exponential decay indicative of an isotropic gap. However the latter is more compatible with the observation of a small coherence peak below T_c and a Balian-Werthamer type relaxation rate immediately below it.

4 MICROSCOPIC SC PAIRING MECHANISM IN HF COMPOUNDS

In this section we illustrate to some detail microscopic concepts and theories that were proposed to describe the superconducting pairing in HF systems or, more generally, in strongly correlated electron compounds including the cuprates and ruthenates. The long history of the subject of non-phononic superconductivity will not be recounted and we refer to the literature for this purpose [6, 141, 142].

Far below the Kondo temperature T^* the ideal HF compound is in a LFL state with quasiparticles that have an effective mass m^* much enhanced compared to the band mass m_b . However due to the presence of virtual high energy excitations a residual on-site quasiparticle repulsion appears. The low energy excitations may then be described by a spectrum of spin fluctuations characterised by a dynamic susceptibility matrix $\mathbf{m}\chi(\mathbf{q}, \omega)$. In the vicinity of a magnetic instability, for example AF order close to a QCP, overdamped critical spin fluctuations called antiferromagnetic paramagnons appear whose spectral density is concentrated around the AF \mathbf{Q} -vector and which has a typical energy $T_{sf} < T^*$ at the maximum of $\mathbf{m}\chi(\mathbf{Q}, \omega)$. The virtual exchange of these excitations mediates an effective interaction between quasiparticles which may lead to a superconducting instability. In contrast to conventional phonon-mediated superconductors the pair states have to be of unconventional (non s-wave) type whose order parameter exhibits a sign change in \mathbf{k} -space to avoid the strong on-site repulsion of quasiparticles. A brief symmetry classification of unconventional SC order parameters was given in sect. 3.1.

Originally the spin fluctuation mechanism in the case of nearly FM systems with paramagnon exchange was proposed to explain superfluidity in ^3He [143, 144]. It was later extended to HF [145] and cuprate superconductors [146]. In the latter one has simple tight binding (TB) hole bands which allows one to carry out fully microscopic calculations based on the fluctuation exchange (FLEX) approximation [147, 148] for the Hubbard model. However the theory in its original single band form is not able to describe the complications of SC pairing in real HF materials, for the following reasons: i) Orbital (spin-orbit) and crystal field effects lead to complicated renormalised band structures with multisheeted FS, therefore the dynamic susceptibility $\mathbf{m}\chi(\mathbf{q}, \omega)$ cannot be reliably calculated, instead empirical forms have to be assumed which also incorporate the vicinity to a possible QCP frequently present in Ce-HF compounds. ii) In the U-compounds 5f- electron have a dual nature, partly localised and partly itinerant. The internal CEF excitations (magnetic excitons) of the former may dominate the effective interactions between itinerant quasiparticles, which is an alternative to the spin fluctuation mechanism that involves only the itinerant 5f electrons.

We shall discuss both electronic pairing mechanisms in the following. While the spin fluctuation mechanism may be appropriate for the Kondo-like Ce HF superconductors, the magnetic exciton mechanism is a serious candidate for a number of U-compounds.

4.1 SPIN FLUCTUATION MECHANISM FOR Ce-BASED HF COMPOUNDS

If one is not too close to the QCP of magnetic order one may assume that the frequency dependence of spin fluctuations is negligible on the scale of the cutoff energy for SC pairing. Then in the effective interaction $V(\mathbf{q}, \omega)$ between quasiparticles $\mathbf{m}\chi(\mathbf{q}, \omega)$ may be replaced by the non-retarded RPA expression $\mathbf{m}\chi(\mathbf{q})$. For the spin dependent part one obtains the spin rotationally invariant interaction

$$V_{\alpha\beta;\gamma\rho}(\mathbf{q}) = V(\mathbf{q})\mathbf{m}\sigma_{\alpha\gamma} \cdot \mathbf{m}\sigma_{\beta\rho} \quad \text{with}$$

$$V(\mathbf{q}) = -\frac{1}{2} \frac{I}{1 - I\chi_0(\mathbf{q})} \simeq -\frac{1}{2} I^2 \chi(\mathbf{q}) \quad \text{and} \quad \chi(\mathbf{q}) = \frac{\chi_0(\mathbf{q})}{1 - I\chi_0(\mathbf{q})} \quad (44)$$

Here I is the residual on-site quasiparticle interaction and $\chi_0(\mathbf{q}) \leq I^{-1}$ their static noninteracting susceptibility. The interaction may be split into singlet ($S=0$) and triplet ($S=1$) channels according to $V_0 = -3V$ and $V_1 = V$, the factor 3 is due to the fact that only longitudinal spin fluctuations contribute in the triplet channel whereas both longitudinal and transverse parts contribute in the singlet channel. In this approximation the SC pairing is completely determined by the static susceptibility $\mathbf{m}\chi(\mathbf{q})$ which may in principle be obtained from diffuse neutron scattering. Its \mathbf{q} -dependence together with the characteristics of the Fermi surface determines the dominant angular momentum component V_S^l of $V_S(\mathbf{q})$ that leads to the stable SC pair state ($l = \text{even}$ for $S=0$ and odd for $S=1$). Obviously the s-wave state is not stable because $V_0^{l=0}$ is always positive (repulsive), pair states with $l > 0$, however, may have attractive $V_l < 0$ and become stable depending on the characteristics of $\chi(\mathbf{q})$. The model has been analysed in some detail in [145] by assuming a spherical FS and a plausible behaviour for $V(\mathbf{q})$ in a cubic lattice with a peak near the AF wave vector \mathbf{Q} to simulate the AF spin fluctuations observed in HF compounds. This analysis predicts that the unconventional even singlet SC state ($l > 0$), e.g. $l = 2$ d-wave state, should be stable because $V_l < 0$ is attractive in this orbital channel.

This result led to the general expectation that AF spin fluctuations favor singlet pairing. While it is true in the simple case of cuprates, and it may be true for some Ce-based HF compounds like CeCoIn_5 (sect. 3.4), it turned out to be misleading for a number of U-compounds like UPt_3 or UNi_2Al_3 and possibly UBe_{13} which exhibit triplet pairing as concluded e.g. from Knight shift results [149]. Therefore the above prediction of singlet pairing may be partly an artefact of the model simplifications and point to the inadequacy of the spin fluctuation model for U-HF superconductors. Indeed the model has obvious deficiencies: i) It completely ignores the orbital structure strongly influenced by spin orbit coupling and CEF effects. ii) It does not take into account the uniaxial crystal anisotropy present in most HF superconductors which possess either tetragonal or hexagonal space groups. iii) It ignores the spin space anisotropy of the pair potential which is assumed as rotationally invariant in eq.(44). In case this symmetry is reduced the triplet state will be less disfavored.

From the low temperature 'power laws' in various thermodynamic and spectroscopic quantities it is also concluded that most HF SC have gap functions with nodes $\Delta(\mathbf{k}) = 0$ along lines on the FS. However if one assumes the strong spin orbit coupling case for quasiparticles, i.e. the crystal double group as symmetry group, 'Blount's theorem' states that triplet pair states can have only point nodes in the SC gap [150]. Therefore the observed power laws which support

line nodes have also been used as an argument for singlet pairing. This argument is misleading however, since the spin orbit coupling is so large that it has to be included already in the orbital basis for band structure calculations within the jj- coupling scheme. The scale of SC pairing energies is much smaller than band energies and therefore it is the 'pseudo-spin' degrees of freedom connected with Kramers degeneracy of quasiparticle band states which are involved in the singlet and triplet pair wave functions. Therefore the pseudo-spins may be assumed to have an effectively weak (pseudo-)spin orbit coupling, and then no contradiction between the existence of line nodes and SC pairing in triplet states for U-compounds appears. We note however that ironically, in UPd₂Al₃, which is the one U compound where the spin fluctuation model is known to be inappropriate probably a singlet SC pair state is realised.

In a series of papers the spin fluctuation mechanism has also been studied within the non-retarded strong-coupling Eliashberg approach [151–154] including the frequency dependence of the pairing interaction and assuming a simple tight binding band with n.n. and n.n.n hopping t and t' respectively for conduction electrons. The frequency dependence is especially important close to a magnetic QCP when the typical energy of spin fluctuations becomes comparable to $2\pi T_c$. Instead of starting from a microscopic model Hamiltonian, a phenomenological effective interaction kernel $V(\mathbf{q}, \omega)$ was used as input for the Eliashberg equation which determines the quasiparticle self energy $\Sigma(\mathbf{k}, i\omega_n)$ and anomalous self energy ('gap function') $\Delta(\mathbf{k}, i\omega_n)$. For singlet ($S=0$) and triplet ($S=1$) pairing it is given in the AF case by

$$\begin{aligned}
 V_S(\mathbf{q}, \omega) &= a_S I^2 \chi(\mathbf{q}, \omega) \quad \text{with } a_0 = -1 \text{ and } a_1 = \frac{1}{3} \\
 \chi(\mathbf{q}, \omega) &= \frac{\chi_0 \kappa_0^2}{\kappa^2 + \hat{q}^2 - i \frac{\omega}{\eta(\hat{q})}} \quad \text{where } \eta(\hat{q}) = T_{sf} \hat{q}_-, \quad \hat{q} = \hat{q}_+ \\
 \hat{q}_\pm^2 &= (4 + 2\alpha_m) \pm 2[\cos q_x + \cos q_y + \alpha_m \cos q_z]
 \end{aligned} \tag{45}$$

Here κ and κ_0 denote the nearly critical and background inverse magnetic correlation lengths respectively (in units of the inverse lattice spacing a^{-1}). In Stoner-RPA theory $\kappa_0^2/\kappa^2 = (1 - I\chi_0)^{-1}$ and $\kappa_0 \sim 2k_F a$. This interaction is mediated by *overdamped* spin fluctuations since the pole of $\chi(\mathbf{q}, \omega)$ is at a purely imaginary frequency, i.e. the spin excitation does not have a real group velocity and therefore is not propagating. This is a natural assumption close to the QCP where the restoring force for spin excitations due to the molecular field breaks down. It is completely different from the phonon case and also the magnetic exciton mechanism discussed later which are both characterised by the exchange of propagating bosons which have a real frequency bigger than the line width. In eq.(45) α_m determines the crystal anisotropy of the spectrum, it is of 2D character when $\alpha_m = 0$ and 3D character for $\alpha_m = 1$. It is still fully isotropic in (pseudo-) spin space as evident from the singlet and triplet classification. According to eq.(45) the interaction in the AF case peaks at the zone boundary vector \mathbf{Q} with a spread given by κ (κ = inverse magnetic correlation length ξ_m^{-1}) and a frequency maximum at $\omega_{max} = \eta(\hat{q}) \kappa^2$. The same type of expression holds for FM spin fluctuations where one has to replace $\hat{q} = \hat{q}_-$. Using the effective pairing in eq. (45) the Eliashberg equation for the gap function $\Delta(\mathbf{k}, i\omega_n)$ (ω_n = Matsubara frequencies) is

$$\Lambda(T) \Delta(\mathbf{k}, i\omega_n) = a_S \frac{T}{N} \sum_{\omega_m} \sum_{\mathbf{k}} \chi(\mathbf{k} - \mathbf{q}, i\omega_n - i\omega_m) |G(\mathbf{q}, i\omega_m)|^2 \Delta(\mathbf{q}, i\omega_m) \tag{46}$$

where $G(\mathbf{q}, i\omega_m)$ is the quasiparticle Green's function renormalised by the normal self energy $\Sigma(\mathbf{q}, i\omega_m)$ that satisfies a similar equation. The solution of this set of self consistent equations determines T_c via the condition that the eigenvalue $\Lambda(T_c) = 1$. The fixed parameters of the model are t, t' (hopping elements), κ_0 (inverse background correlation length), and T_{sf} (spin fluctuation energy scale). The critical temperature $T_c(\lambda, \kappa)$ is studied as function of the dimensionless coupling constant $\lambda = I^2\chi_0/t$ and the inverse magnetic correlation length κ which determines the width of the AF spin fluctuation peak in \mathbf{k} -space. In reality this parameter may be varied experimentally by applying pressure, i.e. tuning the distance to the magnetic QCP where $\kappa = 0$. In the spirit of Ginzburg-Landau theory, at T_c the gap function should belong to a single representation Γ of the spatial symmetry group whose \mathbf{k} -dependence is characterised by the basis function $\Phi_\Gamma(\mathbf{k})$. The stable SC state is the one which has the highest T_c among the representations Γ and pair spins $S = 0, 1$. The $T_c(\lambda, \kappa)$ variation of the stable state may then be calculated. This has been done e.g. for the $d_{x^2-y^2}$ -state in the 2D case appropriate for cuprates, or, with suitable redefinition of bandwidth and T_{sf} also for CeCoIn_5 . Without going to great detail the essential results with the above procedure can be summarised as follows [151–153]:

- When $\mathbf{Q} = 0$ (FM) the p-wave state ($S=1$) is favored (has the largest T_c) and for the AF $\mathbf{Q} = (\frac{1}{2}, \frac{1}{2})$ (2D) or $\mathbf{Q} = (\frac{1}{2}, \frac{1}{2}, \frac{1}{2})$ (3D) the d-wave state ($S=0$) is preferred.
- In both cases T_c increases monotonously with coupling constant λ for any κ . For constant λ it first increases with κ and reaches a maximum at $\kappa^2 \simeq 0.5$ and then shows slow monotonic decrease with κ . When λ decreases the optimum T_c position moves towards $\kappa = 0$, i.e. to the AF QCP.
- Generally the achievable T_c 's under equal conditions are larger in 2D than in 3D, and they are much larger for AF spin fluctuations leading to even pair states as compared to FM spin fluctuations associated with the odd SC states. The latter also depend more strongly on parameters, e.g. on κ .

This result is somewhat counter-intuitive: In the FM case the effective interaction in real space is purely attractive while it is oscillating in the AF case. However as mentioned above, for triplet pairing only longitudinal spin fluctuations contribute, leading to the reduction factor $a_1=1/3$ in eq. (45) whereas in the AF singlet pairing case the additional transverse contributions lead to $|a_0|=1$. This advantage of singlet pairing depends on the isotropy of the effective interaction in spin space. In the opposite limit with maximal Ising type anisotropy in spin space, the disadvantage of triplet pairing is removed as will be discussed in sect. 5.2.

4.2 T_c -DEPENDENCE ON SPECTRAL PROPERTIES OF SPIN FLUCTUATIONS

In the above considerations the change of T_c under variation of global interaction parameters and characteristics is considered. This does not answer the question how the variation of the spectrum of spin fluctuations for a specific \mathbf{q}^* and ω_0 influences T_c , specifically one would like to know which parts of the spectrum are most favorable for achieving a large T_c for a given pair state. For the electron-phonon superconductor this has been first investigated in [155]. It was found that every part of the e-ph interaction function $\alpha^2F(\omega)$ contributes positively with $2\pi T_c$

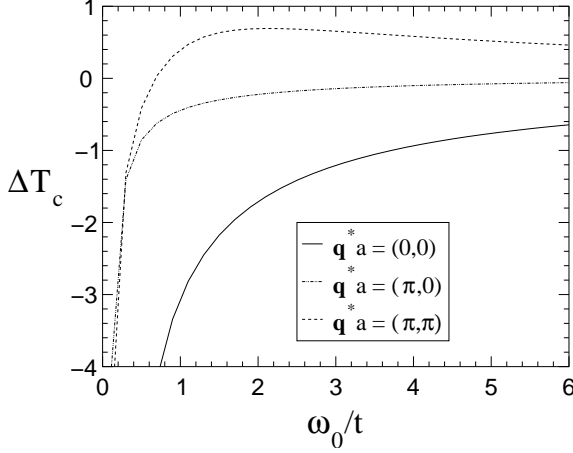


Figure 24: Dependence of ΔT_c on spin fluctuation frequency ω_0 (t = hopping energy) for various momenta \mathbf{q}^* in the 2D AF case with $\mathbf{Q} = (0.5, 0.5)$ (in r.l.u.). Coupling constant $\Gamma^2 \chi_0/t = 10$; $\kappa^2 = \xi_m^{-2} = 0.5$, $\kappa_0^2 = 12$ and $T_{sf} = 0.67t$. Only spin fluctuations at $\mathbf{q}^* = (\pi/a, \pi/a) \equiv \mathbf{Q}$ or close to \mathbf{Q} contribute positively to T_c above the crossover frequency $\omega_{cr}(\mathbf{q}^*) \simeq 0.5t$. Below $\omega_{cr}(\mathbf{q}^*)$ they are pair breaking. [154].

being the optimum phonon frequency while phonons with frequencies much larger or much smaller frequencies contribute little to T_c .

This analysis has been extended later [156] to the spin fluctuation model for HF systems, albeit using an unrealistic effective interaction that factorises with respect to frequency and momentum. As a main result it was found that, for any momentum \mathbf{q} , adding spectral weight below a crossover frequency ω_{cr} reduces T_c , i.e. low energy spin fluctuations act pair breaking. However a subsequent analysis by McHale and Monthoux [154] using the more realistic effective interaction in eq. (45) has modified this picture considerably. By adding an infinitesimal amount of spectral weight to $\chi(\mathbf{q}, \omega)$ at fixed wave vector \mathbf{q}^* and frequency ω_0 and $-\omega_0$, i.e. adding two delta-functions, the change in the critical temperature $\Delta T_c(\mathbf{q}^*, \omega_0)$ was computed numerically. A representative result in 2D for three different \mathbf{q}^* is shown in fig. 24 for the nearly AF spin fluctuation spectrum with 2D incipient ordering vector $\mathbf{Q} = (\frac{1}{2}, \frac{1}{2})$. It clearly shows that the effect of the added intensity to the spectrum also depends strongly on \mathbf{q}^* , i.e. where it is added in the BZ, in addition to the ω_0 dependence. For $\mathbf{q}^* = (0,0)$ or $(\frac{1}{2}, 0)$ which are far away from the AF $\mathbf{Q} = (\frac{1}{2}, \frac{1}{2})$ the added intensity reduces T_c for all frequencies ω_0 . Only when it is added at the incipient ordering wave vector \mathbf{Q} or close to it one has $\Delta T_c > 0$ for frequencies $\omega > \omega_{cr}(\mathbf{q}^*)$. The crossover frequency ω_{cr} from pair breaking to pair formation therefore strongly depends on the wave vector \mathbf{q}^* of the added intensity relative to \mathbf{Q} . Sufficiently far away from their spectral maximum at \mathbf{Q} spin fluctuations with *all* frequencies ω_0 are pair breaking ($\Delta T_c(\mathbf{q}^*, \omega_0) < 0$). The pair forming fluctuations are constrained to the region around \mathbf{Q} which means that the pairing occurs mostly through the short range magnetic fluctuations, except very close to the QCP ($\kappa \rightarrow 0$). The analysis again shows that $\Delta T_c(\mathbf{q}^*, \omega_0)$ is much more robust in the AF case as compared to FM case ($\mathbf{Q} = 0$). From the $\Delta T_c(\mathbf{q}^*, \omega_0)$ curves in the AF case it is also found that the optimum ω_0 where ΔT_c is largest lies above the spectral maximum of $\chi(\mathbf{q}, \omega)$ for $\kappa^2 \ll 1$ (nearly critical case) and vice versa for $\kappa^2 \gg 1$. Despite the complications the optimum ω_0 is of the same order of magnitude given by $2\pi T_c$ as for the electron-phonon mechanism.

These results show that the formation of the SC state is not determined by the very low energy critical spin fluctuations which are responsible for the NFL anomalies in compounds like CePd_2Si_2 . It explains qualitatively why compounds like CeCu_2Ge_2 or CeRh_2Si_2 which exhibit LFL behaviour around the critical pressure for destruction of AF order may nevertheless be spin fluctuation mediated superconductors (see also sect. 3.3).

The previous analysis also suggests another reason why triplet pairing should be relatively scarce. In strongly correlated electron systems not too close to a QCP dominant spin fluctuations involve mostly nearest neighbors, i.e. they have wave vectors \mathbf{Q} at the zone boundary, these are however triplet-pair breaking for all frequencies in the spin fluctuation mechanism. Considering this fact and the observation that most U-based HF superconductors seem to have triplet pairs it seems doubtful whether the spin fluctuation model is appropriate for them and one has to think about other possibilities.

4.3 MAGNETIC EXCITON MECHANISM FOR SUPERCONDUCTIVITY IN U- BASED HF COMPOUNDS

The origin of mass enhancement in Ce- and U-based compounds is not the same as explained in sect. 2. This is due to the multiple 5f-shell occupation and strongly orbital dependent hybridisation in U compounds which, in some cases like UPd₂Al₃, UPt₃ and possibly UBe₁₃ leads to a partly itinerant and partly localised nature of 5f electrons. In a strong-coupling theory for the quasiparticles, mass enhancement and effective pair interactions are two sides of the same coin. Therefore we discuss now the origin of SC pairing within the dual model of 5f electrons. This idea has been proposed and explored to some extent in [157–159] for UPd₂Al₃ as discussed further in sect. 5.2.

In the dual model the localised 5f² electrons occupy specific total angular momentum orbitals which are split by the CEF. For simplicity we consider only the two lowest CEF states which are assumed to be nonmagnetic singlets. They are then described by a pseudo-spin ($S=\frac{1}{2}$) variable where $S_z = \pm\frac{1}{2}$ correspond to singlet CEF states with energies $\pm\frac{\delta}{2}$. They have an effective inter- site coupling (superexchange) as well as a coupling to the itinerant 5f electrons of the conduction band $\epsilon_{\mathbf{k}}$. The latter couples only with the σ_z - conduction electron spin component due to the (Ising-type) anisotropy introduced by the singlet CEF states which have only transition matrix elements for the local S_x pseudo-spin operator. This dual 5f-model is described by [159]

$$H = \sum_{\mathbf{k}\sigma} \epsilon_{\mathbf{k}} c_{\mathbf{k}\sigma}^\dagger c_{\mathbf{k}\sigma} + \delta \sum_i S_{iz} - J_{ff} \sum_{\langle ij \rangle} S_x^i S_x^j - I \sum_i \sigma_{iz} S_{ix}. \quad (47)$$

The localised part may be diagonalised separately. Due to the effective inter-site interaction $J(\mathbf{q})$ which contains the superexchange J_{ff} and a RKKY contribution from the last term the local CEF excitations at an energy δ evolve into propagating magnetic exciton modes with a dispersion given by

$$\omega_E(\mathbf{q}) = \delta \left[1 - \frac{J(\mathbf{q})}{2\delta} \tanh \frac{\beta}{2} \delta \right] \quad (48)$$

If $J(\mathbf{q})$ has its maximum $J_e = J(\mathbf{Q})$ at an AF zone boundary vector \mathbf{Q} the mode frequency becomes soft at \mathbf{Q} at the Néel temperature where induced AF appears;

$$T_N = \frac{\Delta}{2 \tanh^{-1}(\frac{1}{\xi})} \quad \xi = \frac{J_e}{2\Delta} \quad (49)$$

provided one has $\xi > 1$ for the control parameter. In reality the softening will be arrested at a finite magnetic exciton gap due to the effect of higher lying CEF states which may shift T_N

slightly to higher temperatures. The magnetic excitons associated with the localised 5f system may be seen in INS as discussed for UPd₂Al₃ in sect. 5.2. For $T \ll \delta$ they are bosonic modes like phonons and then a canonical transformation on eq. (47) leads to a more convenient dual model Hamiltonian [159]

$$H = \sum_{\mathbf{k}\sigma} \varepsilon_{\mathbf{k}} c_{\mathbf{k}\sigma}^\dagger c_{\mathbf{k}\sigma} + \sum_{\mathbf{q}} \omega_E(\mathbf{q}) (\alpha_{\mathbf{q}}^\dagger \alpha_{\mathbf{q}} + \frac{1}{2}) - I \int d\mathbf{r} \psi_\alpha^\dagger(\mathbf{r}) \sigma_{\alpha\beta}^z \psi_\beta(\mathbf{r}) \phi(\mathbf{r}) \quad (50)$$

where $c_{\mathbf{k}\sigma}^\dagger$ and $\alpha_{\mathbf{q}}^\dagger$ create conduction electrons and magnetic excitons respectively and $\psi_\alpha^\dagger(\mathbf{r})$, $\phi(\mathbf{r})$ are the associated field operators. It is indeed very similar to the electron-phonon Hamiltonian, except that magnetic excitons do not couple to the electronic density but (in this simplified model) only to the z-component of the itinerant spin density. The resulting normal self energy of conduction electrons due to dressing by virtual magnetic excitons has been discussed before. Complementary virtual exchange processes involving magnetic excitons lead to an effective quasiparticle interaction given by ($v_n = 2\pi nT$) [159]

$$\hat{V}(\mathbf{q}, i\nu_n) = -I^2 D^0(\mathbf{q}, i\nu_n) \hat{\sigma}^z \hat{\sigma}^z = \left(\frac{I^2 \Delta}{2} \right) \frac{\hat{\sigma}^z \hat{\sigma}^z}{v_n^2 + \omega_E(\mathbf{q})^2} \quad (51)$$

This effective pairing breaks spin rotational symmetry in a maximal (Ising type) manner. This is enforced by the anisotropy of the CEF states and has important consequences for the classification of SC pair states, one now has to use the equal spin pairing (ESP) states $|\chi\rangle = |\uparrow\uparrow\rangle$ and $|\downarrow\downarrow\rangle$, and opposite spin pairing (OSP) states, given by

$$|\chi\rangle = \begin{cases} \frac{1}{\sqrt{2}} (|\uparrow\downarrow\rangle - |\downarrow\uparrow\rangle) \\ \frac{1}{\sqrt{2}} (|\uparrow\downarrow\rangle + |\downarrow\uparrow\rangle) \end{cases} \quad (52)$$

This aspect is completely different from the previous spin fluctuation theory which leads to a spin rotationally invariant pairing potential and the pair states are classified as (pseudo-) spin singlet ($S = 0$) and triplet ($S = 1$) states. As a consequence, because $p = \langle \chi | \hat{\sigma}^z \hat{\sigma}^z | \chi \rangle$ is +1 for ESP and -1 for OSP respectively, the coupling strength of the effective potential in eq. (51) is equal for OSP and ESP states, in contrast to the enhancement factor 3 of singlet vs. triplet pair interaction in the spin fluctuation model. Thus the present mechanism with its Ising type spin anisotropy in eq. (51) does not disfavor the odd parity states over even parity states, in fact they may be degenerate as will be discussed for a concrete case in UPd₂Al₃.

The magnetic exciton mediated pairing mechanism is due to the interaction between itinerant 5f electrons caused by the exchange of excitations within the localised 5f-CEF states. On one hand it is similar to the electron-phonon mechanism because propagating modes are involved and not overdamped spin fluctuations, on the other hand it is repulsive in the s-wave channel and contains the conduction electron spin variables leading to the possibility of unconventional or nodal pair states.

5 U- BASED HF SUPERCONDUCTORS

Most ambient pressure HF superconductors are intermetallic U compounds like UBe₁₃ [160], UPt₃ [161], URu₂Si₂ [162], UPd₂Al₃ [163] and UNi₂Al₃ [164]. This may partly be caused by

the enhanced delocalisation of 5f as compared to 4f electrons. Due to the multiply occupied 5f shell in U which hosts between two and three electrons, the origin of heavy electron mass enhancement in U compounds is in fact quite different as compared to Ce compounds with nearly singly occupied 4f orbitals. In the latter, heavy quasiparticles originate from coherent resonant scattering in the Kondo lattice [4]. For some U-HF systems however the dual, i.e. localised and itinerant nature of 5f electrons in different orbitals generates the mass enhancement [28, 29] (sect. 2) and may also dominate the SC pairing mechanism. The AF QCP scenario so prevalent in Ce-compounds is not of general importance in U-based HF superconductors with the possible exception of UBe_{13} . One rather observes that SC phases in U-compounds are embedded in a region of reduced moment AF order. In the more recently discovered FM U-based superconductors like UGe_2 or URhGe however QCP of FM or even hidden order may indeed be associated with the observed unconventional SC phases. On the other hand these superconductors are not really HF materials as witnessed by their low γ -values and they will not be discussed here.

In this review we shall not give a complete overview on U-based HF superconductors but shall focus on two examples, $\text{U}_{1-x}\text{Th}_x\text{Be}_{13}$ and UPd_2Al_3 where new results have been obtained recently. Some of the other classical U-compounds, notably the unique multicomponent superconductor UPt_3 are reviewed in [6, 8, 9] while URu_2Si_2 is reviewed in [6].

5.1 MULTIPHASE SUPERCONDUCTIVITY IN THE NON-FERMI LIQUID COMPOUND $\text{U}_{1-x}\text{Th}_x\text{Be}_{13}$

The cubic Be-cage compound UBe_{13} was the second HF superconductor discovered [160, 165] but remains only partly understood. The SC transition takes place in a normal state with pronounced NFL behaviour, as can be seen from the C/T behaviour for fields above H_{c2} . The thorated UBe_{13} has a complicated x-T phase diagram with two distinct SC phases and possibly a coexisting magnetic phase. In fact it is surprising that SC survives up to about $x = 0.06$ since the potential scattering of normal Th impurities should lead to a strong pair breaking for an unconventional SC state and an ensuing a rapid reduction of T_c . Instead a pronounced non-monotonic behaviour of $T_c(x)$ is found. The x-T phase boundaries are still partly a conjecture and may have to be revised according to recent flux creep experiments [166]. The most interesting issue is doubtlessly the origin of small magnetic moments in the low temperature SC phase (C) in the regime $0.02 < x < 0.045$. They may either be caused by a non-unitary SC C-phase which breaks time reversal symmetry as suggested by μSR experiments [167] or they may be associated with the formation of a long range SDW order suggested by thermal expansion experiments [168–170]. Theoretically the former scenario has been explored within the context of a Ginzburg-Landau approach assuming that the $T_c(x)$ of two distinct SC phases cross [5]. The SC/SDW scenario on the other hand has been theoretically proposed in [171]. It should be noted however that assumptions on the gap function symmetry remain purely speculative. Even in the pure UBe_{13} it is not known although the presence of nodes in the gap function and hence its unconventional nature is assured, e.g. from the existence of a zero-bias conductance peak in tunneling experiments [172] which provides evidence for a sign change of the gap function $\Delta(\mathbf{k})$.

5.1.1 ELECTRONIC STRUCTURE AND NFL-LIKE NORMAL STATE

The 5f states in UBe_{13} show both signatures of localisation and itineracy. On one hand the 5f- orbital energy is close to the Fermi level according to photoemission results. This disfavors the Kondo picture with a localised $5f^3$ configuration as origin of the extremely large mass enhancement characterised by $\gamma = 1100 \text{ mJ/mol K}^2$ corresponding to a quasiparticle band width of $T^* \simeq 8 \text{ K}$. LDA calculations [173] with fully itinerant 5f electrons however lead to only $\gamma_b = 13 \text{ mJ/mol K}^2$ implying a large many body enhancement factor of $m^*/m_b = 85$. The Fermi surface consists of two closed hole sheets with nesting properties and one closed electron sheet.

On the other hand Schottky-type specific heat anomalies [174] suggest the presence of CEF excitations $\simeq 180 \text{ K}$ out of a $\Gamma_6(5f^3)$ Kramers doublet ground state. An alternative model [175] assuming a nonmagnetic $\Gamma_3(5f^2)$ ground state can be ruled out because it predicts the wrong sign of the nonlinear susceptibility $\chi^{(3)}(T)$ at low temperatures [176]. A mixed valent model involving both nonmagnetic Γ_3 and magnetic Γ_6 doublets has also lead to the conclusion that the ground state must be the magnetic Γ_6 to obtain qualitative agreement with the observed $\chi^{(3)}(T)$ behaviour [177]. In the pure Γ_6 picture the Kondo effect would lead to a LFL state with enhanced m^* . However a further temperature scale below T^* given by $T_m \simeq 2 \text{ K}$ has been found from a clear maximum structure in resistivity, specific heat and thermal expansion [169, 170]. This indicates that UBe_{13} has not yet reached a true LFL state when SC sets in at $T_c \simeq 0.9 \text{ K}$. Indeed for fields above H_{c2} a pronounced NFL behaviour with logarithmic increase in $\gamma(T)$ and no saturation to the lowest temperatures has been observed [178, 179] in UBe_{13} . In addition a universal field-independent $\rho(T)/\rho_{1K}$ behaviour is observed for $T \geq 1.2K$ and $4T \leq H \leq 10T$ in the normal state. One finds $\rho(T) \sim T$ at elevated and $(\rho(T) - \rho_0) \sim T^{3/2}$ at lower T [179, 180]. The origin of NFL behaviour may reside in the vicinity of a QCP for SDW or possibly hidden order, this would be in accordance with the nesting properties of electronic bands in UBe_{13} and with the evolution of $T_m(x)$ which hits the maximum of $T_c(x)$ in $\text{U}_{1-x}\text{Th}_x\text{Be}_{13}$ as concluded from resistivity measurements [169, 170]. Another possibility is provided by the $T_m(B^*)$ dependence, implying $T_m \rightarrow 0$ for $B^* \rightarrow 5T$ (fig. 25), i.e. a field-induced QCP of short-range AF correlations [179].

5.1.2 THE SUPERCONDUCTING PHASE DIAGRAM OF $\text{U}_{1-x}\text{Th}_x\text{Be}_{13}$

The symmetry of the SC state in pure UBe_{13} is not known with any confidence, but its anisotropic nature is suggested by power law behaviour of specific heat, penetration depth and NMR relaxation and by tunneling results mentioned before. As usual from the power law exponents no consensus has emerged whether the gap function is characterised by point or line nodes and therefore we do not discuss these results. A strong indication of nonconventional SC is obtained from a giant ultrasonic absorption anomaly immediately below T_c [181, 182] which was attributed to damping by domain walls formed by a multicomponent SC order parameter [5]. Also the B-T phase diagram (fig. 25) is quite anomalous, it exhibits a line of anomaly $B^*(T)$ deep in the SC regime which starts at $T_L(x=0) = 0.7 \text{ K}$ signifying the onset of short range AF correlations. As function of x they eventually develop into a long range SDW order discussed below. The SC phase diagram of thoriated $\text{U}_{1-x}\text{Th}_x\text{Be}_{13}$ ($x \leq 0.1$) has required a great effort to unravel and the task is still not finished. It displays a bewildering richness of different phases and lines of anomalies which have been obtained mostly from specific heat, resistivity and ther-

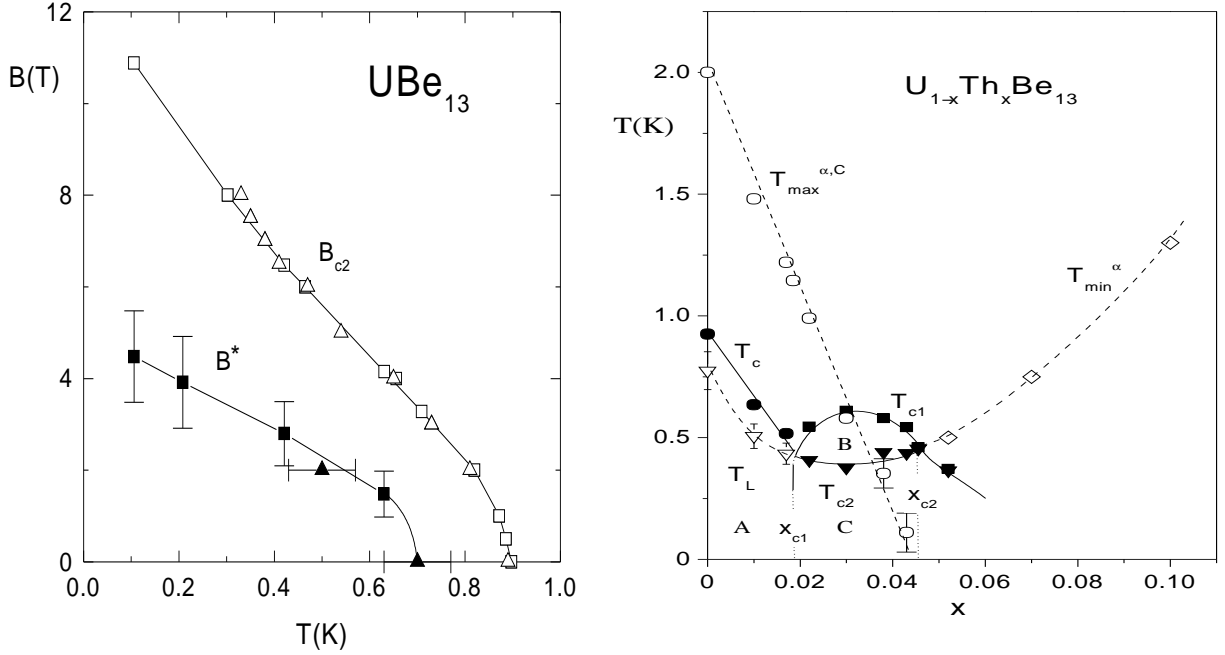


Figure 25: Left panel: B-T phase diagram of UBe_{13} with additional anomaly line $B^*(T)$ obtained from specific heat (squares) and thermal expansion (triangles) experiments. Right panel: SC phase diagram of $\text{U}_{1-x}\text{Th}_x\text{Be}_{13}$. Full lines and symbols denote boundaries of different thermodynamic phases, broken lines and open symbols denote lines of anomalies. T_L and T_{\min}^{α} are anomaly lines obtained from the minimum in thermal expansion $\alpha(T)$. $T_{\max}^{\alpha,C} \equiv T_m$ is the line of anomalies from the maximum in $C(T)$ and $\alpha(T)$. A, B and C are the distinct SC phases in the T_c -crossing model. [169, 170, 183]

mal expansion (magnetostriction) measurements [169, 170]. The salient feature of the phase diagram is a nonmonotonic variation of the $T_c(x)$ curve with a cusp at $x_{c1} \approx 0.02$ and associated with it a splitting in two SC transitions $T_{c1}(x)$ and $T_{c2}(x)$ in the range $x_{c1} < x < x_{c2}$ with $x_{c2} \approx 0.045$ [184]. This leads to three distinct SC regions A, B and C in the x - T plane. When crossing from B to C, H_{c1} exhibits a sudden change in slope [185] and small magnetic moments $\mu \simeq 10^{-3} \mu_B$ seen in μSR experiments [167] appear which are absent below x_{c1} (A) and above x_{c2} . There are presently two distinct scenarios, denoted by I and II, to explain these observations.

(I) The T_c -crossing model

The most widely accepted interpretation has been given quite early in [5, 186] in terms of a Ginzburg-Landau model involving only SC order parameters. The fundamental assumption is that two SC phases with gap functions belonging to different representations, e.g. Γ_1 and Γ_5 of the cubic symmetry group O_h , have close transition temperatures $T_c(\Gamma_1, x)$ and $T_c(\Gamma_5, x)$ which cross at a critical concentration x_{c1} . Below x_{c1} $T_c(\Gamma_5, x) > T_c(\Gamma_1, x)$ and the unconventional Γ_5 (A) phase which has gap nodes is stable. Above x_{c1} the inequality is reversed and the conventional (fully symmetric) Γ_1 (B) phase is stable immediately below $T_{c1} = T_c(\Gamma_1, x)$. For lower temperatures ($T < T_{c2}(x)$) higher order mixing terms in the GL free energy functional stabilise a mixed $\Gamma_1 \otimes \Gamma_5$ (C) SC phase with a different H_{c1} , hence the observed kink. The C- phase gap

function may be non-unitary and time reversal symmetry breaking, thus leading to condensate magnetic moments induced around impurities and defects which allegedly have been observed in the μ SR experiments. For even larger concentrations enhanced pairbreaking or the reduction of the spin excitation energy scale $T_m(x)$ involved in pair formation leads to a decrease in $T_c(\Gamma_1, x) = T_{c1}$ and a second crossing point appears. However a GL expansion around x_{c1} cannot naturally explain the second crossing.

(II) *The SC/SDW coexistence model*

An alternative scenario to explain the phase diagram in fig. 25 (right panel) has appeared as a result of investigations of the differential thermal expansion $\alpha = l^{-1} \partial l / \partial T$ [169, 170]. In this explanation the SC phases A and B are assumed as identical unconventional SC phases as inferred from the almost equal pressure dependence away from the critical x_{c1} . In phase C the SC order parameter is unchanged by a SDW modulation which appears within the unconventional SC phase. This was previously already proposed theoretically in [171] within the context of a model calculation for coexistence of a necessarily unconventional SC and a SDW phase. The moments seen in the C phase are then associated with the SDW. The main reason for this alternative interpretation of the x-T phase diagram is the discovery of a new line of anomaly $T_L(x)$ in $\alpha(T)$ for subcritical $x < x_{c1}$ which starts at a $T_L(0)$ identical to the temperature for which $B^*(T) = 0$ as seen in the B-T phase diagram. With growing x the $\alpha(T)$ anomaly becomes increasingly sharp and $T_L(x)$ exactly joins the T_{c2} line at x_{c2} . This suggests to interpret $T_L(x)$ as the onset temperature of short range magnetic correlations which turn into the long range SDW state at x_{c1} . The $\alpha(T)$ anomaly line is seen to continue even far above x_{c2} . The shape of the $\alpha(T)$ anomaly above x_{c1} is indeed familiar from other magnetic transitions. It is also in accord with the interpretation of a huge (Cr-type) anomaly in the ultrasonic attenuation [187]. The SC/SDW coexistence scenario lacks however a natural explanation for the observed kink in H_{c1} at T_{c2} .

Recent flux-creep experiments [166, 188] have further complicated the picture. A steep drop in the flux creep rate was observed below T_{c2} which may naturally be explained within the T_c -crossing model because the nonunitary C-phase may have domain walls which pin vortices very effectively [189]. Using this effect for mapping out the C/A-phase boundary it was found that contrary to the original view shown in fig. 25 the C-phase boundary is not perpendicular at x_{c1} but rather has a low temperature tail extending down to $x = 0$, i.e. the drop in flux creep indicating a transition into the C-phase is even seen in pure UBe_{13} .

5.2 NODAL SUPERCONDUCTIVITY IN UPd_2Al_3 MEDIATED BY MAGNETIC EXCITATIONS

Since its discovery in 1991 by Geibel et al. [163] the extensive experimental studies on this antiferromagnetically ordered moderate HF superconductor (see table 4) have lead to two important conclusions: Firstly the 5f electrons have a dual nature, partly localised and partly itinerant where the former carry the magnetic moments and the latter become superconducting [190, 191]. Secondly there is now compelling evidence that the internal low energy excitations of the localised 5f subsystem mediate an effective pairing potential between the itinerant electrons. This leads to a superconducting state which has an anisotropic gap function with line

nodes [157]. Moreover the virtual low energy excitations of localised 5f electrons lead to a quasiparticle mass enhancement factor m^*/m_b which is thought to be the origin of the normal HF state of UPd_2Al_3 [29]. Indeed this new mechanism gives consistent T_c and mass enhancement factor within a strong coupling approach based on a dual 5f electron model Hamiltonian [159]. As discussed in sect. 4, HF superconductivity is assumed to exhibit a non-phononic SC pairing mechanism leading to nodal gap functions because the strong on-site repulsion of quasi-particles prevents the (nearly) isotropic SC state most favored by the electron-phonon mechanism. However, UPd_2Al_3 is the only case known so far where this theoretical conjecture has actually been proven by experiment. This was achieved by complementary INS [192–195] and quasiparticle tunneling experiments [196] which, respectively, probe the two aspects of the dual nature of 5f electrons: (1) The internal singlet-singlet CEF excitations ($\delta \simeq 6$ meV) of localised 5f electrons which form propagating magnetic exciton bands in the range of 1-8 meV due to inter-site interactions. (2) The tunneling current which probes the superconducting gap of itinerant 5f electrons in epitaxially grown UPd_2Al_3 - AlO_x -Pb tunneling devices. There is a considerable interaction between localised and itinerant 5f electrons signified on one hand by the appearance of a resonance in the INS scattering function associated with the SC gap. On the other hand, even more compelling is the presence of typical 'strong coupling' signatures in the tunneling DOS at about the magnetic exciton energy in the center of the AF BZ as determined in INS. This is a direct proof that the exchange of these magnetic bosons mediates the SC pairing in UPd_2Al_3 . This important new mechanism is distinctly different from both the electron-phonon and the spin fluctuation mechanism (sect.4).

5.2.1 PHYSICAL PROPERTIES

Further experimental evidence for the dual nature of 5f electrons comes from susceptibility measurements [197] above T_c where $\chi(T)$ for field perpendicular to c shows a pronounced maximum below $T = 50$ K, typical for the effect of CEF states which originate from the $5f^2$ configuration of the U^{4+} ions. The presence of localised states is also seen in Knight shift measurements [191] and optical experiments [198]. There in addition the formation of heavy itinerant quasiparticles below T^* was concluded from an analysis of the Drude peak in the optical conductivity. The low lying CEF states of localised 5f electrons are of singlet-singlet (doublet) type with a splitting $\delta \simeq 6$ meV as obtained from a fit to the overall magnetic exciton dispersion [158]. This means that the AF ordering (table 4) found below T_N is of the induced moment type. The FM ordered ab planes are stacked along c with an AF wave vector $\mathbf{Q} = (0,0,0.5)$ (r.l.u.) [199, 200] and an easy axis [100]. Moment reorientation can only be observed for fields in the ab plane and the phase diagram was determined in [200].

The superconducting state below T_c was investigated in numerous experiments, but a definite conclusion on the symmetry of the pair state has not been achieved yet. Upper critical field measurements show a flattening of $H_{c2}(T)$ for low temperatures [201] which is interpreted as the effect of Pauli limiting in a spin singlet pair state. This hypothesis was further investigated by ^{27}Al Knight shift experiments [202] which shows a considerable reduction below T_c again in favor of singlet pairing, however, the interpretation is not unambiguous due to a large local moment contributions to K_s . The ^{27}Al NMR relaxation rate T_1^{-1} was found to exhibit clear T^3 power law [202], naively interpreted as evidence for line nodes in the gap function $\Delta(\mathbf{k})$ leading

| | $\gamma [\frac{mJ}{molK^2}]$ | T_N [K] | μ [μ_B] | T_c [K] | $\frac{\Delta C(T_c)}{\gamma T_c}$ [K] | $\frac{\Delta S(T_N)}{R \ln 2}$ |
|----------------------------------|------------------------------|-----------|-------------------|-----------|--|---------------------------------|
| UPd ₂ Al ₃ | 140 | 14.3 | 0.85 | 1.8 | 1.2 | 0.67 |
| UNi ₂ Al ₃ | 120 | 4.6 | 0.20 | 1.2 | 0.2-0.4 | 0.12 |

Table 4: Material parameters of UPd₂Al₃ and its isostructural sister compound UNi₂Al₃.

to a quasiparticle DOS $\sim |E|$. This was also suggested by ¹⁰⁵Pd NMR/NQR [203]. Conclusions from the low temperature specific heat $C(T)$ which should be $\sim T^2$ for line nodes are hampered by the difficult subtraction of the nuclear contribution. A $C(T) = \gamma_0 T + aT^3$ behaviour was found where the residual value γ_0 scales with the width of the SC transition [204] that characterises sample quality. The isostructural sister compound UNi₂Al₃ is also a superconductor with co-existing incommensurate magnetic order (table 4). However, contrary to UPd₂Al₃ its 5f states have all a delocalised character as is obvious from the much smaller moment, the incommensurate ordering wave vector and the small entropy release ΔS at T_N which is only one sixth of the value in UPd₂Al₃. Therefore, superconductivity in this compound is thought to be mediated by spin fluctuations of conduction electrons rather than localised 5f excitations as in UPd₂Al₃. However, as in UPt₃, a spin triplet gap function has been proposed for UNi₂Al₃ [205] which according to NMR results should have a line node. Note that this is in conflict with the simple theory of isotropic AF spin fluctuations proposed for U-HF compounds since they would rather prefer spin singlet pairing (sect. 4) [145]. Also it suggests that Blount's theorem which predicts the absence of line nodes for strong spin-orbit coupling cannot naively be applied to real U-HF superconductors (sect. 4). Finally we note that from recent H_{c2} -measurements on epitaxially grown thin films [206] a considerable paramagnetic Pauli-limiting effect was deduced for both a and c directions which led the authors to the opposite conclusion that UNi₂Al₃ should also have a SC singlet pair state.

5.2.2 ELECTRONIC STRUCTURE, THE DUAL MODEL

Within conventional LDA type band structure calculations for UPd₂Al₃ [207–209] there is no way to treat the partly localised and partly itinerant character of 5f electrons properly, all 5f orbitals are incorporated in the basis set for the band states. While the FS topology corresponds reasonably to dHvA results [210] the effective masses of the various sheets are far too small. Even within a modified LSDA (local spin density approximation) treatment including self interaction corrections [211] the effective masses are still too small by an overall factor of ten. The dual model opens an attractive way to remove this discrepancy [29]. The coupling of itinerant 5f- electrons to the low lying discrete CEF excitations of the localised subsystem offers an effective mechanism of mass enhancement (sect. 2). In this approach the calculation of heavy bands proceeds in three steps: 1) 5f orbitals in the jj-coupling limit ($j = \frac{5}{2}$) are used and those with $j_z = \pm \frac{5}{2}, \pm \frac{1}{2}$ are excluded from the basis set of LDA bands which comprises only $j_z = \pm \frac{3}{2}$ states. The band center is fixed to obtain the correct 5f count. 2) The multiplet structure of localised states 5f is calculated using the proper intra-shell Coulomb interactions. The ground

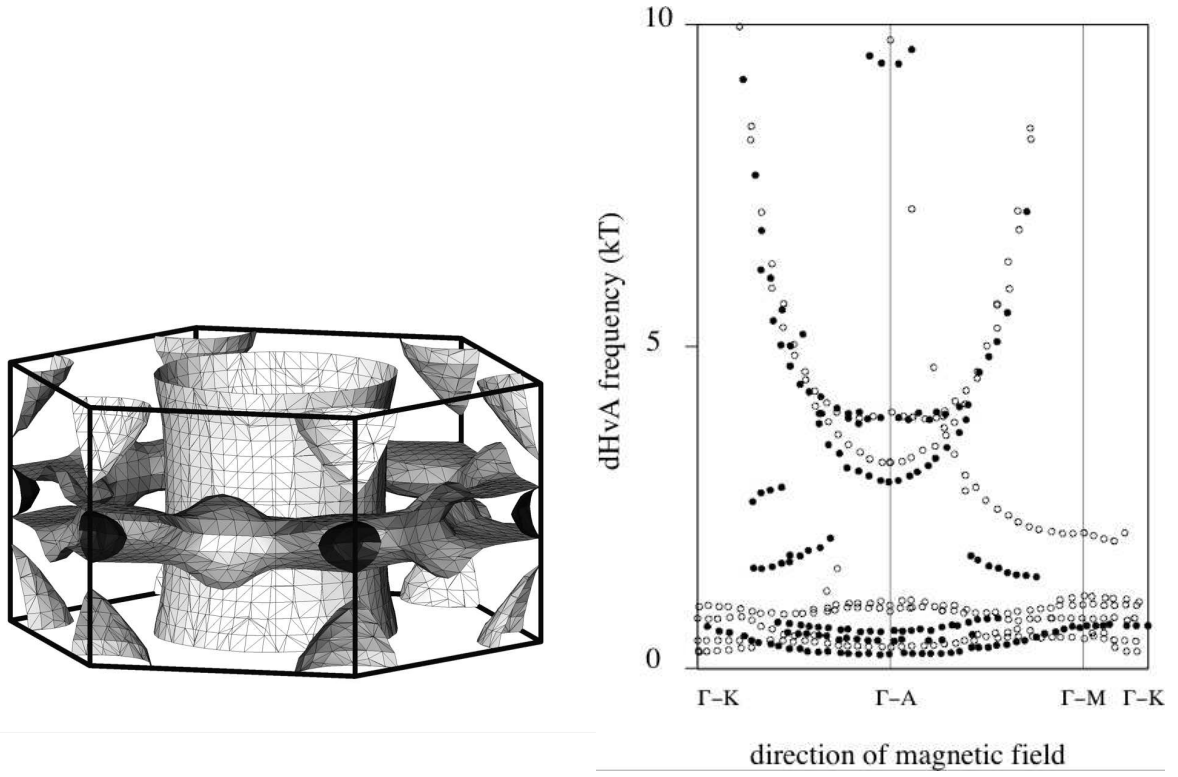


Figure 26: Left panel: Fermi surface of UPd_2Al_3 calculated within the dual model [29]. The main cylinder part has a heavy mass with $m^* = 19 - 33 m$ and the torus ('crown') has $m^* = 65 m$. Right panel: Comparison of experimental dHvA frequencies (black symbols) from [209] and calculated frequencies (open symbols) from the dual model [29]. Large parabolas correspond to the corrugated main FS cylinder. Small arc on top of Γ -A corresponds to the crown sheet.

state is a doublet $|J = 4, J_z = \pm 3\rangle$ which is further split by the CEF potential into two singlets

$$|\Gamma_{3,4}\rangle = \frac{1}{\sqrt{2}}(|J = 4; J_z = 3\rangle \pm |J = 4; J_z = -3\rangle) \quad (53)$$

The splitting energy $\delta \simeq 6 \text{ meV}$ is taken as an empirical parameter obtained from INS. 3) The scattering of localised band states from CEF excitations leads to the mass renormalisation of the former. In the simplest case, without including the dispersion which turns the localised CEF transitions with energy δ into a band of magnetic excitons and neglecting strong coupling effects the mass enhancement would be given by

$$\frac{m^*}{m_b} = 1 + 2 \frac{I^2 N(\epsilon_F)}{\delta} \quad (54)$$

with I defined in eqs. (47) and (50). A more refined treatment for $\frac{m^*}{m_b}$ appropriate for UPd_2Al_3 is described below. In this approach the different treatment of $5f$ orbitals with $j = \frac{5}{2}$ and different j_z cannot be explained on the single particle level because their hybridisation matrix elements are rather similar. The amplification of the orbital dependence of hybridisation due to many body effects has been proposed in [30] and is described in detail in sect. 2.2.

Although the starting point is indeed very different from standard LDA, with only a single delocalised 5f electron, the main FS sheets are reproduced quite well as is obvious from fig. 26. The most prominent FS sheet has the form of a slightly corrugated cylinder oriented along c . It has also a large mass enhancement of $m^*/m \simeq 33$ (m = free electron mass). In the following model discussion one may therefore restrict to this main FS sheet.

5.2.3 MASS ENHANCEMENT AND SC PAIRING DUE TO MAGNETIC EXCITONS

The great advantage of the dual model as compared to the pure LDA approach is its natural explanation of the mass enhancement factor of $m^*/m_b \simeq 10$ (m_b = LDA band mass) which is due to the contribution of virtual singlet-singlet CEF excitations to the conduction electron self energy. Assuming the value of $\delta = 6$ meV from INS the proper mass enhancement is predicted without further adjustable parameters. In addition to the mass enhancement the interaction between the subsystems leads to induced AF magnetic order [157, 158] of localised 5f moments and superconductivity in the itinerant part [157–159]. In its most rudimentary form a model Hamiltonian is given by eq. (50). In UPd_2Al_3 the conduction electrons corresponding to the main FS cylinder in fig. 26 have only dispersion $\perp c$ with $\varepsilon_{\perp \mathbf{k}} = \varepsilon_{\perp}(\mathbf{k}_{\perp}/k_0)^2$. The magnetic exciton dispersion $\omega_E(\mathbf{q})$ which originates from the $\Gamma_3 \leftrightarrow \Gamma_4$ CEF transitions given by eq. (48) is of central importance. For large T eq. (48) describes isolated CEF transitions at an energy δ which develop a dispersion at lower temperature due to an effective exchange $J(\mathbf{q})$. In this RPA expression a complete softening at the Nèel temperature T_N in eq. (49) for induced AF order is expected at the AF ordering wave vector $\mathbf{Q} = (0,0,\frac{1}{2})$. Note that, unlike spin waves the magnetic excitons which originate in singlet-singlet CEF transitions may exist already above T_N and their softening signifies the approaching induced AF order. The experimental investigation of magnetic excitons was undertaken in many INS studies [157, 194, 212, 213]. In the former the overall dispersion up to the maximum $\simeq 8$ meV was determined and theoretically analysed in [158]. The latter focused on high resolution analysis of the low energy excitations around the AF wave vector \mathbf{Q} . The result is shown in the left panel of fig. 27. Indeed, contrary to the above simple RPA singlet-singlet result a magnetic exciton gap of about 1 meV appears. This may be caused by the effect of higher magnetic CEF states whose contribution to the staggered susceptibility leads to AF order slightly before complete softening is achieved and also by self energy effects beyond RPA. The dispersion along c is much larger than in the hexagonal ab-plane which may lead to a considerable DOS for the low energy magnetic excitons around 1 meV. The spectral shape of magnetic excitons is Lorentzian above T_c and evolves into a double peak structure where the lower has the appearance of a sharp resonance within the SC gap region [157, 213]. This is a signature of the strong residual interaction between itinerant (SC) electrons and the excitations within the localised 5f subsystem. A model analysis of the INS spectra at \mathbf{Q} leads to conclude that $\Delta/\omega_E(\mathbf{Q}) \simeq 1$, i.e. SC gap amplitude and magnetic exciton gap are nearly degenerate.

Complementary evidence for this interaction was found in the quasiparticle tunneling spectra of c -axis oriented epitaxially grown UPd_2Al_3 films [196] which probe the SC electrons. The differential conductivity dI/dV of the UPd_2Al_3 - AlO_x -Pb tunneling barrier is proportional to the quasiparticle DOS $N_S(\omega)$. In the weak coupling BCS limit it shows the monotonic square root singular behaviour above $\Delta(\mathbf{k} \parallel c)$. However, retardation effects in the strong coupling limit for

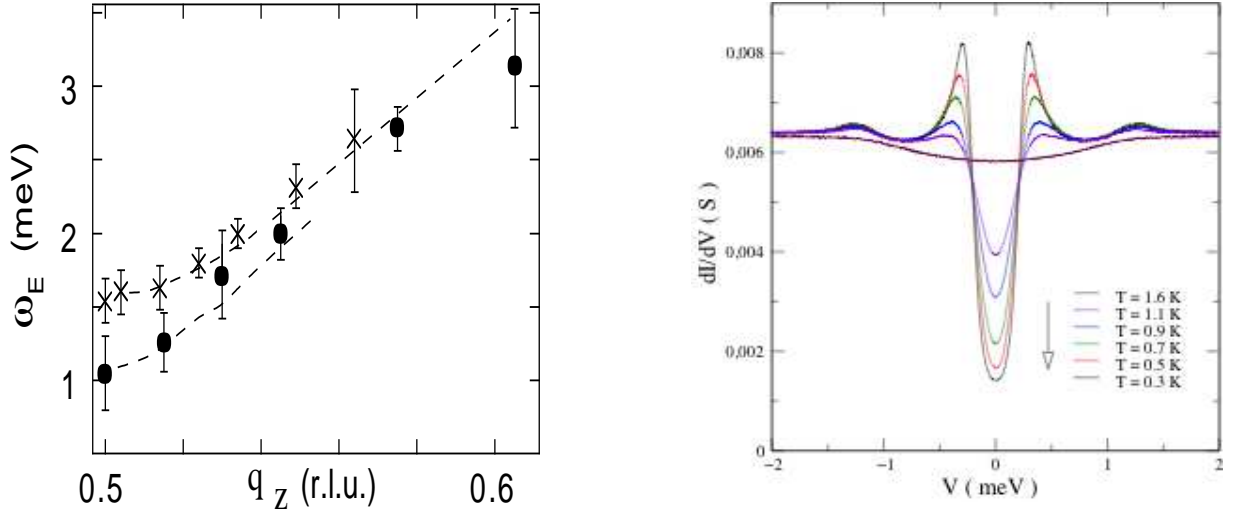


Figure 27: Left panel: Magnetic exciton dispersion $\omega_E(\mathbf{q})$ ($\mathbf{q}=(0,0,q_z)$) derived from low energy INS [157] for temperatures above (crosses) and below (circles) T_c . Right panel: Differential conductivity from tunneling for various temperatures (the arrow indicates the sequence of curves). The hump at 1 meV is a strong coupling signature of the magnetic exciton at $\mathbf{Q} = (0,0,0.5)$ (cf. left panel) which mediates Cooper pairing [196].

the effective pairing interaction lead to characteristic signatures in $dI/dV \sim N_S(\omega)$ at an energy which corresponds to typical energies of the bosons which mediate the interaction. This is well known in the case of strong-coupling electron-phonon superconductors. In their breakthrough tunneling experiment in UPd_2Al_3 Jourdan et al. [196] have for the first time seen evidence of the boson that mediates superconductivity in a HF metal. Its signature can clearly be seen in the tunneling spectra in the right panel of fig. 27 at an energy slightly above 1 meV. This is far too small for characteristic phonon frequencies, since the Debye energy is of the order 13 meV. Instead it corresponds directly to the magnetic exciton energy at the AF vector \mathbf{Q} for $T < T_c$ in the left panel. This strongly suggests that magnetic excitons mediate SC pair formation in UPd_2Al_3 . The coupling between the itinerant heavy quasiparticles and the magnetic exciton in the center of the AF BZ ($q_z = 0.5$) shows substantial retardation because the group velocity ($\partial\omega_E/\partial q_z$) of the latter is much smaller than the Fermi velocity v_F^* of heavy quasiparticles due to the flatness of $\omega_E(q_z)$ over a considerable part of the BZ along c^* [213]. Within Eliashberg theory the quasiparticle DOS can be explained by using a phenomenological retarded potential centered at $\omega_E(\mathbf{Q})$, the analysis [157] leads to the conclusion $2\Delta/T_c = 5.6$ in agreement with the gap estimate above and also with NMR results [214]. Together the two complementary results shown in fig. 27 present the first direct evidence for a non-phononic SC pairing mechanism in a HF superconductor. The magnetic exciton-mediated pairing identified here is distinctly different from both the conventional electron-phonon mechanism and the common spin-fluctuation mechanism (sect. 4) which does not involve any localised electron component.

5.2.4 SYMMETRY OF THE SC GAP FUNCTION AND ELIASHBERG THEORY

The question of the symmetry of the gap function $\Delta(\mathbf{k})$ is most difficult to resolve in unconventional superconductors, and perhaps with the exception of UPt₃ (see [6, 9] for a review) has not been unambiguously achieved for any of the HF superconductors. And yet this is very important because the nodal structure of the gap function and the associated low temperature thermodynamic and transport properties are directly determined by the symmetry class of the gap function. It was suggested [195, 215] that the INS double peak structure for $T \ll T_c$ mentioned previously requires the translational symmetry property $\Delta(\mathbf{k} + \mathbf{Q}) = -\Delta(\mathbf{k})$. Furthermore Knight shift and H_{c2} results mentioned above have lead to the proposal of a spin singlet gap with $\Delta(-\mathbf{k}) = \Delta(\mathbf{k})$. Together this suggest a gap function with node lines $\Delta(\mathbf{k}) = 0$ perpendicular to c at the AF Bragg planes $\mathbf{k} = \pm \frac{1}{2}\mathbf{Q}$ (A_{1g} in table 5). To investigate the consistency of the magnetic exciton model strong coupling calculations based on the Hamiltonian in eq. (50) have been performed [159]. Such model calculations cannot predict reliably the symmetry of the gap function, but they may decide which one is the most favorable within a restricted class of possible gap functions. In addition one may at the same time obtain the mass enhancement (m^*/m_b) of normal quasiparticles from the self energy and T_c from the Eliashberg equations. Both quantities are determined by the effective retarded potential due to magnetic exchange given in eq. (51). For simplicity we use an empirical form for $\omega_E(\mathbf{q})$ with a finite gap and no dispersion $\perp c$, given by

$$\omega_E(q_z) = \omega_E^0[1 + \beta \cos(q_z)] \quad (55)$$

The parameters ω_E^0 , α and β (fig. 28) are chosen to describe the experimental dispersion along c obtained from INS [212]. The effective interaction of eq. (51) breaks spin rotational symmetry in a maximal (Ising type) manner. As explained in sect. 4 this leads to a classification into ESP and OSP pair states with spin projection factors $p = \pm 1$. The Eliashberg equation for the gap function is then given by

$$\Lambda(T)\Delta(\mathbf{k}, i\omega_n) = p \frac{T}{N} \sum_{\mathbf{k}' \omega'_n} V(\mathbf{k} - \mathbf{k}', i\omega_n - i\omega'_n) |G(\mathbf{k}', i\omega'_n)|^2 \Delta(\mathbf{k}', i\omega'_n). \quad (56)$$

where $G(\mathbf{k}, i\omega_n)$ is the renormalised conduction electron Green's function and T_c is obtained from $\Lambda(T_c) = 1$. The result for the T_c of various gap function candidates as function of the dimensionless coupling parameter \hat{g} are shown in fig. 28. Likewise the dependence of m^*/m_b on \hat{g} which is roughly linear may be calculated. From dHvA results the enhancement factor for the main FS cylinder in fig. 26 is $m^*/m_b \simeq 10$. This would imply $\hat{g} = 2$. The corresponding theoretical value $T_c = 2.9$ K for the degenerate A_{1g} and A_{1u} states from fig. 28 is a factor 1.6 larger than the experimental value of 1.8 K. Given that the latter is reduced due to the action of static AF order, this result shows that the magnetic exciton mechanism gives both mass enhancement and a T_c which are consistent. This supports the previous empirical conjecture for this new mechanism of HF superconductivity.

The dispersion of $\omega_E(\mathbf{k})$ and hence the \mathbf{k} -dependence of the interaction is strongest along c . Therefore one may restrict to SC candidate states of the type $\Delta(\mathbf{k}) = \Delta \Phi(k_z)$ with a few possible form factors $\Phi(k_z)$ given in table 5. It is seen in fig. 28 that the A_{1g} and A_{1u} OSP spin pairing states have the highest and equal T_c 's. This degeneracy between even and odd parity

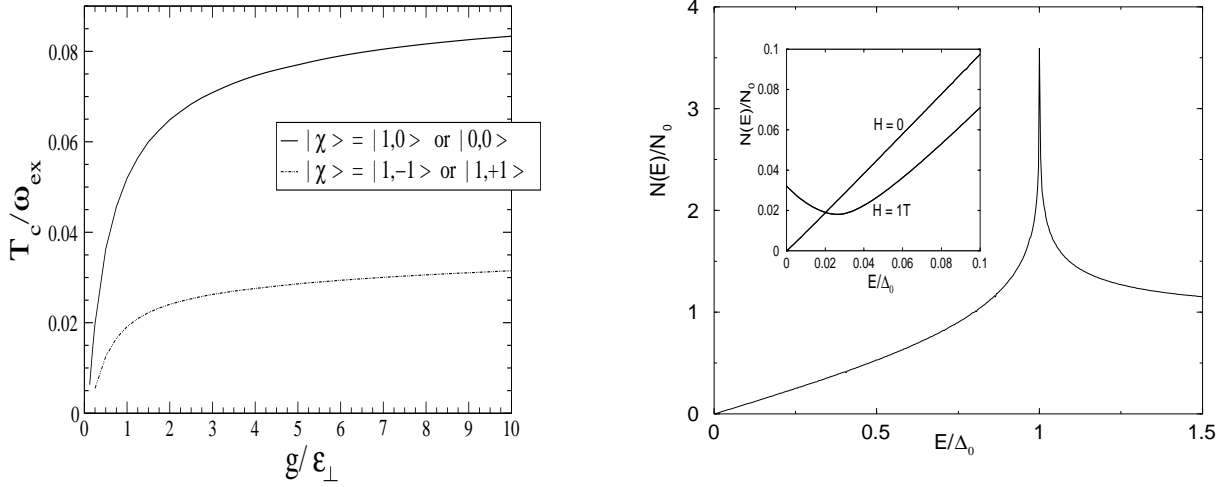


Figure 28: Left panel: Critical temperature as function of the dimensionless coupling constant $\hat{g} = g/\epsilon_{\perp} = \frac{I^2 \Delta N(\epsilon_F)}{2 \omega_E^2}$. Model parameters for $\omega_E(\mathbf{q})$ are $\omega_E^0 = 0.01 \epsilon_{\perp}$ (ϵ_{\perp} = conduction band width) and $\beta = 0.8$. Full (dashed) curve: OSP (ESP) SC states (see table 5) [159]. Right panel: DOS in the A_{1g} state of table 5 with $N(E) \sim E$ for $E \ll \Delta_0$. Inset shows the DOS for field of 1T and orientation $\parallel c$ ($\theta = 0$). Finite $N(0)$ is induced by the Doppler shift of quasiparticles and contributes to specific heat and transport [216].

states is due to the Ising type anisotropy of the effective interaction in spin space signified by their equal spin projection factors $p = -1$ (table 5). It will be lifted by the interaction of the SC order parameters with the background AF order. The respective node lines for $\Phi(\mathbf{k}_z)$ would be at $k_z = \pm\pi/c$ (zone boundary) for A_{1g} and $k_z = 0$ for A_{1u} (zone center). Note that both states have $S_z = 0$ and therefore both should show Pauli limiting of H_{c2} and a Knight shift reduction below T_c . For the odd parity state this is due to the fact that the other 'triplet' components with $S_z = \pm 1$ are not stable, i.e. the \mathbf{d} - vector is pinned along c . Note that although A_{1g} with $\Delta(\mathbf{k}) = \Delta_0 \cos k_z$ has a node line, it is not an unconventional order parameter in the strict sense since it has the full D_{6h} symmetry. The quasiparticle DOS of the A_{1g} state is shown in fig. 28 is linear for $E \ll \Delta_0$ due to the node line at $k_z = \pm\frac{\pi}{2}$. The inset shows that an external field induces a finite residual DOS at $E = 0$ according to the Doppler shift expression of eq. (42). The residual DOS depends on the field direction relative to the nodal position. This leads to a polar field-angle dependent residual $\gamma(\theta)$ -coefficient and thermal conductivity $\kappa_{ii}(\theta)$. There is no azimuthal ϕ -dependence due to cylindrical FS symmetry. The residual κ_{ii} normalised to the normal state κ_n is given by

$$\begin{aligned} \kappa_{ii}(T, \theta)/\kappa_n &= \frac{3}{4\pi^2} \frac{1}{T^3} \int_0^\infty \frac{d\omega}{\cosh^2(\omega/2T)} \hat{\tau}(\omega) \langle \hat{v}_{ik}^2 \rangle_{FS}^{-1} \langle \langle \hat{v}_{ik}^2 K(\omega, \hat{\mathbf{k}}\hat{\mathbf{r}}) \rangle \rangle_{FS,V} \\ K(\omega, \hat{\mathbf{k}}\hat{\mathbf{r}}) &= \frac{2}{\hat{\omega}} [\hat{\omega}^2 - \Delta(\hat{\mathbf{k}})^2]^{\frac{1}{2}} \Theta_H(\hat{\omega}^2 - \Delta(\hat{\mathbf{k}}^2)) \end{aligned} \quad (57)$$

Table 5: Spin and orbital structure of the possible gap functions which are solutions of the Eliashberg equations for the dual model of UPd₂Al₃. The A_{1g} OSP state is fully symmetric and its node line ($k_z = \pm\pi/c$) is not enforced by symmetry.

| p | $ \chi\rangle = S, S_z\rangle$ | D _{6h} repres. | spin pairing | $\Phi(k_z)$ |
|-----|--|-------------------------|--------------|---------------|
| -1 | $ 0, 0\rangle = \frac{1}{\sqrt{2}}(\uparrow\downarrow\rangle - \downarrow\uparrow\rangle)$ | $\Gamma_1^+ (A_{1g})$ | OSP | $\cos(ck_z)$ |
| -1 | $ 1, 0\rangle = \frac{1}{\sqrt{2}}(\uparrow\downarrow\rangle + \downarrow\uparrow\rangle)$ | $\Gamma_1^- (A_{1u})$ | OSP | $\sin(ck_z)$ |
| +1 | $ 1, \pm 1\rangle = \uparrow\uparrow\rangle, \downarrow\downarrow\rangle$ | $\Gamma_1^- (A_{1u})$ | ESP | $\sin(2ck_z)$ |

Here $\hat{\omega} = \omega - \mathbf{v}_s(\mathbf{r}, \hat{\theta}) \cdot \mathbf{k}$ is the Doppler shifted energy of the quasiparticle, \mathbf{k} and \mathbf{r} are its momentum and its position with respect to the vortex core oriented along $\hat{\theta}$. The double average is performed over the FS and the inter-vortex region and Θ_H is the Heaviside function. Furthermore $\hat{\tau}(\omega)$ is the effective quasiparticle lifetime. As already mentioned in sect. 3.4 for CeCoIn₅ angle-resolved measurements of thermal conductivity give important information the position of the node lines of $\Delta(\mathbf{k})$ with respect to the crystal axes. This is of great help in the determination of gap symmetry. One should have $H \ll H_{c2}$ to minimise the background effect of the H_{c2} anisotropy. These experiments, which were proposed in [158], have recently been performed on UPd₂Al₃ single crystals [217] in a rotating field geometry with heat current perpendicular to the field (vortex) direction to probe the itinerant quasiparticle contribution (fig. 29). For fields rotated in the hexagonal ab-plane no oscillations have been found excluding the presence of node lines perpendicular to the ab plane as has been proposed in the model of [218]. On the other hand field rotation in the ac-plane clearly leads to twofold oscillations for $H \ll H_{c2}$ proving the existence of a node line which is parallel to the ab-plane as is predicted by the magnetic exciton model of SC in UPd₂Al₃ [159] (fig. 29). Because of the cylindrical FS geometry the oscillations are qualitatively similar for the three gap functions of table 5. Thus thermal transport measurements alone are in this case not able to fix the position of the horizontal node line. However if one accepts that the Knight shift results point to singlet (OSP) pairing, then the A_{1g}-gap function in table 5 is the proper one for UPd₂Al₃.

6 SUMMARY AND OUTLOOK

The understanding of the heavy fermion state in Ce- and U- intermetallics and its SC phases has made great progress in recent years. In the normal state it has become clear that the origin of quasiparticle mass enhancement may be profoundly different. It is described by the Kondo lattice mechanism in 4f-Ce compounds and by a dual (multiorbital) model of localised and itinerant 5f electrons in U compounds. For Ce systems the heavy electron bands may be described by the renormalised band theory where the single 4f electron is treated as itinerant with a resonant phase shift. Within the dual model for U-compounds, two electrons are treated as being localised in CEF states. The remaining 5f electron forms itinerant conduction bands and its coupling to magnetic excitons, i.e. propagating CEF excitations, leads to the mass enhancement. These different approaches lead to realistic Fermi surfaces in cases like CeCu₂Si₂, UPt₃, UPd₂Al₃ and the mass enhancement may be incorporated naturally.

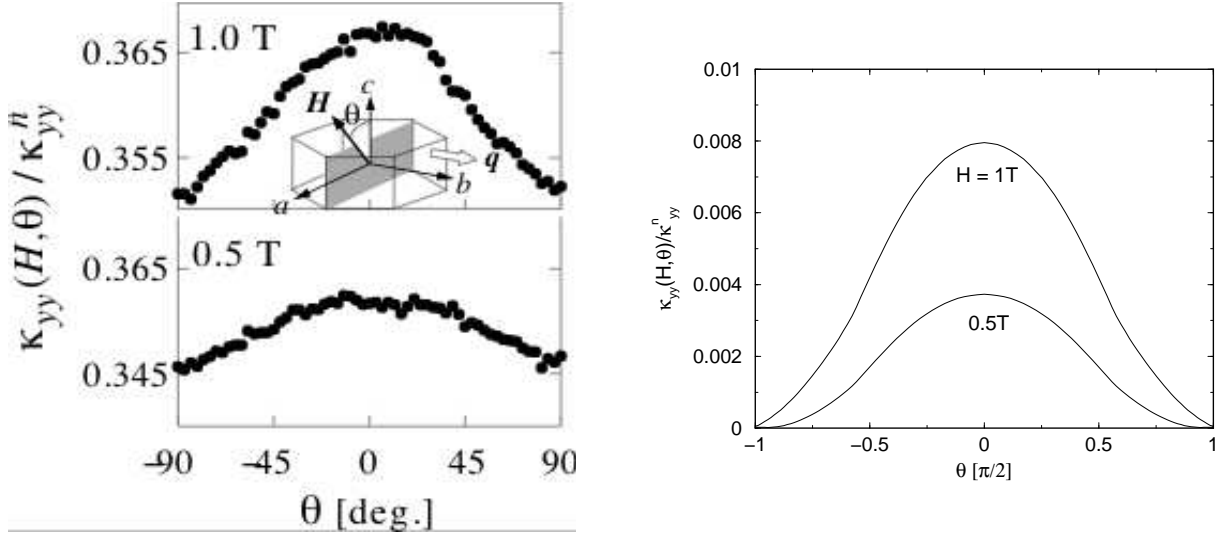


Figure 29: Left panel: Angular variation of the normalised b-axis thermal conductivity $\kappa_{yy}(\mathbf{H}, \theta)$. Field is rotated in the ac -plane \perp to the heat current \mathbf{q} [217]. Right panel: Theoretical calculation of $\kappa_{yy}(\mathbf{H}, \theta)$ according to eq. (57) for the corrugated FS cylinder of UPd_2Al_3 and the A_{1g} gap function. Twofold oscillations in θ proves the existence of a node line in the ab plane [216].

The Kondo lattice mechanism in Ce-compounds implies the competition between HF state and AF ordering as illustrated in the Doniach phase diagram. When AF order is destroyed by variation of a control parameter, pressure or chemical substitution, the normal state behaviour around the QCP shows distinct NFL behaviour. It is characterised by anomalous scaling exponents in the temperature and field dependences of specific heat, resistivity, thermal expansion and other properties. In Ce-compounds these NFL exponents may largely be understood by considering the dressing of quasiparticle with a spectrum of soft magnetic spin fluctuations, this picture seems especially appropriate for CeNi_2Ge_2 but also for CeCu_2Si_2 and CePd_2Si_2 . Simultaneously effective quasiparticle interactions mediated by soft spin fluctuations favor SC pair formation as predicted by Eliashberg theory. In fact in many Ce-compounds SC domes exist around the QCP and frequently but not necessarily is associated with NFL behaviour.

Mass enhancement and SC pairing are closely related. The importance of virtual magnetic exciton exchange for SC pair formation in HF-U compounds with dual 5f electron behaviour may therefore be supposed. Indeed this novel mechanism has been identified in the model compound UPd_2Al_3 by complementary tunneling and INS measurements. The former exhibit a characteristic strong coupling feature at the energy of the zone center magnetic exciton mode which identifies the latter as the exchanged boson that mediates pairing. This observation is quite unique for HF-compounds, it has not been achieved for the spin fluctuation Ce-compounds which is explicable since the latter are overdamped modes whereas magnetic excitons are propagating modes with a real group velocity. Whether SC in other U-HF compounds may be explained with a similar mechanism is a matter of debate. UBe_{13} is the only SC U compound which possibly exhibits a magnetic QCP and may therefore be more similar to Ce-based SC, while UPt_3 and URu_2Si_2 where SC is embedded in a magnetic (or hidden

order) phase are more plausible candidates for the magnetic exciton mechanism. Also the AF spin fluctuation model in its simple versions strongly favors singlet pairing whereas a number of U-HF compounds, notably UPt₃, exhibit triplet pairing. The latter is not disfavored in the magnetic exciton model due to an inherent spin space anisotropy of the effective interaction.

The most important property of unconventional HF SC is the symmetry class of the gap function. Progress in understanding these symmetries for specific compounds has been slow in the past since the traditional method, i.e. interpreting 'power law' behaviour of thermodynamic and transport quantities etc. is ambiguous and often contradictory. Recently the situation has improved considerably with the advent of angle-resolved specific heat and magnetotransport measurements that can identify or restrict nodal positions of the gap functions in **k**-space. Together with Knight shift measurements they are the most powerful tool to investigate the gap symmetry in ultra-pure stoichiometric samples. Up to now the SC gap is known with some certainty only for three cases: f-wave triplet (E_{2u}) in UPt₃, nodal singlet (A_{1g}) in UPd₂Al₃ and d-wave singlet (B_{1g} or B_{2g}) in CeCoIn₅.

An issue of permanent interest in HF SC is the coexistence/competition with long range AF or SDW order away from the QCP. This is now fairly well understood for the 'A-phase' SDW state in CeCu₂Si₂ and CeCu₂(Si_{1-x}Ge_x)₂, both experimentally and within theoretical models involving a realistic FS geometry. A similar approach may be possible for Ce115 materials like CeRh_{1-x}Co_xIn₅.

The vortex phase can give further insight into the SC state. For UPt₃ the appearance of three distinct SC regions in the B-T plane was a sure sign of a multicomponent SC order parameter. More recently the observation of a distinct SC vortex phase in the low temperature and high field corner close to H_{c2} for CeCoIn₅ has been interpreted as the long-sought FFLO phase where SC pairs have finite momentum which leads to a segmentation of vortices.

Many fundamental issues in HF materials, like the importance of unconventional density wave states for NFL behaviour, QCP scenarios with a local breakup of quasiparticles, the effect of time reversal and inversion symmetry breaking in unconventional SC states, the vortex and FFLO phase for nodal SC gap functions and many others, are still incompletely understood. This guarantees that heavy fermion physics will be a thriving field in the future.

Acknowledgements

The authors are grateful for collaboration and discussion with numerous colleagues, especially T. Dahm, E. Faulhaber, P. Fulde, P. Gegenwart, C. Geibel, K. Izawa, K. Maki, Y. Matsuda, P. McHale, M. Neef, F. Pollmann, N. Sato, B. Schmidt, G. Varelogiannis, T. Watanabe, A. Yaresko, H.Q. Yuan and Q. Yuan.

List of acronyms

| | |
|---------|--|
| AF | antiferromagnet, antiferromagnetism, antiferromagnetic |
| AFBZ | antiferromagnetic Brillouin zone |
| ARPES | angle resolved photoemission spectroscopy |
| BIS | bremsstrahlung isochromat spectroscopy |
| BZ | Brillouin zone |
| CDW | charge density wave |
| CEF | crystalline electric field |
| CPT | cluster perturbation theory |
| dHvA | de Haas-van Alphen |
| DLRO | diagonal long range order |
| DOS | density of states |
| ESP | equal spin pairing |
| FFLO | Fulde-Ferrell-Larkin-Ovchinnikov |
| GL | Ginzburg-Landau |
| LFL | Landau-Fermi liquid |
| FLEX | fluctuation exchange |
| FM | ferromagnet, ferromagnetism, ferromagnetic |
| FS | Fermi surface |
| HF | heavy fermion |
| IC | incommensurate |
| INS | inelastic neutron scattering |
| LDA | local density approximation |
| LSDA | local spin density approximation |
| mf | mean field |
| NFL | non-Fermi liquid |
| n.n. | next neighbor |
| n.n.n. | next nearest neighbor |
| NMR | nuclear magnetic resonance |
| NQR | nuclear quadrupole resonance |
| ODLRO | off-diagonal long range order |
| OSP | opposite spin pairing |
| PES | photoemission spectroscopy |
| QCP | quantum critical point |
| RPA | random phase approximation |
| RKKY | Ruderman-Kittel-Kasuya-Yoshida |
| SC | superconductor, superconductivity, superconducting |
| SIC-LDA | self interaction corrected local density approximation |
| SDW | spin density wave |
| s.o. | spin orbit |
| TB | tight binding |

REFERENCES

- [1] P. Fulde, J. Phys. F 18 (1988) 601.
- [2] N. Grewe and F. Steglich, *Handbook on the Physics and Chemistry of Rare Earths* (Elsevier Science Publishers B. V., Amsterdam, 1991), vol. 14, chap. Heavy Fermions, p. 343.
- [3] Y. Kuramoto and Y. Kitaoka, *Dynamics of Heavy Electrons*, vol. 105 of *International Series of Monographs in Physics* (Clarendon Press, Oxford, 2000).
- [4] A. C. Hewson, *The Kondo Problem to Heavy Fermions* (Cambridge University Press, 1993).
- [5] M. Sigrist and K. Ueda, Rev. Mod. Phys. 63 (1991) 239.
- [6] P. Thalmeier and G. Zwicknagl, *Handbook on the Physics and Chemistry of Rare Earths (cond-mat/0312540)* (Elsevier, 2004), vol. 34.
- [7] V. P. Mineev and K. V. Samokhin, *Introduction to Unconventional Superconductivity* (Gordon and Breach Science Publishers, 1999).
- [8] J. A. Sauls, Adv. Phys. 43 (1994) 113.
- [9] R. Joynt and L. Taillefer, Rev. Mod. Phys. 74 (2002) 237.
- [10] L. D. Landau, Sov. Phys. JETP 3 (1956) 920.
- [11] L. D. Landau, Soviet Physics - JETP 32 (1957) 59.
- [12] L. D. Landau, Soviet Physics - JETP 35 (1958) 97.
- [13] A. A. Abrikosov, L. P. Gorkov, and I. E. Dzyaloshinski, *Methods of Quantum Field Theory in Statistical Physics* (Dover, New York, 1975).
- [14] J. W. Allen, *Resonant Photoemission of Solids with Strongly Correlated Electrons* (Plenum Press, New York, 1992), vol. 1 of *Synchrotron Radiation Research: Advances in Surface and Interface Science*, chap. 6, p. 253.
- [15] D. Malterre, M. Grioni, and Y. Baer, Adv. Phys. 45 (1996) 299.
- [16] F. Reinert, D. Ehm, S. Schmidt, G. Nicolay, S. Hüfner, J. Kroha, O. Trovarelli, and C. Geibel, Phys. Rev. Lett. 87 (2001) 106401.
- [17] K. G. Wilson, Rev. Mod. Phys. 47 (1975) 773.
- [18] P. Nozières, J. Low Temp. Phys. 17 (1974) 31.
- [19] G. Zwicknagl, Adv. Phys. 41 (1992) 203.

- [20] G. Zwicknagl and U. Pulst, *Physica B* 186 (1993) 895.
- [21] G. Zwicknagl, *Physica Scripta T* 49 (1993) 34.
- [22] G. G. Lonzarich, *J. Magn. Magn. Mat.* 76 / 77 (1988) 1.
- [23] H. Aoki, S. Uji, A. K. Albessard, and Y. Onuki, *Phys. Rev. Lett.* 71 (1993) 2110.
- [24] F. S. Tautz, S. R. Julian, G. J. McMullen, and G. G. Lonzarich, *Physica B* 206-207 (1995) 29.
- [25] D. L. Cox and A. Zawadowski, *Exotic Kondo effects in retals: Magnetic ions in a crystalline electric field and tunnelling centres* (Taylor and Francis, 1999).
- [26] R. White and P. Fulde, *Phys. Rev. Lett.* 47 (1981) 1540.
- [27] G. Zwicknagl and P. Fulde, *J. Phys. Condens. Matter* 15 (2003) S1911.
- [28] G. Zwicknagl, A. N. Yaresko, and P. Fulde, *Phys. Rev. B* 65 (2002) 081103(R).
- [29] G. Zwicknagl, A. Yaresko, and P. Fulde, *Phys. Rev. B* 68 (2003) 052508.
- [30] D. V. Efremov, N. Hasselmann, E. Runge, P. Fulde, and G. Zwicknagl, *Phys. Rev. B* 69 (2004) 115114.
- [31] F. Pollmann, Diplomarbeit, Techn. Universität Braunschweig (2004).
- [32] E. Runge, P. Fulde, D. V. Efremov, N. Hasselmann, and G. Zwicknagl, *Phys. Rev. B* 69 (2004) 155110.
- [33] E. Dagotto, *Rev. Mod. Phys.* 66 (1994) 763.
- [34] D. Senechal, D. Perez, and D. Plouffe, *Phys. Rev. B* 66 (2002) 075129.
- [35] G. L. G. Sleijpen and H. A. V. der Vorst, *SIAM J. Matrix Anal. Appl. (SIMAX)* 17 (1996) 401.
- [36] S. Fujimori, Y. Saito, M. Seki, K. Tamura, M. Mizuta, K. Yamaki, K. Sato, T. Okane, A. Tanaka, N. Sato, T. Komatsubara, Y. Tezuka, S. Shin, S. Suzuki, and S. Sato, *Journal of Electron Spectroscopy and Related Phenomena* 101-103 (1999) 439.
- [37] S.-K. Ma, *Modern Theory of Critical Phenomena*, Frontiers in Physics (W. A. Benjamin Inc., Reading, Massachusetts, 1976).
- [38] S. Sachdev, *Quantum Phase Transitions* (Cambridge University Press, 1999).
- [39] M. A. Continentino, *Quantum Scaling in Many-Body Systems* (World Scientific Publishing, Singapore, 2001).
- [40] J. A. Hertz, *Phys. Rev. B* 14 (1976) 1165.

- [41] L. Zhu, M. Garst, A. Rosch, and Q. Si, Phys. Rev. Lett. 91 (2003) 066404.
- [42] R. Takke, M. Nicksch, W. Assmus, B. Lüthi, R. Pott, R. Schefzyk, and D. K. Wohlleben, Z. Phys. b 44 (1981) 33.
- [43] P. Thalmeier and P. Fulde, Europhys. Lett. 1 (1986) 367.
- [44] P. Fulde, J. Keller, and G. Zwicknagl, in *Solid State Physics*, edited by F. Seitz, D. Turnbull, and H. Ehrenreich (Academic Press, New York, 1988), vol. 41, p. 1.
- [45] P. Thalmeier and B. Lüthi, *Handbook on the Physics and Chemistry of Rare Earths* (North-Holland, 1991), vol. 14, chap. 96, p. 225.
- [46] M. A. Continentino, cond-mat/0408217 (2004).
- [47] L. Zhu, M. Garst, A. Rosch, and Q. Si, cond-mat/0408230 (2004).
- [48] R. K  chler, N. Oeschler, P. Gegenwart, T. Cichorek, K. Neumaier, O. Tegus, C. Geibel, J. A. Mydosh, F. Steglich, L. Zhu, and Q. Si, Phys. Rev. Lett. 91 (2003) 066405.
- [49] A. Rosch, Phys. Rev. Lett. 82 (1999) 4280.
- [50] A. J. Millis, Phys. Rev. B 48 (1993) 7183.
- [51] U. Z  licke and A. J. Millis, Phys. Rev. B 51 (1995) 8996.
- [52] T. Moriya, *Spin Fluctuations in Itinerant Electron Magnets* (Springer Verlag, Berlin, 1985).
- [53] G. R. Stewart, Rev. Mod. Phys. 73 (2001) 797.
- [54] F. Steglich, J. Aarts, C. Bredl, W. Lieke, D. Meschede, W. Franz, and H. Sch  fer, Phys. Rev. Lett. 43 (1979) 1892.
- [55] O. Stockert, E. Faulhaber, G. Zwicknagl, N. Stuesser, H. Jeevan, T. Cichorek, R. Loewenhaupt, C. Geibel, and F. Steglich, Phys. Rev. Lett. 92 (2004) 136401.
- [56] O. Trovarelli, M. Weiden, R. M  ller-Reisener, M. G  mez-Berisso, P. Gegenwart, M. Deppe, C. Geibel, J. G. Sereni, and F. Steglich, Phys. Rev. B. 56 (1997) 678.
- [57] D. Jaccard, H. Wilhelm, K. Alami-Yadri, and E. Vargoz, Physica B 259-261 (1999) 1.
- [58] H. Q. Yuan, F. M. Grosche, M. Deppe, C. Geibel, G. Sparn, and F. Steglich, Science 302 (2003) 2104.
- [59] C. Petrovic, R. Movshovich, M. Jaime, P. G. Pagliuso, M. F. Hundley, J. L. Sarrao, Z. Fisk, and J. D. Thompson, Europhys. Lett. 53 (2001) 354.
- [60] K. Izawa, H. Yamaguchi, Y. Matsuda, H. Shishido, R. Settai, and Y. Onuki, Phys. Rev. Lett. 87 (2001) 05700.

- [61] H. Aoki, T. Sakakibara, H. Shishido, R. Settai, Y. Onuki, P. Miranovic, and K. Machida, J. Phys. Condens. Matter 16 (2004) L13.
- [62] A. Bianchi, R. Movshovich, C. Capan, A. Lacerda, P. G. Pagliuso, and J. L. Sarrao, Phys. Rev. Lett. 91 (2003) 187004.
- [63] T. Watanabe, Y. Kasahara, K. Izawa, T. Sakakibara, C. van der Beek, T. Hanaguri, H. Shishido, R. Settai, Y. Onuki, and Y. Matsuda, cond-mat/0312062 (2003).
- [64] E. Bauer, G. Hilscher, H. Michor, C. Paul, E. W. Scheidt, A. Griбанov, Y. Seropegin, H. Noel, M. Sigrist, and P. Rogl, Phys. Rev. Lett. 92 (2004) 027003.
- [65] L. N. Bulaevskii, A. A. Guseinov, and A. I. Rusinov, Sov. Phys. JETP 44 (1976) 1243.
- [66] P. Frigeri, D. Agterberg, A. Koga, and M. Sigrist, Phys. Rev. Lett 92 (2003) 097011.
- [67] G. Bruls, D. Weber, B. Wolf, P. Thalmeier, B. Lüthi, A. de Visser, and A. Menovsky, Phys. Rev. Lett 65 (1990) 2294.
- [68] W. Sun, M. Brand, G. Bruls, and W. Assmuss, Z. Phys. B 80 (1990) 249.
- [69] O. . Stockert, M. Deppe, E. Faulhaber, H. Jeevan, R. Schneider, N. Stüsser, C. Geibel, M. Loewenhaupt, and F. Steglich, preprint (2004).
- [70] A. T. Holmes, D. Jaccard, and K. Miyake, Phys. Rev. B 69 (2004) 024508.
- [71] Y. Onishi and K. Miyake, J. Phys. Soc. Jpn. 69 (2004) 3955.
- [72] F. Steglich, P. Gegenwart, C. Geibel, P. Hinze, M. Lang, C. Langhammer, G. Sparn, T. Tayama, O. Trovarelli, N. Sato, T. Dahm, and G. Varelogiannis, *More is different- fifty years of condensed matter physics* (Princeton University Press, 2001), chap. 13, p. 191.
- [73] G. Bruls, B. Wolf, D. Finsterbusch, P. Thalmeier, I. Kouroudis, W. Sun, W. Assmus, B. Lüthi, M. Lang, K. Gloos, F. Steglich, and R. Modler, Phys. Rev. Lett. 72 (1994) 1754.
- [74] F. Weickert, unpublished.
- [75] P. Gegenwart, C. Langhammer, C. Geibel, R. Helfrich, M. Lang, G. Sparn, F. Steglich, R. Horn, L. Donnevert, A. Link, and W. Assmus, Phys. Rev. Lett. 81 (1998) 1501.
- [76] F. Thomas, J. Thomasson, C. Ayache, C. Geibel, and F. Steglich, Physica B 186-188 (1993) 303.
- [77] A. Onodera, S. Tsuduki, Y. Onishi, T. Watanuki, K. Ishida, Y. Kitaoka, and Y. Onuki, Solid State Commun. 123 (2002) 113.
- [78] J. Roehler, J. Klug, and K. Keulerz, J. Magn. Magn. Mater 76-77 (1988) 340.

- [79] Y. Kawasaki, K. Ishida, S. Kawasaki, T. Mito, G. q. Zheng, Y. Kitaoka, C. Geibel, and F. Steglich, *J. Phys. Soc. Jpn.* 73 (2004) 194.
- [80] K. Ishida, Y. Kawasaki, K. Tabuchi, K. Kashima, Y. Kitaoka, and K. Asayama, *Phys. Rev. Lett.* 82 (1999) 5353.
- [81] F. Steglich and S. Suellow, *Encyclopedia of Materials: Science and Technology* (2001).
- [82] M. Neef, *Diplomarbeit, Techn. Universität Braunschweig* (2004).
- [83] M. Neef and G. Zwicknagl, preprint (2004).
- [84] G. Zwicknagl and P. Fulde, *Z. Phys. B* 43 (1981) 23.
- [85] P. Fulde and G. Zwicknagl, *J. Appl. Phys.* 53 (1982) 8064.
- [86] U. Rauchschwalbe, W. Lieke, C. D. Bredl, F. Steglich, J. Aarts, K. M. Martini, and A. C. Mota, *Phys. Rev. Lett.* 49 (1982) 1448.
- [87] R. Konno and K. Ueda, *Phys. Rev. B* 40 (1989) 4329.
- [88] M. Ozaki and K. Machida, *Phys. Rev. B* 39 (1989) 4145.
- [89] O. Stockert, unpublished (2004).
- [90] G. Knebel, M. Brando, J. Hemberger, M. Nicklas, W. Trinkl, and A. Loidl, *Phys. Rev. B* 59 (1999) 12390.
- [91] P. Gegenwart, J. Custers, T. Tayama, K. Tenya, C. Geibel, G. Sparn, N. Harrison, P. Kersch, D. Eckert, K.-H. Müller, and F. Steglich, *J. Low Temp. Phys.* 133 (2003) 3.
- [92] D. Jaccard, K. Behnia, and J. Sierro, *Phys. Lett. A* 163 (1992) 475.
- [93] R. Movshovich, T. Graf, D. Mandrus, J. D. Thompson, and a. Z. F. J. L. Smith, *Phys. Rev. B* 53 (1996) 8241.
- [94] N. D. Mathur, F. M. Grosche, S. R. Julian, I. R. Walker, D. M. Freye, R. K. W. Haselwimmer, and G. G. Lonzarich, *Nature* 394 (1998) 39.
- [95] F. M. Grosche, I. R. Walker, S. R. Julian, N. D. Mathur, D. M. Freye, M. J. Steiner, and G. G. Lonzarich, *J. Phys.: Condens. Matter* 13 (2001) 2845.
- [96] A. Demuer, A. T. Holmes, and D. Jaccard, *J. Phys. Condens. Matter* 14 (2002) L529.
- [97] M. G. Berisso, P. Pedrazzini, J. G. Sereni, O. Trovarelli, C. Geibel, and F. Steglich, *Eur. Phys. J. B* 30 (2002) 343.
- [98] S. Araki, R. Settai, T. C. Kobayashi, H. Harima, and Y. Onuki, *Phys. Rev. B* 64 (2001) 224417.

- [99] N. H. van Dijk, B. Fak, T. Charvolin, P. Lejay, and J. M. Mignot, *Phys. Rev. B* 61 (2000) 8922.
- [100] Y. Onuki, R. Settai, K. Sugiyama, T. Takeuchi, T. C. Kobayashi, Y. Haga, and E. Yamamoto, *J. Phys. Soc. Jpn.* 73 (2004) 769.
- [101] T. Graf, J. D. Thompson, M. Hundley, R. Movshovich, Z. Fisk, D. Mandrus, R. A. Fisher, and N. E. Philips, *Phys. Rev. Lett.* 78 (1997) 3769.
- [102] N. Oeschler, P. Gegenwart, M. Lang, R. Movshovich, J. L. Sarrao, J. D. Thompson, and F. Steglich, *Phys. Rev. Lett.* 91 (2003) 076402.
- [103] J. D. Thompson, M. Nicklas, A. Bianchi, R. Movshovich, A. Llobet, W. Bao, A. Malinowski, M. F. Hundley, N. O. Moreno, P. G. Pagliuso, J. L. Sarrao, S. Nakatsuji, Z. Fisk, R. Borth, E. Lengyel, N. Oeschler, G. Sparn, F. S. E. Lengyel, N. Oeschler, G. Sparn, and F. Steglich, *Physica B* 329-333 (2003) 446.
- [104] H. Shishido, R. Settai, D. Aoki, S. Ikeda, H. Nakawaki, N. Nakamura, T. Iizuka, Y. Inada, K. Sugiyama, T. Takeuchi, K. Kindo, T. C. Kobayashi, Y. Haga, H. Harima, Y. Aoki, T. Namiki, H. Sato, and Y. Onuki, *J. Phys. Soc. Japan* 71 (2002) 162.
- [105] T. Maehira, T. Hotta, K. Ueda, and A. Hasegawa, *J. Phys. Soc. Jpn.* 72 (2003) 854.
- [106] T. Ueda, H. Shishido, S. Hashimoto, T. Okubo, M. Yamada, Y. Inada, R. Settai, H. Harima, A. Galatanu, E. Yamamoto, N. Nakamura, K. Sugiyama, T. Takeuchi, K. Kindo, T. Namiki, Y. Aoki, H. Sato, and Y. Onuki, *J. Phys. Soc. Jpn.* 73 (2004) 649.
- [107] A. D. Christianson, J. M. Lawrence, P. G. Pagliuso, N. O. Moreno, J. L. Sarrao, J. D. Thompson, P. S. Riseborough, S. Kern, E. A. Goremychkin, and A. H. Lacerda, *Phys. Rev. B* 66 (2002) 193102.
- [108] Y. Kitaoka, S. Kawasaki, Y. Kawasaki, T. Mito, and G. q. Zheng, *cond-mat/0405348* (2004).
- [109] V. S. Zapf, E. J. Freeman, E. D. Bauer, J. Petricka, C. Sirvent, N. A. Frederick, R. P. Dickey, and M. B. Maple, *Phys. Rev. B* 65 (2001) 014506.
- [110] P. G. Pagliuso, C. Petrovic, R. Movshovich, D. Hall, F. Hundley, J. L. Sarrao, J. D. Thompson, and Z. Fisk, *Phys. Rev. B* 64 (2001) 100503(R).
- [111] T. Muramatsu, T. C. Kobayashi, K. Shimizu, K. Amaya, D. Aoki, Y. Haga, and Y. Onuki, *Physica C* 388-389 (2003) 539.
- [112] G. Zheng, Y. Yamaguchi, H. Kan, Y. Kitaoka, J. L. Sarrao, P. G. Pagliuso, N. O. Moreno, and J. D. Thompson, *Phys. Rev. B* 70 (2004) 014511.
- [113] M. Nicklas, V. A. Sidorov, H. A. Borges, P. G. Pagliuso, C. Petrovic, Z. Fisk, J. L. Sarrao, and J. D. Thompson, *Phys. Rev. B* 67 (2003) 020506(R).

- [114] J. S. Kim, J. Alwood, G. R. Stewart, J. L. Sarrao, and J. D. Thompson, Phys. Rev. B 64 (2001) 134524.
- [115] J. Paglione, M. A. Tanatar, D. G. Hawthorn, E. Boaknin, F. Ronning, R. W. Hill, M. Sutherland, L. Taillefer, C. Petrovic, and P. C. Canfield, cond-mat/0405157 (2004).
- [116] V. A. Sidorov, M. Nicklas, P. G. Pagliuso, J. L. Sarrao, Y. Bang, A. V. Balatsky, and J. D. Thompson, Phys. Rev. Lett. 89 (2002) 157004.
- [117] Y. Nakajima, K. Izawa, Y. Matsuda, S. Uji, T. Terashima, H. Shishido, R. Settai, Y. Onuki, and H. Kotani, J. Phys. Soc. Jpn. 73 (2004) 5.
- [118] R. Bel, K. Behnia, Y. Nakajima, K. Izawa, Y. Matsuda, H. Shishido, R. Settai, and Y. Onuki, Phys. Rev. Lett. 92 (2004) 217002.
- [119] N. Oeschler, P. Gegenwart, F. Steglich, N. A. Frederick, E. D. Bauer, and M. B. Maple, Acta Phys. Pol. B 34 (2003) 959.
- [120] J. S. Kim, N. O. Moreno, J. L. Sarrao, J. D. Thompson, and G. R. Stewart, Phys. Rev. B 69 (2004) 024402.
- [121] M. Yashima, S. Kawasaki, Y. Kawasaki, G. Zheng, Y. Kitaoka, H. Shishido, R. Settai, Y. Haga, and Y. Onuki, J. Phys. Soc. Jpn. 73 (2004) 2073.
- [122] Y. Kohori, Y. Yamato, Y. Iwamoto, T. Kohara, E. D. Bauer, M. B. Maple, and J. L. Sarrao, Phys. Rev. B 64 (2001) 134526.
- [123] G. E. Volovik, JETP Lett. 58 (1993) 469.
- [124] N. Nagai, P. Miranović, M. Ichioka, and K. Machida, preprint (2004).
- [125] K. Izawa, H. Takahashi, H. Yamaguchi, Y. Matsuda, M. Suzuki, T. Sasaki, T. Fukase, Y. Yoshida, R. Settai, and Y. Onuki, Phys. Rev. Lett. 86 (2001a) 2653.
- [126] K. Izawa, H. Yamaguchi, T. Sasaki, and Y. Matsuda, Phys. Rev. Lett. 88 (2002) 027002.
- [127] K. Izawa, K. Kamata, Y. Nakajima, Y. Matsuda, T. Watanabe, M. Nohara, H. Takagi, P. Thalmeier, and K. Maki, Phys. Rev. Lett. 89 (2002a) 137006.
- [128] K. Izawa, Y. Nakajima, J. Goryo, Y. Matsuda, S. Osaki, H. Sugawara, H. Sato, P. Thalmeier, and K. Maki, Phys. Rev. Lett. 90 (2003) 1170013.
- [129] P. Thalmeier and K. Maki, Acta Physica Polonica B 34 (2003) 557.
- [130] A. Bianchi, R. Movshovich, N. Oeschler, P. Gegenwart, F. Steglich, J. D. Thompson, P. G. Pagliuso, and J. L. Sarrao, Phys. Rev. Lett. 89 (2002) 137002.
- [131] H. A. Radovan, N. A. Fortune, T. P. Murphy, S. T. Hannahs, E. C. Palm, S. W. Tozer, and D. Hall, Nature 425 (2003) 51.

- [132] T. Tayama, A. Harita, T. Sakakibara, Y. Haga, H. Shishido, R. Settai, and Y. Onuki, Phys. Rev. B. 65 (2002).
- [133] L. W. Gruenberg and L. Gunther, Phys. Rev. Lett. 16 (1966) 996.
- [134] K. Kakuyanagi, M. Saito, K. Kumagai, S. Takashima, M. Nohara, H. Takagi, and Y. Matsuda, cond-mat/0405661 (2004).
- [135] P. W. Anderson, Phys. Rev. B 30 (1984) 1549.
- [136] E. Bauer, G. Hilscher, H. Michor, M. Sieberer, E. W. Scheidt, A. Griбанov, Y. Seregopin, P. Rogl, A. Amato, W. Y. Song, J. G. Park, D. T. Adroja, M. Nicklas, G. Sparn, M. Yogi, and Y. Kitaoka, cond-mat/0408244 (2004).
- [137] N. Metoki, K. Kaneko, T. D. Matsuda, A. Galatanu, T. Takeuchi, S. Hashimoto, T. Ueda, R. Settai, Y. Onuki, and N. Bernhoeft, J. Phys. Condens. Matter 16 (2004) L207.
- [138] T. Yasuda, H. Shishido, T. Ueda, S. Hashimoto, R. Settai, T. Takeuchi, T. D. Matsuda, Y. Haga, and Y. Onuki, J. Phys. Soc. Jpn. 73 (2004) 1657.
- [139] P. A. Frigeri, D. F. Agterberg, and M. Sigrist, cond-mat/0405179 (2004).
- [140] M. Yogi, Y. Kitaoka, S. Hashimoto, T. Yasuda, R. Settai, T. D. Matsuda, Y. Haga, Y. Onuki, P. Rogl, and E. Bauer, cond-mat/0405493 (2004).
- [141] T. Moriya and K. Ueda, Adv. Phys. 49 (2000) 555.
- [142] D. Vollhardt and P. Wölfle, *The superfluid phases of ^3He* (Taylor and Francis, New York, 1990).
- [143] S. Nakajima, Prog. Theor. Phys. 50 (1973) 1101.
- [144] P. W. Anderson and W. F. Brinkman, Phys. Rev. Lett. 30 (1973) 1108.
- [145] K. Miyake, S. Schmitt-Rink, and C. M. Varma, Phys. Rev. B 34 (1986) 6554.
- [146] D. J. Scalapino, E. Loh, and J. E. Hirsch, Phys. Rev. B 34 (1986) 8190.
- [147] C. H. Pao and N. E. Bickers, Phys. Rev. Lett. 72 (1994) 1870.
- [148] T. Dahm and L. Tewordt, Phys. Rev. Lett. 74 (1995) 793.
- [149] H. Tou, K. Ishida, and Y. Kitaoka, cond-mat/0308562 (2003).
- [150] G. E. Volovik and L. P. Gor'kov, Sov. Phys. JETP 61 (1985) 843.
- [151] P. Monthoux and G. G. Lonzarich, Phys. Rev. B 59 (1999) 14598.
- [152] P. Monthoux and G. G. Lonzarich, Phys. Rev. B 63 (2001) 054529.
- [153] P. Monthoux and G. G. Lonzarich, Phys. Rev. B 66 (2002) 224504.

- [154] P. McHale and P. Monthoux, *Phys. Rev. B* 67 (2003) 214512.
- [155] G. Bergmann and D. Rainer, *Z. Phys.* 263 (1973) 59.
- [156] A. J. Millis, S. Sachdev, and C. M. Varma, *Phys. Rev. B* 37 (1988) 4975.
- [157] N. K. Sato, N. Aso, K. Miyake, R. Shiina, P. Thalmeier, G. Varelogiannis, C. Geibel, F. Steglich, P. Fulde, and T. Komatsubara, *Nature* 410 (2001) 340.
- [158] P. Thalmeier, *Eur. Phys. J. B* 27 (2002) 29.
- [159] P. McHale, P. Fulde, and P. Thalmeier, *Phys. Rev. B* 70 (2004) 014513.
- [160] H. R. Ott, H. Rudigier, Z. Fisk, and J. L. Smith, *Phys. Rev. Lett.* 50 (1983) 1595.
- [161] G. R. Stewart, Z. Fisk, J. O. Willis, and J. L. Smith, *Phys. Rev. Lett.* 52 (1984) 679.
- [162] W. Schlabit, J. Baumann, B. Pollit, U. Rauchschwalbe, W. M. Meyer, U. Ahlheim, and C. C. Bredl, *Z. Phys. B* 62 (1986) 171, (and abstracts of the ICVF, Cologne, 1984).
- [163] C. Geibel, C. Schank, S. Thies, H. Kitazawa, C. D. Bredl, A. Böhm, M. Rau, A. Grauel, R. Caspary, R. Helfrich, U. Ahlheim, G. Weber, and F. Steglich, *Z. Phys. B* 84 (1991) 1.
- [164] C. Geibel, S. Thies, D. Kaczorowski, A. Mehner, A. Grauel, B. Seidel, U. Ahlheim, R. Helfrich, K. Petersen, C. D. Bredl, and F. Steglich, *Z. Phys.* 83 (1991) 305.
- [165] H. R. Ott, H. Rudigier, T. M. Rice, K. Ueda, Z. Fisk, and J. L. Smith, *Phys. Rev. Lett.* 82 (1984).
- [166] A. C. Mota and T. Cichorek, unpublished (2003).
- [167] R. H. Heffner, J. L. Smith, J. O. Willis, P. Birrer, C. Baines, F. N. Gygax, B. Hitti, E. Lippelt, H. R. Ott, A. Schenk, E. A. Knetsch, J. A. Mydosh, and D. E. MacLaughlin, *Phys. Rev. Lett.* 65 (1990) 2816.
- [168] F. Kromer, R. Helfrich, M. Lang, F. Steglich, C. Langhammer, A. Bach, T. Michels, J. Kim, and G. Stewart, *Phys. Rev. Lett.* 81 (1998) 4476.
- [169] F. Kromer, M. Lang, N. Oeschler, P. Hinze, C. Langhammer, and F. Steglich, *Phys. Rev. B* 62 (2000) 12477.
- [170] F. Kromer, N. Oeschler, T. Tayama, K. Tenya, T. Cichorek, M. Lang, F. Steglich, J. S. Kim, and G. R. Stewart, *J. Low Temp. Phys.* 126 (2002) 815.
- [171] M. Kato and K. Machida, *J. Phys. Soc. Jpn.* 56 (1987) 2136.
- [172] C. Wälti, H. R. Ott, Z. Fisk, and J. L. Smith, *Phys. Rev. Lett.* 84 (2000) 5616.
- [173] T. Maehira, A. Higashiya, M. Higuchi, H. Yasuhara, and A. Hasegawa, *Physica B* 312-313 (2002) 103.

- [174] R. Felten, F. Steglich, G. Weber, H. Rietschel, F. Gompf, B. Renker, and J. Beuers, *Europhys. Lett.* 2 (1986).
- [175] D. L. Cox, *Phys. Rev. Lett.* 59 (1987) 1240.
- [176] A. P. Ramirez, P. Chandra, P. Coleman, Z. Fisk, J. L. Smith, and H. R. Ott, *Phys. Rev. Lett.* 73 (1994) 3018.
- [177] A. Schiller, F. B. Anders, and D. L. Cox, *Phys. Rev. Lett.* 81 (1998) 3235.
- [178] R. Helfrich, Dissertation, TU Darmstadt (1996).
- [179] P. Gegenwart, C. Langhammer, R. Helfrich, N. Oeschler, M. Lang, J. S. Kim, G. R. Stewart, and F. Steglich, cond-mat/0307420 (2004).
- [180] P. Gegenwart, Dissertation, TU Darmstadt (1997).
- [181] B. Golding, D. J. Bishop, B. Batlogg, W. H. Haemmerle, Z. Fisk, J. L. Smith, and H. R. Ott, *Phys. Rev. Lett.* 55 (1985) 2479.
- [182] V. Müller, D. Maurer, E. W. Scheidt, C. Roth, K. L. amd E. Bucher, and H. E. Bömmel, *Solid State Commun.* 57 (1986) 319.
- [183] F. Kromer, Dissertation, TU Dresden (2000).
- [184] H. R. Ott, H. Rudiger, Z. Fisk, and J. L. Smith, *Phys. Rev. B* 31 (1985) 1651.
- [185] U. Rauchschwalbe, F. Steglich, G. R. Stewart, A. L. Giorgi, P. Fulde, and K. Maki, *Europhys. Lett.* 3 (1987) 751.
- [186] M. Sigrist and T. M. Rice, *Phys. Rev. B* 39 (1989) 2200.
- [187] B. Batlogg, D. Bishop, B. Golding, C. M. Varma, Z. Fisk, J. L. Smith, and H. R. Ott, *Phys. Rev. Lett.* 55 (1985) 1319.
- [188] E. Dumont and A. C. Mota, *Phys. Rev. B* 65 (2002) 144519.
- [189] M. Sigrist and D. Agterberg, *Prog. Theor. Phys.* 102 (1999) 965.
- [190] R. Caspary, P. Hellmann, M. Keller, C. Wassilew, R. Köhler, G. Sparn, C. Schank, C. Geibel, F. Steglich, and N. E. Phillips, *Phys. Rev. Lett.* 71 (1993) 2146.
- [191] R. Feyerherm, A. Amato, F. N. Gygax, A. Schenck, C. Geibel, F. Steglich, N. Sato, and T. Komatsubara, *Phys. Rev. Lett.* 73 (1994) 1849.
- [192] N. Sato, N. Aso, G. H. Lander, B. Roessli, T. Komatsubara, and Y. Endoh, *J. Phys. Soc. Jpn.* 66 (1997) 1884.
- [193] N. Sato, N. Aso, G. H. Lander, B. Roessli, T. Komatsubara, and Y. Endoh, *J. Phys. Soc. Jpn.* 66 (1997) 2981.

- [194] N. Bernhoeft, N. Sato, B. Roessli, N. Aso, A. Hiess, G. H. Lander, Y. Endoh, and T. Komatsubara, Phys. Rev. Lett. 81 (1998) 4244.
- [195] N. Bernhoeft, Eur. Phys. J. B 13 (2000) 685.
- [196] M. Jourdan, M. Huth, and H. Adrian, Nature 398 (1999) 47.
- [197] A. Grauel, A. Böhm, H. Fischer, C. Geibel, R. Köhler, R. Modler, C. Schank, F. Steglich, and G. Weber, Phys. Rev. B 46 (1992) 5818.
- [198] M. Dressel, N. Kasper, K. Petukhov, B. Gorshunov, G. Grüner, M. Huth, and H. Adrian, Phys. Rev. Lett. 88 (2002) 186404.
- [199] A. Krimmel, P. Fischer, B. Roessli, H. Maletta, C. Geibel, C. Schank, A. Grauel, A. Loidl, and F. Steglich, Z. Phys. B 86 (1992) 161.
- [200] H. Kita, A. Dönni, Y. Endoh, K. Kakurai, N. Sato, and T. Komatsubara, J. Phys. Soc. Jpn. 63 (1994) 726.
- [201] J. Hessert, M. Huth, M. Jourdan, H. Adrian, C. T. Rieck, and K. Scharnberg, Physica B 230-232 (1997) 373.
- [202] H. Tou, Y. Kitaoka, K. Asayama, C. Geibel, C. Schank, and F. Steglich, J. Phys. Soc. Jpn. 64 (1995) 725.
- [203] K. Matsuda, Y. Kohori, and T. Kohara, Phys. Rev. B. 55 (1997) 15223.
- [204] F. Steglich, B. Buschinger, P. Gegenwart, C. Geibel, R. Helfrich, P. Hellmann, M. Lang, A. Link, R. Modler, D. Jaccard, and P. Link, *Physical Phenomena in High Magnetic Fields -II* (World Scientific, Singapore, 1996), p. 125.
- [205] K. Ishida, K. Okamoto, Y. Kawasaki, Y. Kitaoka, O. Trovarelli, C. Geibel, and F. Steglich, Phys. Rev. Lett. 89 (2002) 107202.
- [206] M. Jourdan, A. Zakharov, M. Foerster, and H. Adrian, Phys. Rev. Lett 93 (2004) 097001.
- [207] L. M. Sandratskii and J. Kübler, Phys. Rev. B 50 (1994).
- [208] K. Knöpfle, A. Mavromaras, L. M. Sandratskii, and J. Kübler, J. Phys. Condens. Matter 8 (1996) 901.
- [209] Y. Inada, H. Yamagami, Y. Haga, K. Sakurai, Y. Tokiwa, T. Honma, E. Yamamoto, Y. Onuki, and T. Yanagisawa, J. Phys. Soc. Jpn. 68 (1999) 3643.
- [210] Y. Inada, A. Ishiguro, J. Kimura, N. Sato, A. Sawada, T. Komatsubara, and H. Yamagami, Physica B 206-207 (1995) 33.
- [211] L. Petit, A. Svane, W. M. Temmerman, Z. Szotek, and R. Tyer, Europhys. Lett. 62 (2003) 391.

- [212] T. E. Mason and G. Aeppli, *Matematisk-fysiske Meddelelser* 45 (1997) 231.
- [213] A. Hiess, N. Bernhoeft, N. Metoki, G. H. Lander, B. Roessli, N. K. Sato, N. Aso, Y. Haga, Y. Koike, T. Komatsubara, and Y. Onuki, preprint (2004).
- [214] M. Kyogaku, Y. Kitaoka, K. Asayama, C. Geibel, C. Schank, and F. Steglich, *J. Phys. Soc. Jpn.* 62 (1993) 4016.
- [215] N. Bernhoeft, A. Hiess, N. Metoki, G. H. Lander, and B. Roessli, preprint (2004).
- [216] P. Thalmeier and P. McHale, preprint (2004).
- [217] T. Watanabe, K. Izawa, Y. Kasahara, Y. Haga, Y. Onuki, P. Thalmeier, K. Maki, and Y. Matsuda, cond-mat/0405211 (2004).
- [218] Y. Nishikawa and K. Yamada, *J. Phys. Soc. Jpn.* 71 (2002) 237.